**UNIVERSIDADE FEDERAL DE MINAS GERAIS**
**Instituto de Geociências**
**Programa de Pós-Graduação em Geologia**

Deniro Felipe Gonçalves Costa

# INTEGRATION OF STRUCTURAL AND GEOCHEMICAL DATA FROM THE PRE-SALT IN IRACEMA, TUPI FIELD, SANTOS BASIN

Belo Horizonte

2025

Deniro Felipe Gonçalves Costa

# INTEGRATION OF STRUCTURAL AND GEOCHEMICAL DATA FROM THE PRE-SALT IN IRACEMA, TUPI FIELD, SANTOS BASIN

Dissertação apresentada ao Programa de Pós-Graduação em Geologia da Universidade Federal de Minas Gerais como requisito parcial para obtenção do título de Mestre em Geologia.

Orientador: Prof. Dr. Tiago Amâncio Novo

Coorientadores: Prof. Dr. Tobias Maia Rabelo Fonte Boa, Prof. Dr. Humberto Luis Siqueira Reis, Prof. Dr. Ross Stevenson

Belo Horizonte

2025

C837i
2025

Costa, Deniro Felipe Gonçalves.

Integration of structural and geochemical data from the pre-salt in Iracema, Tupi field, Santos Basin / Deniro Felipe Gonçalves Costa. – 2025.

114 f., enc. il. (principalmente color.)

Orientador: Tiago Amâncio Novo.

Co-orientadores: Tobias Maia Rabelo Fonte Boa, Humberto Luis Siqueira Reis, Ross Stevenson.

Dissertação (mestrado) – Universidade Federal de Minas Gerais, Instituto de Geociências, 2025.

Área de concentração: Geologia Econômica e Aplicada.

Bibliografia: f. 87-110.

Inclui apêndices e anexos.

1. Petróleo – Geologia – Teses. 2. Falhas (Geologia) – Brasil, Sudeste – Teses. 3. Geologia estrutural – Teses. 4. Geologia estratigráfica – Teses. 5. Geoquímica – Teses. 6. Isótopos – Teses. I. Novo, Tiago Amâncio. II. Fonte-Boa, Tobias Maia Rabelo. III. Reis, Humberto Luis Siqueira. IV. Stevenson, Ross. V. Universidade Federal de Minas Gerais. Instituto de Geociências. VI. Título.

CDU: 553.982 (815)

Ficha catalográfica elaborada por Nathalia Machado Laponez Maia – CRB-6/3002
Biblioteca “Vitória Pedersoli”, Instituto de Geociências da UFMG

**UNIVERSIDADE FEDERAL DE MINAS GERAIS**

**PROGRAMA DE PÓS-GRADUAÇÃO EM GEOLOGIA DO IGC/UFMG**

# FOLHA DE APROVAÇÃO

**Integration of structural and geochemical data from the pre-salt in Iracema, Tupi field, Santos Basin**

## DENIRO FELIPE GONÇALVES COSTA

Dissertação submetida à Banca Examinadora designada pelo Colegiado do Programa de Pós-Graduação em GEOLOGIA, do Instituto de Geociências (IGC), da Universidade Federal de Minas Gerais (UFMG), como **REQUISITO PARCIAL** para obtenção do grau de Mestre em GEOLOGIA, área de concentração GEOLOGIA ECONÔMICA E APLICADA, pelo Programa de Pós-graduação em Geologia do IGC/UFMG.

Aprovada em 04 de fevereiro de 2025, pela banca constituída pelos membros:

gov.br Documento assinado digitalmente
TIAGO AMANCIO NOVO
Data: 05/02/2025 10:04:24-0300
Verifique em https://validar.iti.gov.br

Prof(a). Dr(a). Tiago Amâncio Novo – Orientador(a)
UFMG

gov.br Documento assinado digitalmente
DANIEL GALVAO CARNIER FRAGOSO
Data: 05/02/2025 11:03:55-0300
Verifique em https://validar.iti.gov.br

Prof(a). Dr(a). Daniel Galvão Carnier Fragoso
UFMG

gov.br Documento assinado digitalmente
HENRIQUE BRUNO
Data: 25/02/2025 13:24:39-0300
Verifique em https://validar.iti.gov.br

Prof(a). Dr(a). Henrique Bruno
UERJ

Belo Horizonte, 04 de fevereiro de 2025.

## ACKNOWLEDGEMENTS

Primarily, I would like to express my sincere gratitude to my advisor, Professor Tiago, and to my co-advisors here at UFMG, Professor Tobias and Humberto, for their continuous support, insightful guidance and unwavering patience in this journey.

I had the opportunity to live in Montréal to perform part of my research and I am deeply thankful for Professor Ross taking me as an advisee during my internship at UQAM. I also thank the Geotop team, besides André Poirier and Julien Gogot (UQAM) and Thi Hao Bui and Professor Galen Halverson (McGill University) for assistance with preparation and analysis of my samples.

I would like to acknowledge the Pró-reitoria de Pós-graduação (PRPg) and the Programa de Pós-graduação em Geologia do Instituto de Geociências (IGC) from UFMG for the institutional and financial support to participate in academic-scientific events. Samples acquisition was carried by Petrobras through the project entitled “Inteligência artificial aplicada à exploração de petróleo na camada pré-sal” (nº 28184). This study was financed in part by the Coordenação de Aperfeiçoamento de Pessoal de Nível Superior – Brasil (CAPES) – Finance Code 001. The scholarship in Canada was provided by the Emerging Leaders in the Americas Program (ELAP).

I especially thank ANP for providing the seismic data and samples used in this work, the DUG company for the DUG Insight academic license applied for seismic visualization, interpretation, analysis, and PE Limited for the MOVE application used for fault analysis and structural restoration.

Thanks so much to Felipe Farias from Petrobras and Professor Gabriel Uhlein from UFMG for their suggestions and constant assistance.

The support and discussion with members of the SÍSMICA research group – along with the friendship –, mainly Mariana, Fernanda, Maria and Caique is also appreciated.

To the amazing Brazilian geologists who made me feel at home in Québec, Julia, Larissa, Mariane and Isabela, you rock! Just like my best friend Gabriela back in BH.

Finally, to be a cliché, I owe a great share of who I am today to those who I may not see every day anymore yet are always in my heart. To my parents Janaíne and Edmilson, and my sister Thaís, thank you.

“Questioning is the piety of thought” (Martin Heidegger, 1954).

## RESUMO

Os reservatórios do pré-sal em depósitos carbonáticos lacustres nas bacias marítimas do sudeste brasileiro são responsáveis pela maior parte da produção petrolífera no país recentemente. Apesar da ampla literatura detalhando a evolução paleoambiental ou integrando uma abordagem quantitativa associada à distribuição espacial/estratigráfica, relacionada ao contexto deposicional ou estrutural, existem questões ainda a serem exploradas. O objetivo principal, portanto, é avaliar a correspondência das estruturas geradas e/ou reativadas durante a evolução tectônica e a deposição das camadas do pré-sal na Bacia de Santos, com foco na Formação Barra Velha (FBV) e seu sinal isotópico. Assim, o contexto tectono-estratigráfico é avaliado com interpretação de seções sísmicas 2D e restauração estrutural. Isso permite analisar a dinâmica da evolução tectônica, quantificar e descrever a distribuição de falhas. Análises isotópicas são essenciais para fornecer restrições críticas sobre o ambiente de formação das rochas-reservatório na região de Iracema, no campo de Tupi. Análises de isótopos estáveis de C e O e de Sr radiogênico foram feitas em fácies de amostras de carbonatos de furos de sondagem em uma coluna de 101 m. Elementos maiores (Ca, Mg, Fe, Mn, Sr e Rb) também tiveram suas concentrações medidas. Valores de $\delta^{13}C$ variam entre + 0,79 e + 3,16‰, com média de +2,22‰. O $\delta^{18}O$ varia entre - 1,22 e + 3,86‰, com média de +1,18‰. Já o $^{87}Sr/^{86}Sr$, varia entre 0,7130 na parte superior da seção e 0,7144 na parte inferior, com média de 0,7135. Os altos valores de $\delta^{13}C$ e $\delta^{18}O$ registram principalmente os efeitos climáticos responsáveis pelo controle da deposição de sedimentos da FBV e acordam com aqueles encontrados na bacia, indicando que os sinais isotópicos podem ter sido conservados até certo ponto. Embora ambientes com altas temperaturas e alta salinidade tendam a favorecer a precipitação de dolomita e/ou calcita rica em Mg, os resultados mostram ausência virtual de dolomita. Outras observações corroboram com um baixo grau de alteração, preservando características mais próximas do carbonato original, como alto Ca/Mg na maioria das amostras e baixas concentrações de Mn e Fe. Altos valores de $^{87}Sr/^{86}Sr$ podem implicar uma contribuição significativa de Sr da erosão continental ou de fontes terrestres, embora possa haver outra origem, como a vulcânica. Durante a diagênese, Rb pode ter sido incorporado em fases minerais secundárias ou materiais de argila associados. A restauração estrutural aponta para a identificação de falhas reativadas durante a deposição carbonática,

havendo estruturas nas direções NW-SE, N-S e NE-SW. Resultados indicam que as estruturas mapeadas podem ter participado de processos diagenéticos tenros no poço amostrado, já que o sistema de falhas pode ter sido responsável pelo transporte simultâneo de Rb e Sr e pela promoção da deposição de argilas Mg na área, sem sugestão de maior componente hidrotermal.

Palavras-chave: carbonatos do pré-sal; isótopos de carbono e oxigênio; isótopos de estrôncio; atividade de falhas; Formação Barra Velha; restauração estrutural.

## ABSTRACT

Lacustrine carbonate deposits from pre-salt reservoirs in the offshore basins of Southeastern Brazil account for most of the oil production in the country in recent years. Despite a large number of studies detailing the paleoenvironmental evolution or integrating a quantitative approach associated with spatial/stratigraphic distribution and related to depositional or structural context, many questions are yet to be explored. The main objective, therefore, is to evaluate the correspondence of structures generated and/or reactivated during the tectonic evolution and the deposition of the pre-salt layers in the Santos Basin, focusing on the Barra Velha Formation (BVF) and its isotopic signal. Thus, the tectono-stratigraphic context is evaluated from the interpretation of 2D seismic sections and structural restoration. This enables us to analyze the dynamics of tectonic evolution, quantify and describe the distribution of faults. Isotopic analyses are essential to provide critical constraints on the formation environment of the reservoir rocks in the Iracema region, Tupi field. Stable isotope analyses of C and O and radiogenic Sr were carried out on carbonate samples from sidewall borehole facies in a 101 m column. Major elements (Ca, Mg, Fe, Mn, Sr and Rb) also had their concentrations measured. The sample values of $\delta^{13}C$ vary between + 0.79 and + 3.16‰, with an average of +2.22‰. The values of $\delta^{18}O$ vary between -1.22 and + 3.86‰, with an average of +1.18‰. The values of $^{87}Sr/^{86}Sr$ vary between 0.7130 at the top of the section and 0.7144 at the bottom, with an average of 0.7135. High $\delta^{13}C$ and $\delta^{18}O$ values mainly record the climatic effects responsible for controlling the deposition of sediments from the BVF and are in accord with those found in the Santos Basin, indicating that isotopic signals may have been conserved to some extent. Even though environments with high temperatures and high salinity tend to favor the precipitation of dolomite and/or calcite rich in Mg, results show virtual absence of dolomite. Other observations corroborate with a low degree of alteration, preserving characteristics closer to the original carbonate, such as high Ca/Mg in most samples and low concentrations of Mn and Fe. High $^{87}Sr/^{86}Sr$ values may implicate a significant contribution of Sr from continental erosion or terrestrial sources, although there may be another origin, such as volcanic. During diagenesis, Rb could have been incorporated into secondary mineral phases or associated clay materials. Structural restoration points to identify reactivated faults during carbonate deposition, with structures in NW-SE, N-S and NE-SW directions. Results indicate that mapped

structures may have participated in weak diagenetic processes in the sampled well, as the fault system may have been responsible for transporting Rb and Sr simultaneously and promoting deposition of Mg-clays in the area, with no suggestion of greater hydrothermal component.

Keywords: pre-salt carbonates; carbon and oxygen isotopes; strontium isotopes; fault activity; Barra Velha Formation, structural restoration.

## LIST OF FIGURES

## LIST OF FIGURES – MANUSCRIPT

## LIST OF TABLES



## LIST OF TABLES – MANUSCRIPT

## LIST OF ACRONYMS

| | |
|---|---|
| BVF | Barra Velha Formation |
| ICP-OES | Inductively Coupled Plasma Optical Emission Spectroscopy |
| IRMS | Isotope Ratio Mass Spectrometry |
| MC-ICP-MS | Multi Collector Inductively Coupled Plasma Mass Spectrometry |
| VPDB | Vienna Pee Dee Belemnite |

**CONTENTS**

# 1 INTRODUCTION

This dissertation is submitted as a partial requirement to obtain the master's degree in Geology from the Programa de Pós-graduação em Geologia at the Universidade Federal de Minas Gerais (UFMG), in the area of concentration "Geologia Econômica e Aplicada". This investigation was conducted under the supervision of Prof. Dr. Tiago Amâncio Novo and co-supervisors Profs. Drs. Tobias Maia Rabelo Fonte Boa and Humberto Luis Siqueira Reis in Brazil and supported by Prof. Dr. Ross Stevenson during the research internship at the Université du Québec à Montréal (UQAM) in Canada. This work integrates the project "Inteligência artificial aplicada à exploração de petróleo na camada pré-sal" (nº 28184). In collaboration between the Departamento de Ciências da Computação (DCC) and the Centro de Pesquisas Professor Manoel Teixeira da Costa (CPMTC), the Instituto de Geociências (IGC) and Petrobras S.A., the PetrobrasIAGeo project is multidisciplinary in nature and aims to bring a new culture to oil and gas exploration, via a feasibility study of models applying AI techniques in different areas. Funding was provided by multiple sources. Beyond obtaining samples through the PetrobrasIAGeo project and conducting geochemical analyses in Canada, this study was financed in part by the Coordenação de Aperfeiçoamento de Pessoal de Nível Superior – Brasil (CAPES) – Finance Code 001.

## 1.1 Objective and geological background

This dissertation aims to correlate geochemical data from the Barra Velha Formation (BVF) carbonates with the tectonostructural context that defines their deposition, on a local and regional scale. To achieve this, analyses of major elements, stable carbon and oxygen isotopes and radiogenic strontium isotopes were conducted. On the structural side, seismic sections were interpreted to identify the distribution of faults and the separation of horizons for the application of structural restoration.

Lacustrine carbonate reservoirs are characterized by their significant geological complexity, with several unresolved aspects that continue to be actively debated in the literature (Terra et al., 2010; Wright and Barnett, 2015; Sabato Ceraldi and Green, 2016; Herlinger et al., 2017). Following the discovery of large pre-salt reservoirs, there has been an increased focus on understanding the environmental conditions that

enabled the deposition of lacustrine carbonates in rift basins, where tectonism controls structural geometry and subsidence rates (e.g., Wright, 2012; Wright and Barnett, 2015; Tosca and Wright, 2018; Arienti et al., 2018; Souza et al., 2018; Farias et al., 2019; Pietzsch et al., 2020).

Published research primarily focuses on the depositional, diagenetic and geochemical facets of the distal pre-salt lacustrine carbonate reservoirs, examining how the primary framework constituents and diagenesis influenced the pore system of the Santos Basin pre-salt carbonates and presenting petrophysical data related to the porosity and permeability of these reservoirs (e.g., Herlinger et al., 2016, 2017; Muniz and Bosence, 2015; Wright and Barnett, 2015; Pietzsch et al., 2018; Lima and De Ros, 2019). Alternatively, other works focus on the geodynamic aspects following the origination and deformation the Brazilian and correlated African basins, such as the regional tectonic regime (e.g., Karner and Gambôa, 2007; Davison, 2007; Strozyk et al., 2017; Kukla et al., 2018). Some studies detail the paleoenvironmental evolution and stratigraphic filling of the sag interval (e.g., Sabato Ceraldi and Green, 2016; Saller et al., 2016) or have integrated a quantitative approach coupled with spatial and stratigraphic distribution and related to the depositional or structural context (e.g., Wright and Barnett, 2020; Gomes et al., 2020; Carramal et al., 2022).

The Iracema region (about 700 km²) in the Tupi (Lula) field, is located in the central portion of the Santos Basin, about 230 km off the coast of Rio de Janeiro city (Figure 1). Petroleum production from pre-salt reservoirs in 2023 corresponded to 76.07% of total production, with the Tupi field alone contributing with 25.04% (ANP, 2023). Few works have provided structural characterization, tectonostratigraphic evolution and paleoenvironmental conditions for the area (e.g., Silva, 2021; Adriano et al., 2022; Almeida Carvalho et al., 2022; Carramal et al., 2022; Sommer et al., 2022). Carvalho et al. (2024), for example, applied structural restoration in the pre-salt layers, which had only been applied to salt and post-salt packages previously.

The Outer High of the Santos Basin hosts most production fields (e.g., Tupi, Búzios, Mero, Sapinhoá, Sépia, Atapu) and pre-salt exploration blocks. NE-SW-trending faults shaped the structure of the Outer High prior to evaporitic deposition (Carminatti et al., 2008). This positive feature of distal location and pronounced elevation provided isolation from external clastic sediments in the region (Buckley et al., 2015). It would

have impacted depositional thickness and accumulation patterns from the pre-salt carbonates to Neogene sediment packages (Gomes et al., 2009).

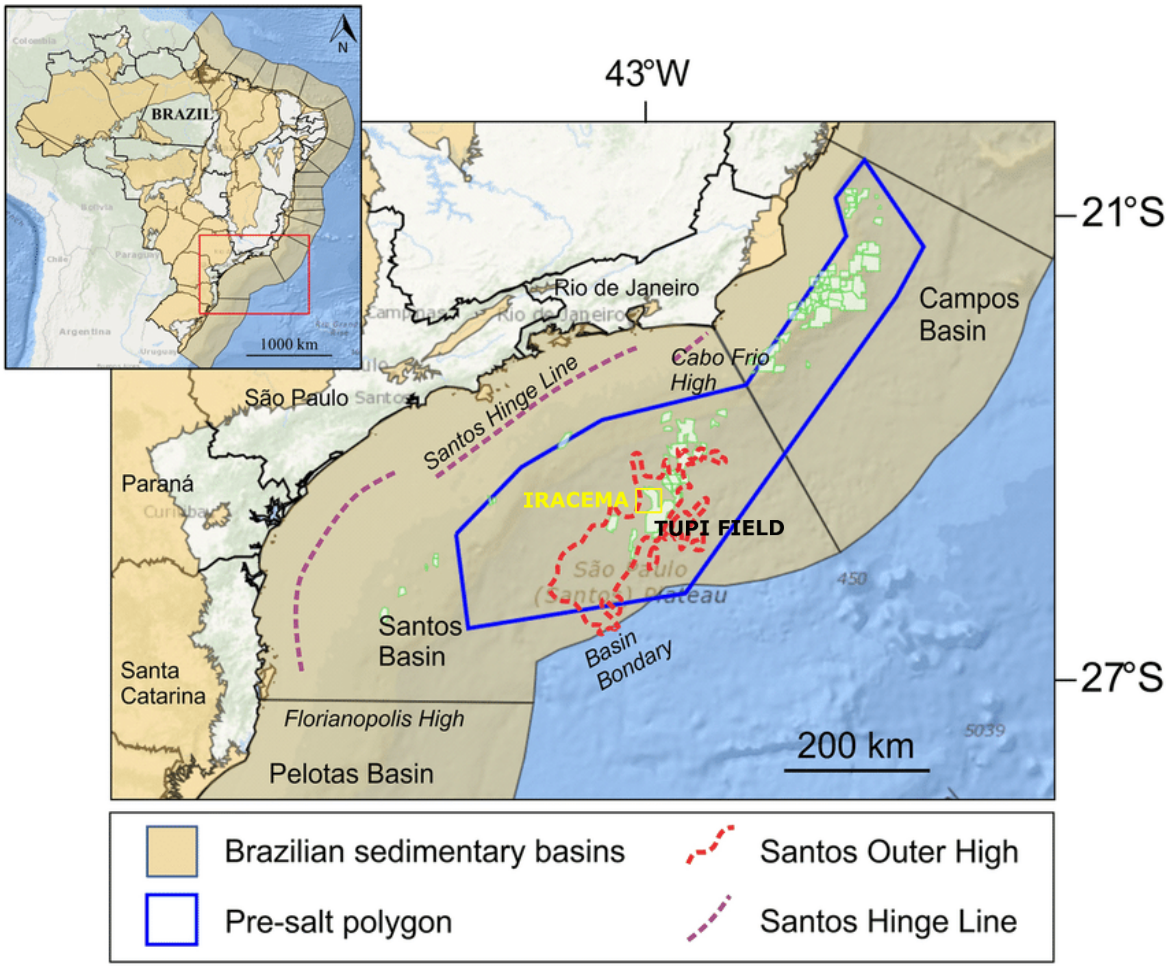


Figure 1 - Location map of the Santos Basin, offshore SE Brazil (adapted from Basso et al., 2020). Santos outer high limits and Santos hinge line were retrieved from Ysaccis et al. (2019) (modified from Basso et al., 2022).

The Outer High presents two individual structures represented by the NE Tupi High, which is segmented by a series of synthetic SE faults; and the SE Pão de Açúcar High, segmented by antithetic NW faults. Both are separated by a large NW-SE transfer zone (Gomes et al., 2009, 2012). The primary NE-SW fracture trend, inherited from basement structures (Stanton et al., 2014), bends in the NW portion of the field, forming the Iracema High (Silva, 2021) (Figure 2).During rift extension, the Iracema transfer zone was generated as the Cabo Frio High remained static (Moulin et al., 2013). The direction of the faults changed to NW-SE, forming an S-shaped feature (Magnavita, 2021) and presenting dextral regional movement (Silva, 2021). In the region, short faults contained only in the pre-salt interval may or may not extend to the base of the salt and are formed due to the transcurrent movement (Silva, 2021). It is suggested

that rifting was active along with all pre-salt deposition, within 3 phases (Lower, Upper and Later Rift) that occur at different extensions in the field (Adriano et al., 2022).

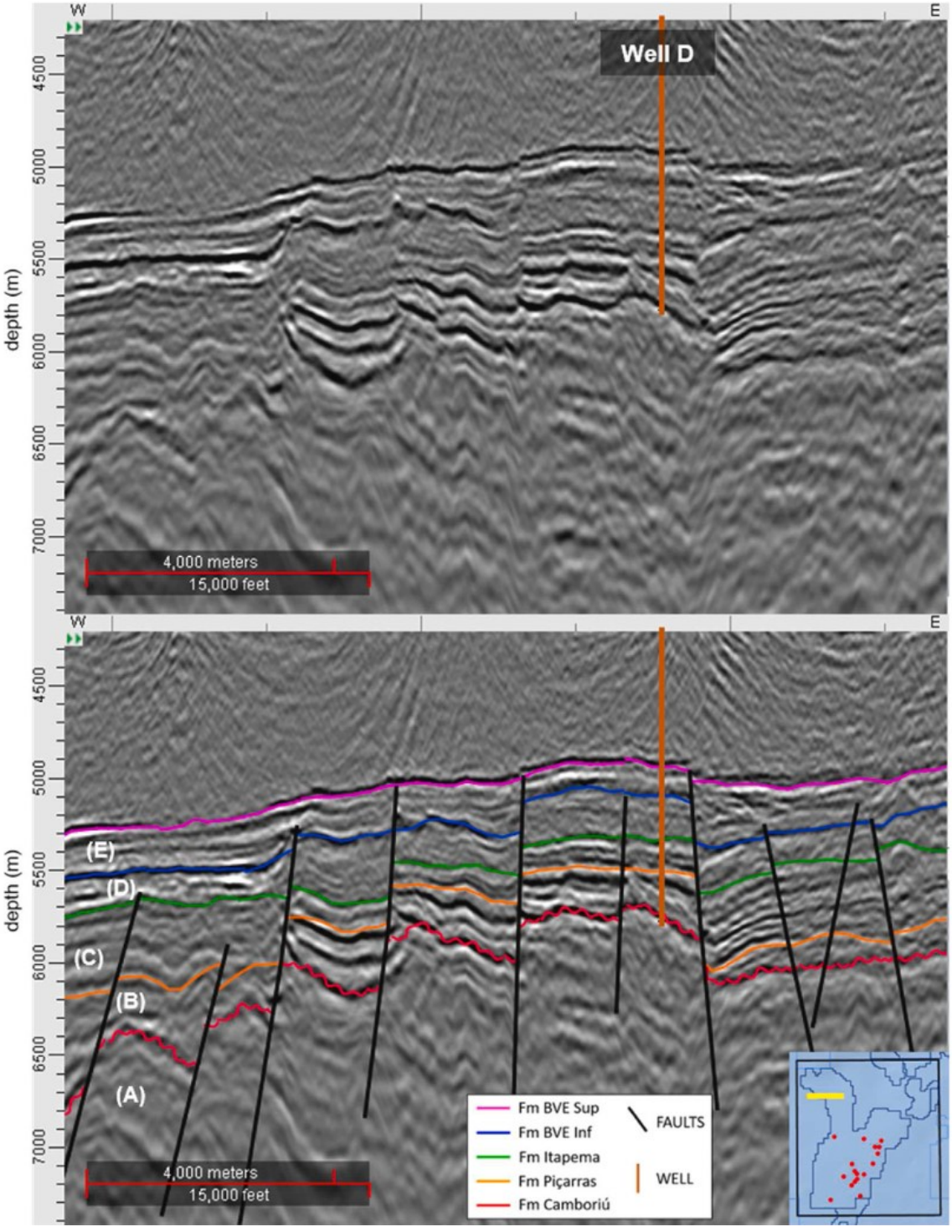


Figure 2 – Detailed view of the Iracema High. Note subparallel reflectors, with good lateral correspondence, for Piçarras, Itapema and Lower Barra Velha Formations, indicating faulting after deposition. The Upper Barra Velha Formation divergent pattern, near faults, indicates syn-depositional conditions (from Adriano et al., 2022).

Considering all this structural context of the study area, a different approach is taken regarding the influence of structures in the upper part of the BVF. Questions about the

generation or reactivation of faults during the deposition of carbonates and the input of elements into the composition of these rocks, as well as diagenetic and possibly hydrothermal processes, are still being raised. Although there has been an increasingly detailed assessment of textures and facies in the region, little has yet been said about stable isotopes, beyond the depositional paleoenvironment, and radiogenic isotopes, in an attempt to explain their origin. This study aims to enhance the understanding of the Tupi field's evolution, extending the analysis to neighboring fields in the Outer High and drawing comparisons with the Campos Basin. It enables us to integrate isotopic data and discuss whether and how there is alteration by tectonostructural influence.

## 1.2 Summary of the dissertation

The dissertation is divided into chapters, as follows:

- **Chapter 2:** corresponds to the geological settings. Topics from the definition of faults, their role during the rifting process in the South Atlantic, along with subsidence mechanisms and an overlook on the Santos Basin are presented;
- **Chapter 3:** presents materials and methods. There is an explanation and brief review of the methods applied before pointing out the materials used;
- **Chapter 4:** represents an adapted version of the manuscript for publication. Note that this section has its own list of figures and tables;
- **Chapter 5:** indicates the conclusions of the dissertation.

After that, references, appendix and annex follow.

# 2 GEOLOGICAL SETTINGS

## 2.1 Structural concepts

Deformation refers to the alteration of an initial geometry into a final form through processes such as rigid body translation, rotation, strain (distortion), and changes in volume (Hasui and Mioto, 1992). Strain involves a change in shape, with or without a change in volume, and indicates that particles within a rock have shifted positions relative to one another. When rocks are heated, they tend to undergo a flow and accumulate permanent deformation, occasionally leading to significant permanent strains (Davis et al., 2011). Stress is a concept frequently used in the context of materials with minimal shear resistance, such as rocks. A rock's response to stress is contingent upon the magnitude of stress applied or the extent of accumulated strain. It is also influenced by factors including anisotropy, temperature, strain rate, pore fluid presence, and confining pressure (Ramsay and Huber, 1984).

Fracture initiation occurs when differential stress surpasses the inherent strength of the rock. They represent planar or sub planar discontinuities, typically much narrower in one dimension compared to the other two, and arise due to external (e.g., tectonic forces) or internal forces (thermal or residual stress). Fractures disrupt continuity in terms of displacement and mechanical properties, often resulting in a reduction or loss of cohesion. While they are typically described as surfaces, fractures possess some degree of thickness when examined at various scales (Fossen, 2010).

Once a fracture forms, it becomes a zone of weakness within the rock (Tiab and Donaldson, 2016). Subsequent stress build-up is more likely to reactivate existing fractures at lower stress levels rather than initiating the formation of new fractures. It is an energy-intensive process involving the growth and linkage of minor flaws in the rock (e.g., Colatina Fracture Zone at the Espírito Santo Basin; Belém, 2014). Reactivation of fractures is a critical step for the development of major faults. Without reactivation, the crust would be filled with numerous short fractures characterized by minimal displacements. The orientation of a preexisting fracture and its frictional properties are key factors influencing reactivation, in addition to the existing stress field (Davis et al., 2011). Fractures and related discontinuities are relatively simple structures, whereas faults are more intricate and capable of accommodating significant strain in the upper crust.

The term "fault" is used variably depending on context. A fundamental definition describes a fault as a surface or narrow zone exhibiting visible shear displacement (Fossen, 2010). In terms of fault geometry, non-vertical faults indicate whether the hanging wall displaced downward (normal fault) or moved upward (reverse fault) relative to the footwall. Lateral movement within the horizontal plane characterizes a strike-slip fault, classified as sinistral (left-lateral) or dextral (right-lateral) according to the direction of displacement (Ramsay and Huber, 1984). When two separate normal faults dip toward each other, they create a downthrown block (graben) and, when they dip away from each other, it results in an upthrown block (horst). In faulted regions, the largest faults (i.e., master faults) are often accompanied by minor faults that dip opposite (antithetic) or in the same direction (synthetic) as the master fault (Hasui and Mioto, 1992) (Figure 3).

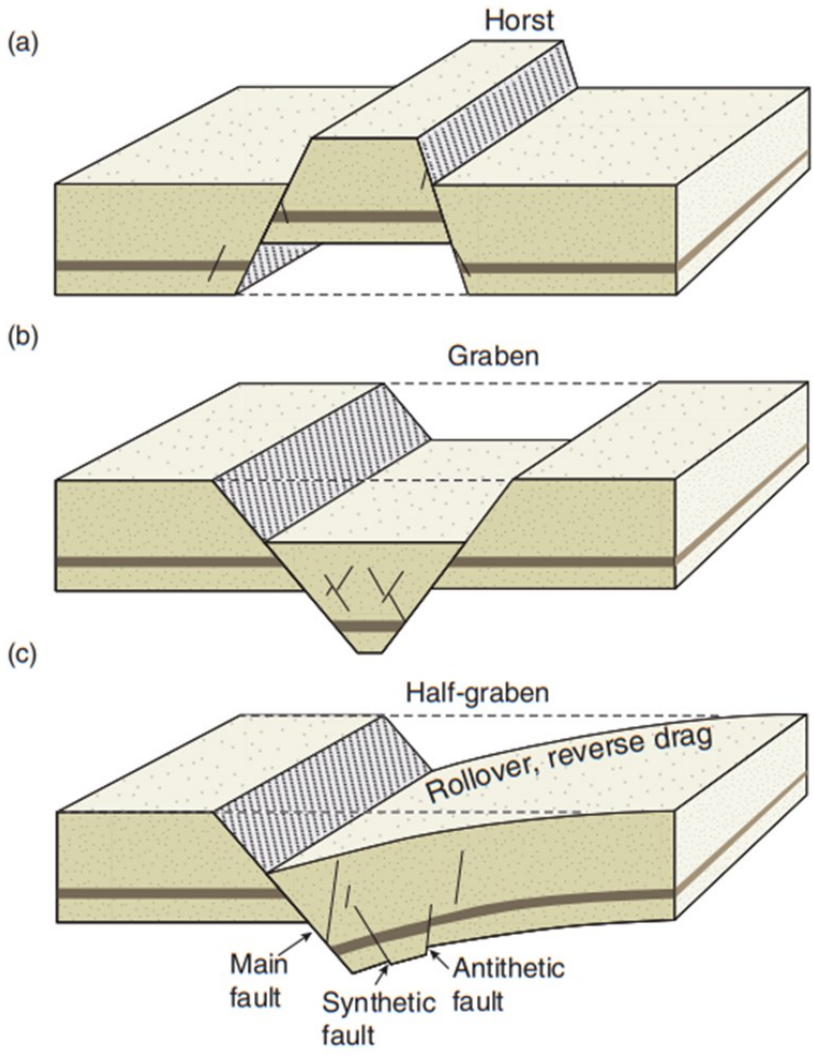


Figure 3 – A horst (a), symmetric graben (b) and asymmetric graben (c), also known as a half-graben. Antithetic and synthetic faults are shown (from Fossen, 2010).

Extensional faults facilitate the stretching of the Earth's crust or specific stratigraphic layers within deformed rock sequences. Field mapping and seismic analysis identify both high-angle and low-angle extensional faults. In many extensional settings, these two types of faults coexist because most rocks exhibit anisotropy inherited from earlier phases of deformation. Thus, steep faults may correspond to reactivated joints or strike-slip faults (Fossen, 2010).

Cross-sections of a rifted portion of the upper crust often display a series of rotated fault blocks arranged like dominoes or overturned books on a partially filled bookshelf. This arrangement illustrates the complex nature of fault systems in geological processes (e.g., Southeastern Brazil).

## 2.2 Rifting: processes and definitions

A rift forms where segments of the continental crust are pulled apart by tectonic forces actively (i.e., controlled by rising mantle plumes that add tensile stress to the domed area) or passively (i.e., controlled by far-field stresses related to plate tectonics along zones of inherited weakness in the lithosphere) (Fossen, 2010). Rifting is a first-order plate tectonic process, primarily described in models of lithospheric stretching (e.g., pure shear, McKenzie, 1978; simple shear, Wernicke, 1985). Following studies (e.g., Lister et al., 1991; Planke et al., 1994) presented the archetypes “magma-poor” (e.g., in Southern Australia; Meeuws et al., 2016) and “magma-rich” (e.g., Pelotas Basin; Stica et al., 2014), from which a wide range of margins is proposed due to different evolutionary stages.

However, the traditional classification of tectonic phases in the evolution of sedimentary basins in rifted margins (i.e., pre-rift, syn-rift, transitional, and passive continental margin; Asmus, 1982; Cainelli and Mohriak, 1998) is no longer sufficient to explain recent observations. Improving our comprehension of plate tectonics depends on gaining deeper insights into local and regional mechanisms controlling thermal and structural processes linked to significant plate tectonic movements (Wildman, 2015).

As the understanding of the way that deformation is coupled with magmatic, thermal, and isostatic processes has evolved, it is widely accepted that rifting is fundamentally multiphase (Peron-Pinvidic et al., 2019). The progression from the rupture of the continental lithosphere to the formation of new plate boundaries and oceanic domains

is currently discussed leading to alternative terminologies in relation to previous definitions of rift phases (Peron-Pinvidic et al., 2013, 2019; Neuharth et al., 2022; Brune et al., 2023). These include morphological terms (platform, terrace, taper break, marginal high), rift domain names (proximal, necking, distal, outer, oceanic, ocean-continent transition, ocean-continent boundary, zone of exhumed continental mantle) and geological processes references (stretching, thinning, exhumation) (Peron-Pinvidic et al., 2013 and references therein, Figure 4).

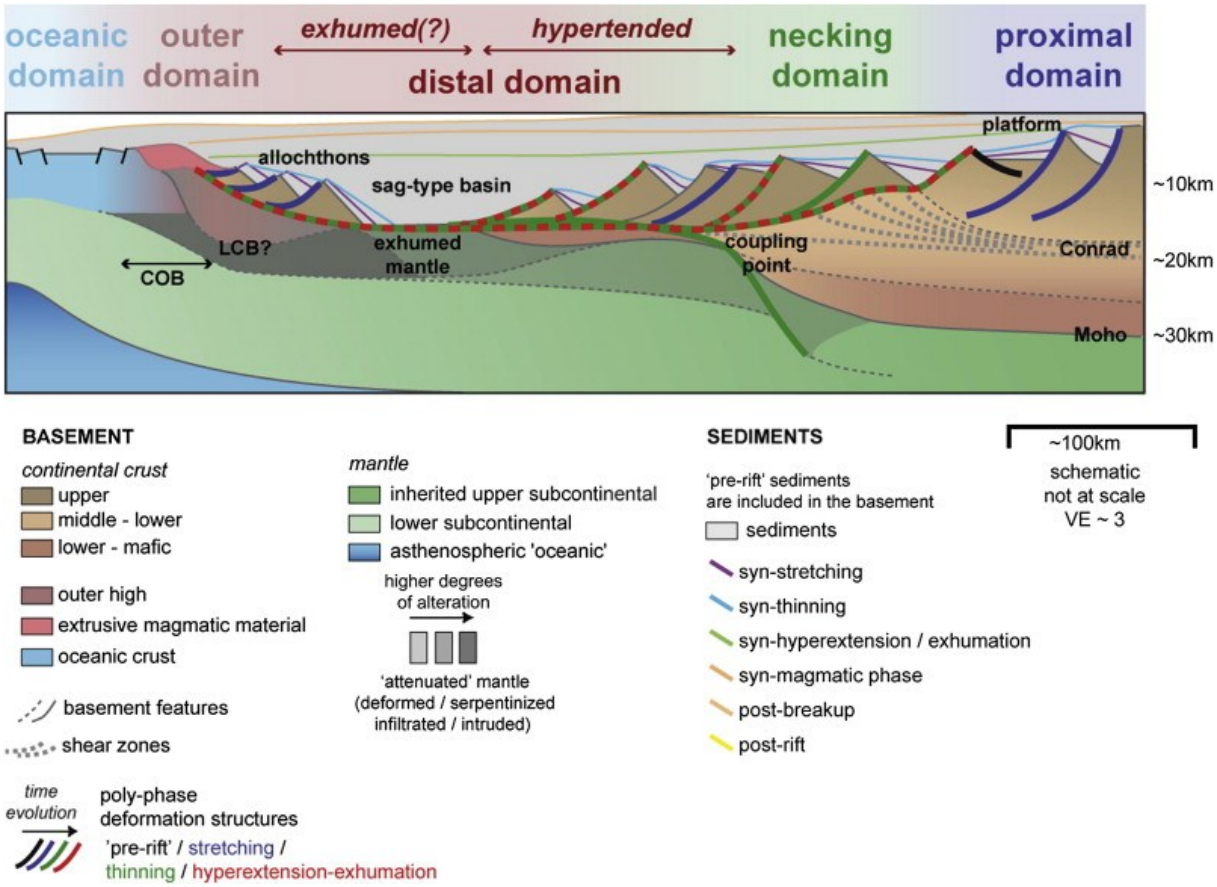


Figure 4 – Schematic section of a typical rifted margin illustrating the various terms used (from Peron-Pinvidic et al., 2013).

Key themes in rifted margin research are considered high-priority targets (e.g., rheology, inheritance, faults, stratigraphy, kinematics, and mantle; Peron-Pinvidic et al., 2019) since the progressive thinning of the crust and mantle lithosphere is a behavior of continental rifts that does not occur in other plate boundary types (Brune et al., 2017a; Naliboff et al., 2017). Actually, some of the earlier phase definitions have been based on changes in layer thickness and its impact on rheology (Lavier and Manatschal, 2006; Huismans and Beaumont, 2014), or the position of faults (Corti, 2012).

**Five rift phases** identified by Neuharth et al. (2022) in terms of active fault network properties were correlated with prior works. Phase one is analogous to the early “stretching phase” (Peron-Pinvidic et al., 2013; Naliboff et al., 2017; Chenin et al., 2021), representing distributed lithospheric deformation and coalescence (e.g., Trøndelag Platform, Norway; Osmundsen et al., 2002). **Phase two** indicates the growth of a fault system, in which large faults define the borders of a central graben (e.g., Malawi and Central Kenya Rifts; Ebinger and Scholz, 2012), associated with the “thinning phase” (Lavier and Manatschal, 2006). It relates to the first phase of two-phase rifting (Agostini et al., 2009; Corti, 2012), whereas the second phase, corresponding to a fault system decline of the “hyperextension phase” (Peron-Pinvidic et al., 2013) is similar to **phase three** (e.g., Main Ethiopian Rift; Corti, 2012). **Phase four** is still part of the definition proposed by Peron-Pinvidic et al. (2013), as the rifting migration generates distinct margin asymmetry (e.g., Central South Atlantic margins, Carminatti et al., 2009). The **final phase** marks the end of continental rifting, the breakup, with the onset of seafloor spreading (e.g., South Atlantic, Heine et al., 2013; Red Sea, Stern and Johnson, 2019).

The conceptual model for the inception and evolution of continental rifts presented by Brune et al. (2023) involves several major phases. **Rift initiation** (e.g., Okavango Rift, Kinabo et al., 2007) is facilitated by structures inherited from previous deformation episodes, which guide deformation, accommodated by brittle faults, ductile shear zones and magmatic dikes. **Rift maturation** generates sedimentary basins as the slip along major faults and ductile thinning of the lower crust cause hanging wall subsidence, in narrow (e.g., Tanganyika Rift; Shaban et al., 2021) to wide rifts (e.g., Basin and Range; Ricketts et al., 2021). Moreover, sublithospheric mantle rises and decompression-driven melts migrate, establishing dikes, sills, and volcanoes. **Oceanization** occurs when a sufficiently thinned crust undergoes intensified magmatic emplacement in the rift center, as deformation migrates to the site where the continental lithosphere ruptures, initiating the transition to mid-ocean spreading. **Post-rift** phase represents a rifted continental margin that tilts due to differing rates of deformation in the proximal part and cooling in the distal part. Offshore subsidence may result from the deposition of sediments transported by river networks, which continue to shape rifted margins until today (e.g., Espírito Santo, Campos and Santos

Basins; Japsen et al., 2012; Jelinek et al., 2014; Engelmann de Oliveira et al., 2016; Fonte-Boa et al., 2022).

Key domains in the Atlantic margins occur nearly in the same order, exhibiting sedimentary and basement geometries and relative temporal evolution (Peron-Pinvidic et al., 2013). Equivalent observations have also been reported from other margins (e.g., Nova Scotia margin, Funck et al., 2004; South China Sea, Franke et al., 2011; Gulf of Aden, Autin et al., 2010; Great Australian Bight margin; Direen et al., 2007; Argentina margin, Blaich et al., 2009; as well as onshore analogues, Manatschal, 2004; Mohn et al., 2010).

## 2.3 Subsidence mechanisms

According to Ingersoll (2011), depositional surfaces may subside due to the following processes (Ingersoll and Busby, 1995 and references therein):

(1) crustal thinning due to stretching, erosion, and magmatic withdrawal;

(2) thickening of the mantle lithosphere during cooling, followed by the cessation of stretching and/or heating;

(3) sedimentary and volcanic loading, where local crustal isostasy and/or regional lithospheric flexure occur;

(4) tectonic loading of both crust and lithosphere during overthrusting and/or underpulling;

(5) subcrustal loading, considering lithospheric flexure during underplating of dense lithosphere;

(6) dynamic effects of asthenospheric flow, commonly due to descent or delamination of subducted lithosphere;

(7) crustal densification, due to changes in pressure/temperature conditions and/or emplacement of higher-density melts into lower-density crust.

As proposed by Allen and Allen (2005), the mechanisms for regional subsidence and uplift might be grouped according to the fundamental geodynamical processes. For

rifts, post-rift, and passive margins, flexural, isostatic, and dynamic mechanisms operate differently.

The sediment infilling a basin acts as a sedimentary load in the rift, amplifying the primary driving mechanism. In the post-rift and at passive margins, there is also a volcanic load component. Flexure, and therefore subsidence, is caused by the loading of the lithosphere, both at the surface and in the subsurface, including the far-field effects of in-plane stresses.

Lithospheric thickness changes (i.e., stretches) in rifts as an isostatic response to crustal thinning, along with brittle fault displacements. On the other hand, gravitational/salt tectonics are more present in the post-rift and passive margins, even with large-scale halokinesis (e.g., Santos Basin). The thickness changes may also be brought purely thermally by lithospheric cooling/densification, where rifting is prolonged while subsequent phases exhibit thermal contraction/re-equilibration of lithosphere.

As for the dynamic effects caused by asthenospheric flow, mantle convection and plumes, the buoyancy effects of changes in temperature in the mantle result in subsidence or uplift. While convection is induced secondarily in the rifts, it is edge-driven in the post-rift and passive margins. Substantial thermal subsidence in the early post-rift characterizes the sag zone, which begins at the beginning of the late syn-rift and continues into the post-rift period. Lithospheric mantle thinning in the sag and distal zones (Figure 5) results in subsidence, as indicated by the finite-element modeling (Huismans and Beaumont, 2008), significant enough to cause the decompression melting in upwelling asthenosphere (Allen and Allen, 2005).

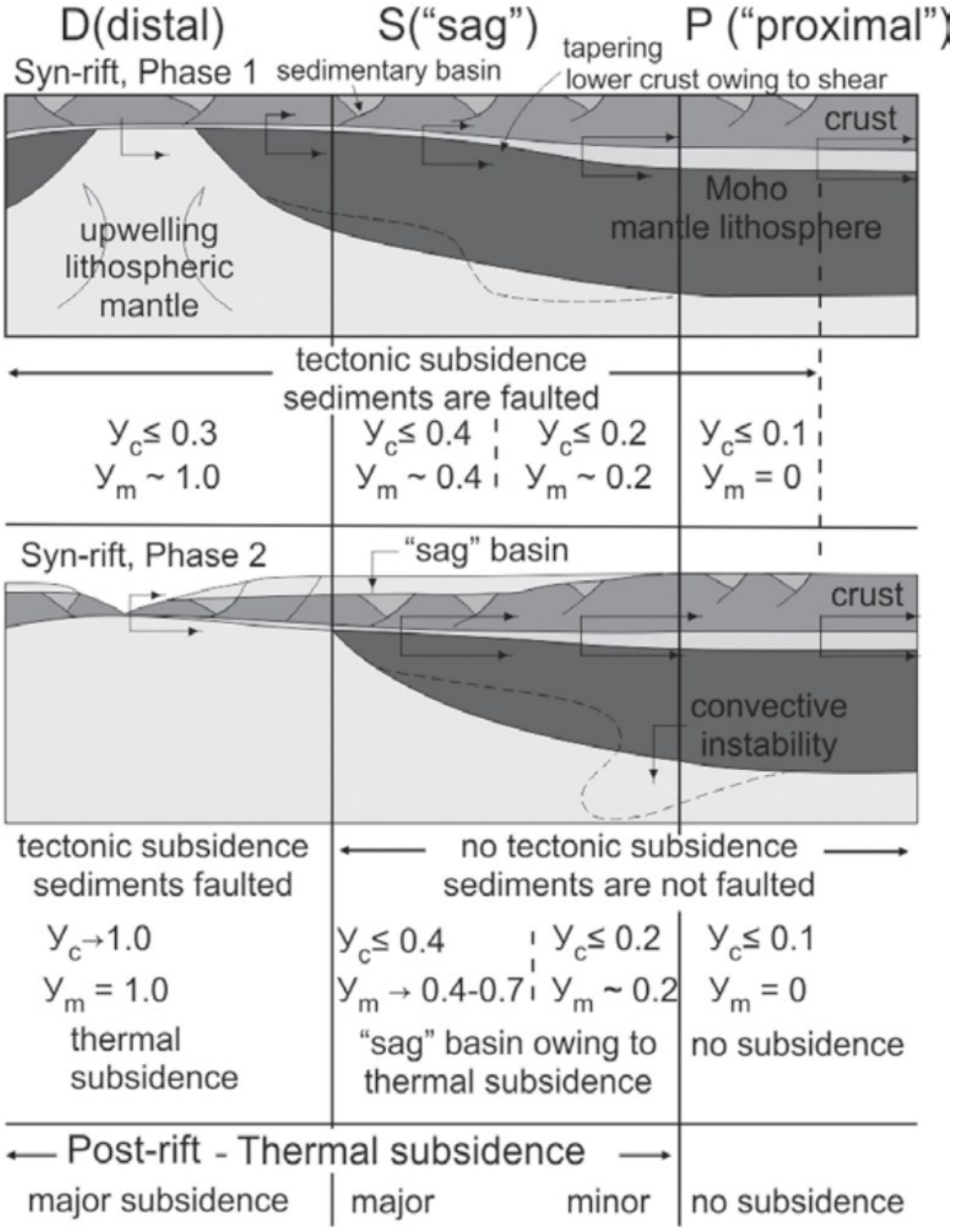


Figure 5 – Figure summarizing main characteristics of dynamic models classified according to zones proximal (P), sag (S), and distal (D) (from Huismans and Beaumont, 2008). $\gamma_c$ and $\gamma_m$ are crustal and lithospheric mantle attenuation factors. Phase 1 crustal extension is distributed, producing limited attenuation and subsidence; basins are faulted. Mantle lithosphere extends by focused necking and ruptures under D with some attenuation under S. Phase 2 crustal extension migrates to the rift axis, D. Additional faulting is confined to basins in D. Mantle lithosphere is advected laterally. Unfaulted "sag" basins develop where there is cooling and thermal subsidence in zone S; transient uplift in S may occur if mantle lithosphere is further attenuated. Post-rift thermal subsidence correlates with $\gamma_m(x)$ and is confined to D and S. Incremental strain at the surface accumulated during each of the stages shown in A, B, and C indicates early deformed syn-rift sediments and late syn-rift sediments are undeformed.

## 2.4 Scenario of the South Atlantic Ocean opening

The South Atlantic can be divided into four segments: Equatorial, Central (which includes the Southeastern Brazilian margin), Austral, and Falkland, bounded from north to south by Marathon, Ascension, Rio Grande, and Agulhas-Falkland fracture zones (Moulin et al., 2010) (Figure 6). The continental rupture associated with the Tristan da Cunha Plume thermal anomaly controlled the formation of the Rio Grande-Walvis volcanic chain (White and McKenzie, 1989), leading to a broader extent of crustal thinning, with a lower stretching rate, and consequent rheological changes (Ponte and Asmus, 1976; Zalán and Oliveira, 2005). Magmatic additions at the early stages of margin formation may partially deplete the mantle, limiting the presence of igneous rocks at later stages (Franke, 2012).

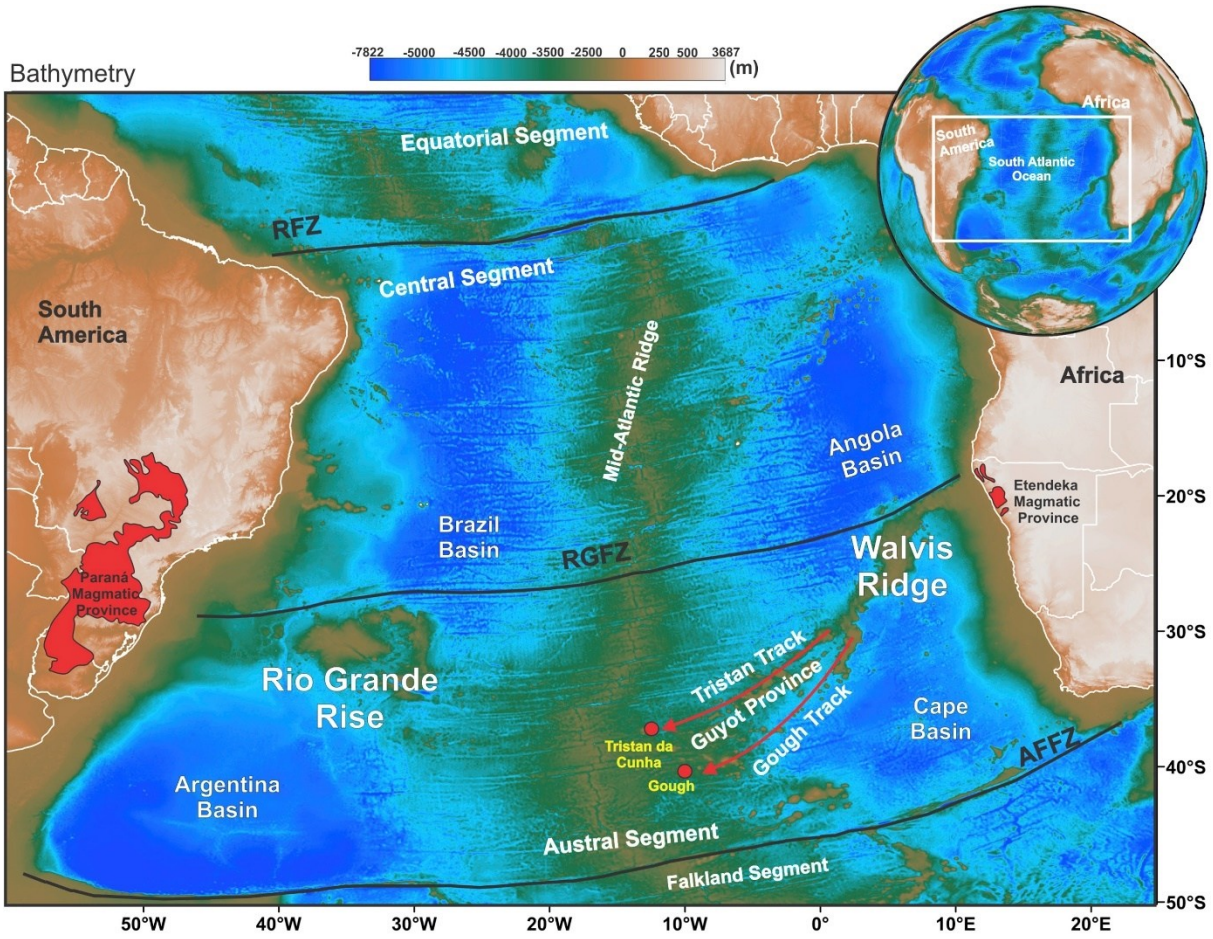


Figure 6 – Regional bathymetric (Amante and Eakins, 2009) map, overlain by a shaded-relief display of free-air gravity anomaly, showing the location of Rio Grande Rise and Walvis Ridge and its Tristan-Gough volcanic track (Guyot Province) in the South Atlantic Ocean (SAO), as well as South Atlantic fracture zones (AFFZ: Agulhas-Falkland Fracture Zone; RGFZ: Rio Grande Fracture Zone; RFZ: Romanche Fracture Zone) dividing the SAO in Central, Austral and Falkland segments. The Equatorial segment belongs to the Equatorial Atlantic. The Rio Grande Rise and Walvis Ridge are located southern of the RGFZ. Paraná-Etendeka Magmatic Provinces are shown in red in the South America and African continents (from Graça et al., 2019).

Previous magmatic and/or tectonic events reduce the static lithospheric strength and allow inherited features (e.g., foliations, faults, suture zones, regions of metasomatized mantle) to remain weak enough to be repeatedly reactivated (Petersen and Schiffer, 2016). Plume-related melting of mantle rocks and subsequent magma ascent heat and weaken the lithosphere facilitating rift initiation (Courtillot et al., 1999; Buck, 2006). In the disassembly of Western Gondwana, the main suture zone between the Neoproterozoic terranes of the basement (Heilbron et al., 2008) followed the trend of the Ribeira Belt, becoming the primary weakness zone where the South Atlantic Ocean formed (Almeida et al., 2013), still contested for its exact timing (Torsvik et al., 2009).

The emplacement of the Paraná-Etendeka Large Igneous Province (LIP) (ca. ~136-131 Ma, Stewart et al., 1996; Kirstein et al., 2001) in both South American and African counterparts most likely triggered or aided the opening. Magmatic rocks are well exposed and associated with dike swarms such as the NW Ponta Grossa (ca. 131-129 Ma; Renne et al., 1996), the NNE Florianópolis (ca. 129 Ma; Deckart et al., 1998) and the NE Santos-Rio de Janeiro (ca. 133-127 Ma; Vieira, 2009) (ages based on K-Ar/Ar-Ar method) in SE Brazil (Almeida, 1986) and Hentis Bay-Outjo in NW Namibia (Renne et al., 1992; Turner et al., 1994; Hawkesworth et al., 2000). The South American Magmatic Province (SAMP) (Szatmari and Milani, 2016) provides evidence of igneous activity in the South Atlantic during the Lower Cretaceous. Basaltic volcanism likely began when the deepest faults reached the anomalously hot subcontinental lithospheric mantle, triggering widespread melting.

Rifting initiation along the central segment of the South Atlantic is of Berriasian age (Karner and Driscoll, 1999; França et al., 2007; Moreira et al., 2007; Winter et al., 2007), indicated by faulted and rotated blocks, with half-grabens enclosing thick sedimentary successions in their depocenters (Milani et al., 2007). Normal faults are oriented preferentially parallel to the southeastern Brazilian coast, defining the regional trend seen in the offshore basins (e.g., Espírito Santo, Campos, Santos; Ojeda, 1982; Chang et al., 1992). The transfer zones that segment these faults nucleated the major transform faults of the seafloor, with evidence of transtensional deformation (Tetzner and Almeida, 2003; Milani et al., 2007; Stanton and Schmitt, 2007). The kinematics of the opening points to an NNE-SSW to N-S-trending rift (Aslanian et al., 2009; Moulin et al., 2010; Heine et al., 2013). Also, to a left-lateral strike-slip reactivation of NE-SW-trending continental-scale fault zones (Szatmari and Milani, 2016) (Figure 7).

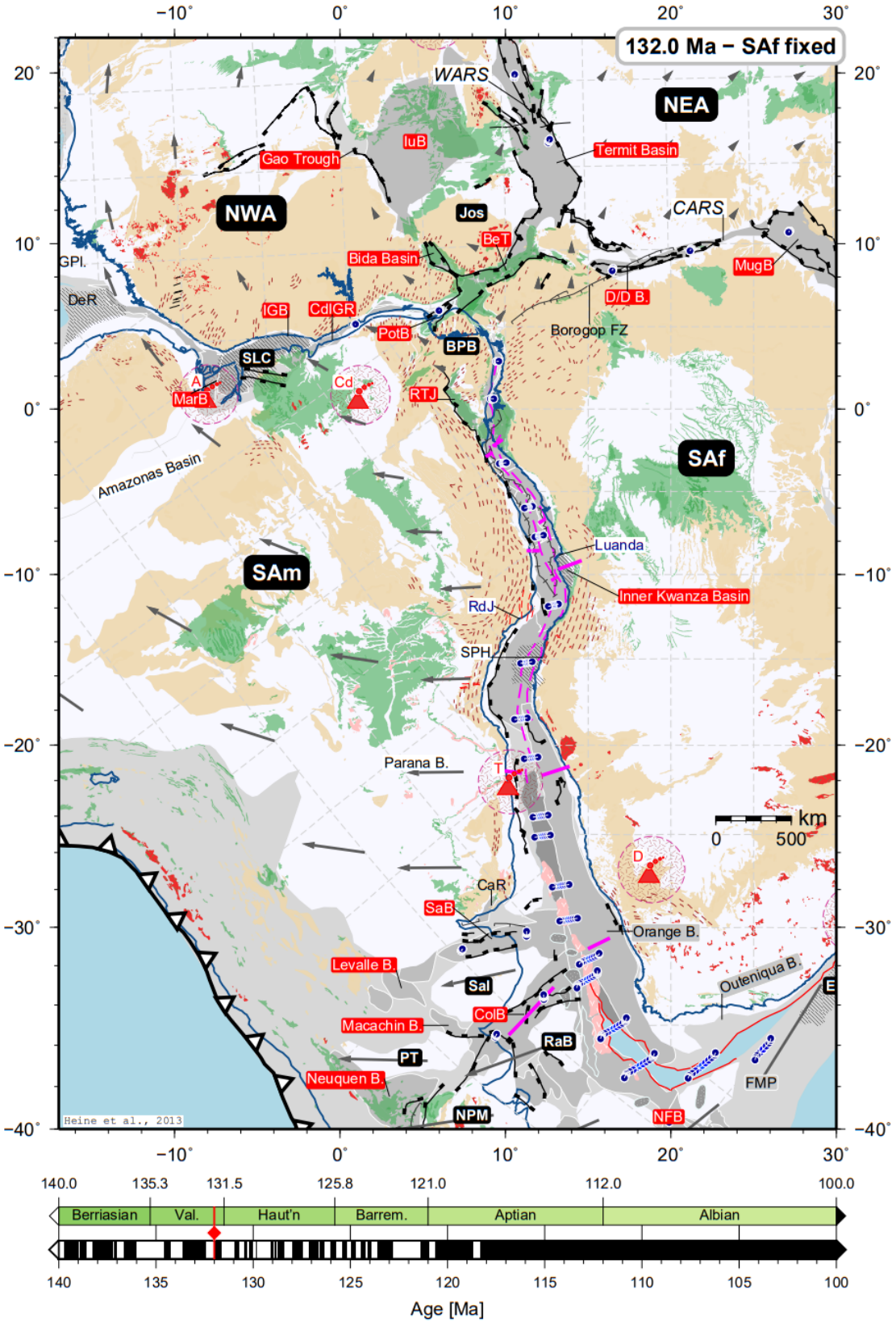


Figure 7 – Plate tectonic reconstruction at 132 Ma, with Africa fixed in present-day coordinates. Initial extension directions along the margin rotate from NW–SE in Gabon/Sergipe–Alagoas segment to W–E in Pelotas/Walvis Basin segment with increasing distance from stage pole location. Flowlines between Patagonian blocks in southern South America and southern austral Africa indicate and initial SW–NE directed motions between these plates (from Heine et al., 2013, abbreviations in there).

Topographic manifestations of continental rifting include basin subsidence and rift shoulder uplift (Weissel and Karner, 1989). The reorganization of preexisting drainage patterns (e.g., Paraíba do Sul River; Zalán and Oliveira, 2005) during the uplift of onshore features (e.g., Serra do Mar and Serra da Mantiqueira; Almeida and Carneiro, 1998), facilitates complete denudation of topographic highs and uninterrupted sedimentation in topographic lows (Vieira et al., 1994; Mohriak, 2003; França et al., 2007). This mass redistribution affects the thermal state and stress of the lithosphere, promoting strain localization (Maniatis et al., 2009). Onshore NNW-SSE fracture zones (e.g., Alegre, Calegari et al., 2016; Colatina, Belém, 2014) and NW-SE to WNW-ESE lineaments (e.g., Paranapanema, Fulfaro, 1974; Tietê, Riccomini, 1995) have influenced the emplacement of dike swarms (e.g., NNW-SSE Vitória-Colatina, Novais et al., 2004; Valente et al., 2009) and granitic intrusions (Santiago et al., 2020). The fracture zones extend offshore along the same trend and control the tectonostructural framework of the Northern Campos and Espírito Santo Basins (Figure 8; Calegari et al., 2016; Costa et al., 2024). Meanwhile, the lineaments switch to a N70E direction and directly affect the pre-salt layer in the Santos Basin (Lúcio et al., 2011).


Figure 8 – Lineaments/Fracture Zones onshore (Calegari et al., (2016), Lourenço et al., (2016) and Pedrosa-Soares et al., (2008)) and offshore (Vincentelli et al., 2016) (from Costa, 2022).

## 2.5 Santos Basin

The Santos Basin covers an area of ~350.000 km$^2$ in Southeastern Brazil with plenty of structural features (e.g., synthetic untilted step-fault blocks, hinges with asymmetric compensation grabens, homoclinal and growth faults with rollover structures, diapirs; Ojeda, 1982). The direction of extension is suggested to follow a main WNW-ESE orientation, based on seismic, structural, and potential field data (Macedo, 1989; Chang et al., 1992; Karner, 2000; Meisling et al., 2001).

The northern limit corresponds to the Cabo Frio High, a sedimentation barrier between the Santos and Campos basins (Mohriak et al., 1990b; Oreiro et al., 2008). It is an elevated portion of the basement that extends across through the continental platform and the São Paulo Plateau, related to tectonomagmatic events (Santonian to Eocene) (Mohriak and Paula, 2005). Main aspect corresponds to a transfer zone expressed by high angle faults or flower structures that displaces blocks from the Albian carbonate platform, characterizing a change in the stratigraphic and structural pattern of the Eastern Brazilian margin (Mohriak et al., 1995). The Florianópolis High designates the southern limit to the Pelotas Basin (Mohriak et al., 2010). This structure is a shallow basement anticline along the Florianópolis Platform, whereas the fracture zone consists of a ridge jump that contributed to the lithospheric mantle exhumation in that region (Gomes et al., 2008; Zalán et al., 2011). Both highs lie at the termination of major oceanic lineaments (Cainelli and Mohriak, 1998).

The western limit confines the basin to the oceanic domain and is represented by the coastal mountain ranges (Serra do Mar and Serra da Mantiqueira), uplifted during the reactivation of ancient basement faults in the Upper Cretaceous (Macedo, 1989). Parallel to the coastline, the (Santos) Cretaceous Hinge Line (Alves, 2002) separates the thick sedimentary Cretaceous deposits to the east from the thin Cenozoic sediments wedge that lie directly onto the shallow basement to the west.

The uplift promoted notable erosion and siliciclastic degradation into the basin (Macedo, 1987, 1989; Almeida and Carneiro, 1998), accommodated in the space created during Paleocene – Eocene subsidence (Moreira and Carminatti, 2004). The ocean-continent boundary has been suggested near the outer edge of the evaporites (Chang et al., 1992) or inferred from the termination of fracture zone trends and on changing directions of gravity anomaly trends (Karner, 2000).

The Cabo Frio Fault (Modica and Brush, 2004; Mohriak and Paula, 2005) presents NE-SW direction with antithetic displacement and has migrated offshore throughout its evolution into the deeper SE basin (Guerra and Underhill, 2012). In that direction, the Santos Outer High appears as a large structural high in the distal central part of the basin, following the same trend (Gomes et al., 2009). It consists of a series of segmented faulted blocks and rift shoulders uplifted and eroded in the Barremian where a transition from the initial volcanoclastic to a carbonate deposition in the Aptian occurs (Buckley et al., 2015). During rift extension, the Iracema transfer zone was generated as the Cabo Frio High remained static (Moulin et al., 2013).

The São Paulo Plateau (Kowsmann et al., 1982; Asmus, 1984) is an E-W-trending, shallow, stretched continental uplift controlled by basement structures (Mascle and Renard, 1976). It stands for the eastern boundary of the basin, where the hyperextend domain probably contains exhumed mantle and thick crustal blocks, while the eastern end would show normal thickness oceanic crust (Moreira et al., 2007; Zalán et al., 2011). To the south, the São Paulo Ridge, a volcanic chain within the submarine basement (Kumar and Gamboa, 1979; Alves, 1981) extends in the same direction.

Moulin et al. (2013) proposed a kinematic reconstruction where the Santos Basin and São Paulo Plateau formed a system that underwent oblique rifting. The existence of transtensional and strike-slip structures, an en-echelon pattern of faults and dykes onshore (Tetzner and Almeida, 2003) and offshore (Souza et al., 2007; Oreiro et al., 2008) and of the basin's depocenters (Karner, 2000; Meisling et al., 2001), points to an oblique rifting in this segment of the margin.

Lithospheric inherited NE-SW onshore features control deformation in the proximal domain, following a continental-type structural pattern, where a series of NE-SW to NNE-SSW-trending normal faults occur along with magnetic basement blocks with an E-W-trending inflexion (Stanton et al., 2014). The necking domain undergoes a structural change due to the NW-SE-trending transfer zones, characterized by oblique magnetic basement highs and lows (E-W and NW-SE) (e.g., Northern Santos Basin; Meisling et al., 2001). The South Atlantic Fracture is adjacent to the distal domain, where subparallel lineaments and transfer zones progressively inflect towards 'new' ENE and E-W trends as they approach the ocean-continent crust transition, where the influence of preexisting structures appears to diminish (Chang et al., 1992; Cainelli and Mohriak, 1998; Mohriak, 2004) (Figure 9).

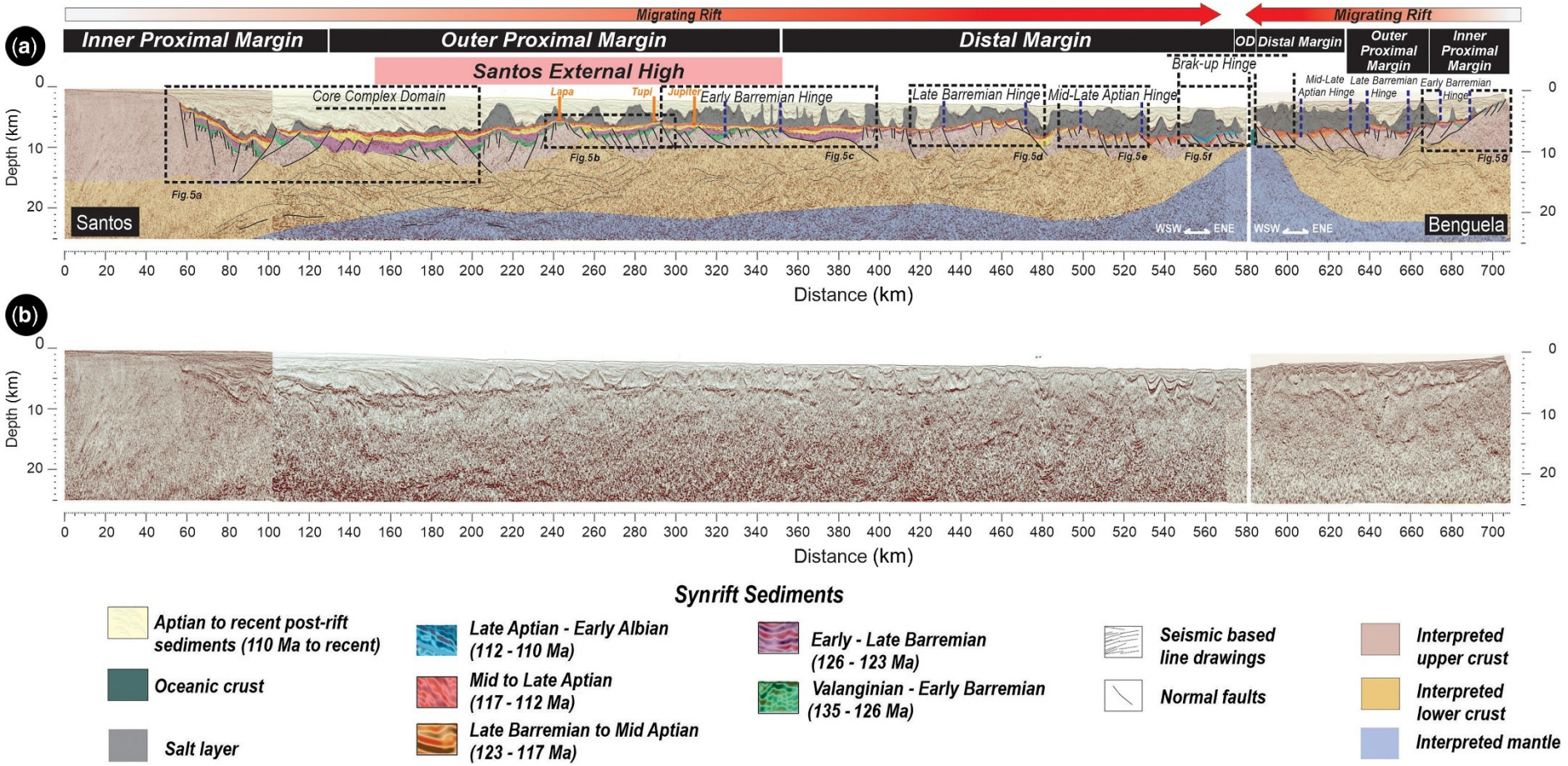


Figure 9 – (a) Interpreted and (b) uninterpreted depth-converted conjugate Santos–Benguela transect through the central portion of the Atlantic. Sections include post-rift deformation, also present in the present-day seismic records. Note that this margin is extremely asymmetric. (a) The wide margin, in the Brazilian side, shows landward-dipping normal faults, which change polarity to basinward faults after passing by a proximal dome defined by deep reflector bands buried below Early-Late Barremian and Late Barremian to Early Albian sediments. This feature is interpreted to be an extensional core complex with exhumed lower crust in its core. To its east, the upper crustal structure is defined by eastward-verging rotated blocks, with syn-rift sediments progressively younging oceanward, separated by basement hinges. In the African side, the Benguela margin is extremely narrow, but shows a similar arrangement of oceanward-younging internal compartments (from Araujo et al., 2023).

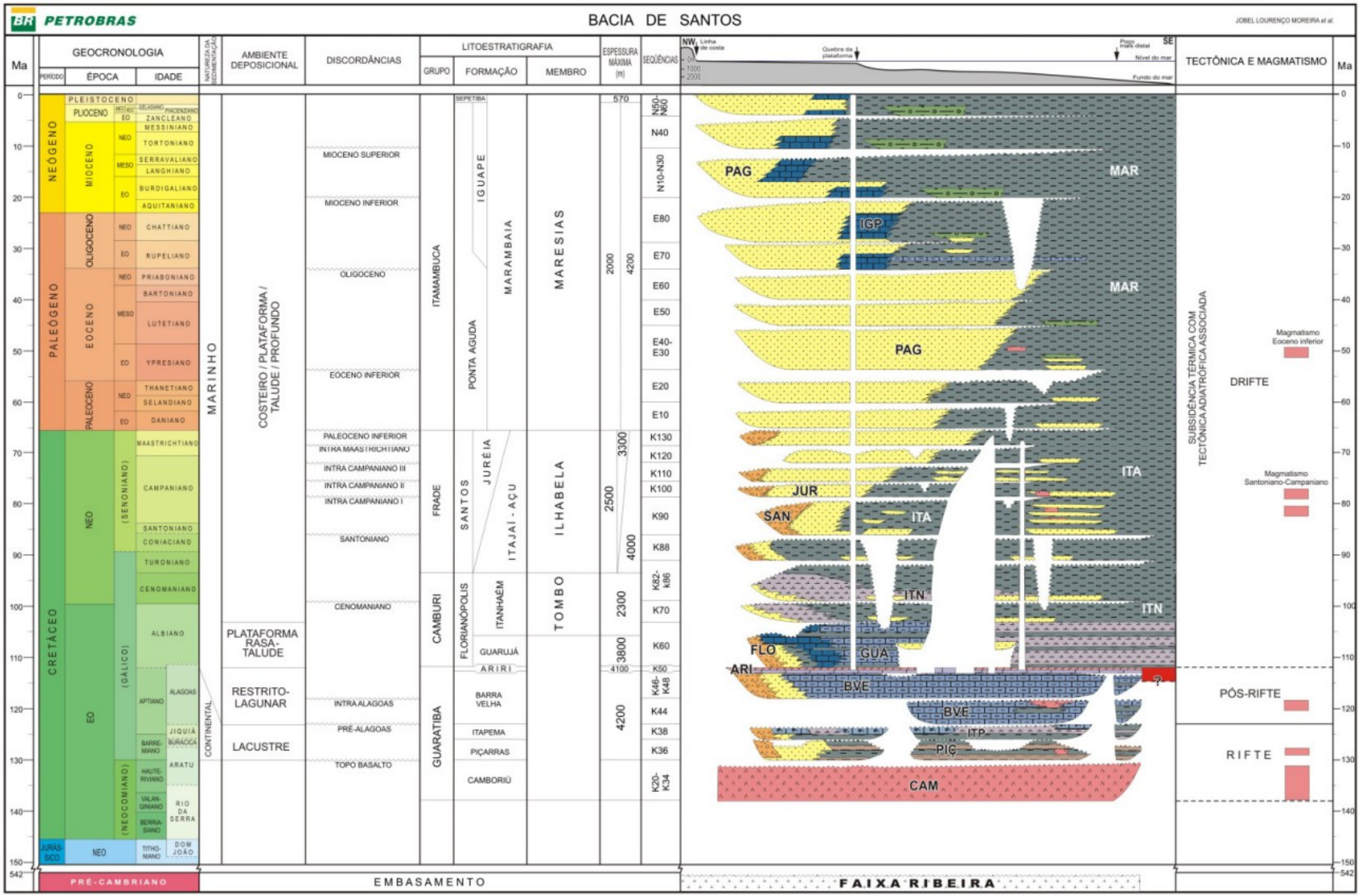


Figure 10 – Chronostratigraphic chart – Santos Basin (from Moreira et al., 2007).

The Santos Basin consists of four unconformity-bounded tectono-sedimentary megasequences (Ponte and Asmus, 1978; Chang et al., 1992): (i) continental (Late Jurassic – Early Cretaceous rift stage with fluvio-lacustrine sediments), (ii) transitional (Aptian evaporites), (iii) restricted-marine (Albian carbonates) and (iv) open-marine (Cenomanian to Present) sequences. While Pereira and Feijó (1994) described Rift, Transitional and Passive Margin phases, Moreira et al. (2007) proposed Rift, Post-rift and Drift sequences and Chang et al. (2008) presented Rift (Syn-rift I and II), Sag (Syn-rift III) and passive margin (Post-rift) phases (Figure 10).

The Precambrian granite-gneisses and metasediments of the Ribeira Belt outcrop in the São Paulo region and consist of the crystalline basement (Heilbron et al., 2000; Trouw et al., 2000; Moreira et al., 2007). The sedimentary section was deposited on a discontinuous crust formed by a mosaic of small blocks, possibly reaching the upper mantle (Hasui et al., 1975; Ferreira, 1982; Macedo, 1989).

The rift phase (Hauterivian – Aptian) comprises the sediments deposited during the Gondwana rifting process. NE-SW synthetic normal faults, with antithetic secondary systems occur with a series of half-grabens with different stretching rates accommodated by NW-SE transfer faults (Cainelli and Mohriak, 1999b; Moreira et al., 2007; Zalán et al., 2011). Three main magmatic events affected the offshore basin, at pre-rift (130 Ma), rifting (130 - 121 Ma) and post-rift phases (Fodor et al., 1984; Pereira and Feijó, 1994; Moreira et al., 2007, based on Ar/Ar method).

The economic basement is characterized by Neocomian tholeiitic basaltic flows of the Camboriú Formation related to the beginning of the structural development of the rifting of the South American and African plates (Chang et al., 2008). This phase is structurally characterized by horsts and grabens controlled by NE-SW structures, normal and regional faults (Zalán et al., 2011). Stress confinement occurred in the portion of the crust that underwent thinning, causing crustal faulting. Strain hardening conditions seemingly predominated when deformation was mostly elastic, reaching rupture under relatively high differential stresses. It led to the formation of edge faults, where thermal plumes did not exist; or uplifted zones, in regions with thermal anomalies (Chang et al., 1992; Karner and Driscoll, 1999). Strain softening processes and formation of fault systems marked by a second hinge line were a consequence of the decrease in shear strength, which conditioned the rupture of the partially thinned lithosphere, with deformation mostly in the upper crustal portions (Chang et al., 2008).

The Piçarras Formation sediments of alluvial fans (conglomerates, polymictic sandstones with basalt, quartz, and feldspar fragments) were deposited in the proximal portions. Sandstones, siltstones, and dark shales with high organic carbon of talc-stevensitic composition comprise the most distal rocks of lacustrine environment, from the initial stage until the maximum activity of the formation of the mid-grabens. Its upper boundary is marked by the Intra-Barremian unconformity (Moreira et al., 2007).

Above this, the Itapema Formation was deposited in the final stage of the asymmetric graben formation when the main faults ceased almost completely (Moreira et al., 2007). Fluctuations of the water level due to the influence of waves and currents (Castro and Azambuja, 1981) implicates on tempestites to shoreface deposits composed mainly of bivalve bioclastic rudstones and grainstones taphonomically distinct (Chinelatto et al., 2020). As this unit corresponds to the Coqueiros Formation (Campos Basin). Carvalho et al., 2000 describes that detrital coquina was deposited by alluvial fans, composed of polymictic conglomerates, lithic to feldspathic sandstones, siltstones, and red shales, whereas pure coquina is represented by lacustrine deposits of bivalve and ostracod coquinas, locally interbedded with siliciclastic facies.

The post-rift phase is a transitional phase between the rift and drift sequences, known as the Alagoas Stage (Buckley et al., 2015). The Barra Velha Formation (BVF) is marked by the Pre-Alagoas unconformity and extends to the base of the salt, transitioning from the clastic-carbonate sedimentary sequence to an evaporitic environment (Moreira et al., 2007; Chang et al., 2008; Carminatti et al., 2009). Wright and Barnett (2015) divided the BVF into two sequences: the Eoaptian Upper Rift, corresponding to the lower portion of the formation, deposited from the platform break; and the Neoaptian Sag, representing the upper section (Figure 11). The Intra-Alagoas unconformity separates the older sequence, composed of limestones, stromatolites and laminites in the proximal portions and shales in the distal portions, from the younger sequence, where limestones interbedded with shales are predominant. The proximal portions of the BVF consist of alluvial fans of sandstones and conglomerates (Moreira et al., 2007).

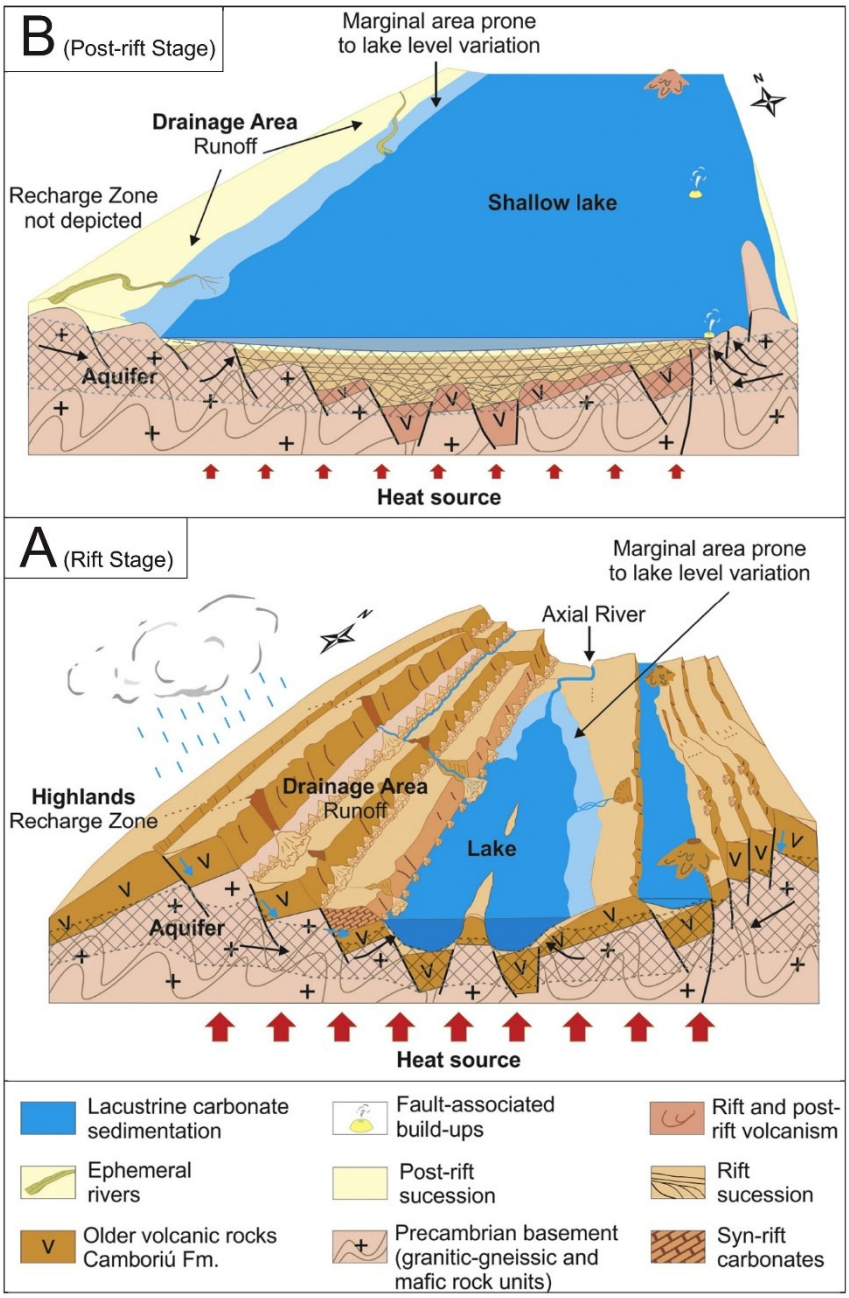


Figure 11 – Simplified conceptual model illustrating the general geology and hydrology of the pre-salt rift system. Small blue arrows show infiltration to and recharge of the aquifers; long black arrows indicate infiltration of groundwater to the lake basin. Thick red arrows underneath represent geothermal heat, which is assumed to decrease from rift to post-rift phase. Hachured areas propose the presence of aquifers relative to the lake basin, flowing mainly through fractured crystalline basement. A) Idealization of the rift phase environment, corresponding to the time of deposition of the Jiquiá sequence, where a deeper lake formed, which could eventually be subjected to water-column stratification. B) Idealization of the post-rift phase environment, at the time of deposition of the Alagoas (Barra Velha) sequence, where a shallower, endorheic lake with a large areal coverage evolved. Illustrations are not to scale (from Pietzsch et al., 2018).

The sag phase represented the evolution of the strain softening process into lithospheric rifting, with the development of a broad, laterally continuous, sag-like depression, characterized by a transitional environment from continental to shallow marine (Chang et al., 2008). Although a period of tectonic quiescence is used to

describe the sag phase, the more distal parts of the rift remained locally active, generating normal faulting activities (Karner and Gamboa, 2007). The reactivation of the pre-existing faults propagates to the base of the evaporites, indicating that extensional deformation happened until the Upper Aptian (Faria et al., 2017).

A series of interconnected lake basins were developed in an extensive system of half-grabens and their periodic isolation originated fluvio-deltaic and lacustrine carbonates with little to no influence from marine water (Braccini et al., 1997; Harris, 2000; Gomes et al., 2009). Marine incursions crossed the São Paulo Ridge from the south at times and the increased evaporation rate relative to the water influx (Mio et al., 2005) resulted in the deposition of thick and widespread neoaptian evaporite deposits of the Ariri Formation (Moreira et al., 2007; Mohriak et al., 2012). Rocks deposited during this stage are characteristic of shallow-water environments or hypersaline epicontinental sea conditioned by the prevalent dry climate (Dias, 2005; Chang et al., 2008).

Although the high mobility of halite would turn the estimated time of evaporites accumulation rate imprecise, the presence of more soluble salts (e.g., tachyhydrite, carnallite) (Moreira et al., 2007) allowed an estimation of 600 m.y. for the deposition of about 2 km of thick evaporitic package (Dias, 2008). This anomalously high subsidence rate, even considering the isostatic effect of the added weight, implies that rifting would also have to act in order to create the deep depression in which the salt deposited. The width of the rift was much larger in the south (700 km in the Santos Basin) than in the north (200 km in Sergipe-Gabon segment) by the time salt deposition started (~113 Ma) (Szatmari and Milani, 2016).

During the drift phase, thermal subsidence dominated over other tectonic processes, allowing the development of a second basin with sag geometry due to normal fault activity reduction (Gamboa et al., 2008; Milani et al., 2007). The deepening of the basin facilitated the establishment of a fully developed ocean once the volcanic and structural obstacles were overcome in the Neoalbian (Azevedo, 2004; Gamboa et al., 2008; Mohriak et al., 2012). Extensive marine carbonate deposits, followed by siliciclastic sediments from the Camburi, Frade and Itamambuca groups were deposited (Moreira et al., 2007). The end of the evaporitic basin resulted from the transition from continental to oceanic crust (Mohriak, 2003) and separation of the South American and African plates (Riccomini et al., 2012).

## 2.6 Depositional environments

Present-day rift lakes (e.g., Great Salt, Jones et al., 2009; Pyramid, Henry et al. 2007; and Mono, Whiticar and Suess, 1998) may provide a better understanding of depositional and spatial models of carbonates in continental rift settings to produce predictive tools for subsurface exploration of lacustrine and spring-related carbonate reservoirs (Harris et al., 2013). For the Itapema Formation, the best potential correlatives are the hypersaline marine environment of Shark Bay in Australia and Lake Tanganyika of the East African rifted lake complex (Thompson et al., 2015), presenting still noticeable difference in water chemistry, salinity and shell types and size.

The pre-salt deposits of the sag phase were initially attributed to microbial-influenced processes, i.e., microbial stromatolites, laminites, and microbialites rich in ‘talc’’ and Mg-clays (Dias, 2005; Moreira et al., 2007; Carminatti et al., 2008; Terra et al., 2010, Muniz and Bosence, 2015; Mercedes-Martín et al., 2016, Sabato Ceraldi and Green, 2016). Microbialites are mentioned as constituent facies of the Barra Velha Formation (Moreira et al., 2007; Carminatti et al., 2008, 2009) and the stromatolites and spherulites from the Brazilian basins follow this classification (Terra et al., 2010). However, the carbonates of the BVF are stated to be partially microbial (Muniz and Bosence, 2015), mentioned to contain a hybrid origin with abiotic predominance for the pre-salt carbonates (Lima and De Ros, 2019). Although the Kwanza Basin contains facies identified as microbial in origin (Saller et al.2016; Sabato Ceraldi and Green 2016), on the Brazilian margin the consensus is that they are largely of abiotic origin and were precipitated by chemical-driven processes (Wright and Barnett, 2015, 2017; Pietzsch et al., 2018, 2020).

Microbial influence is virtually ruled out since macro and microscopic evidence of microbial activity is rare in these carbonates and absent in the BVF (Wright and Barnett, 2015). The abiotic models (Wright and Barnett, 2015; Herlinger et al., 2017; Farias et al., 2019; Gomes et al., 2020) also emphasize that alkaline waters with pH as high as 10-10.5 (Tutolo and Tosca, 2018) where stevensite represents a source of elements for dolomite and silica precipitation (Wright and Barnett, 2015; Farias et al., 2019) reduces the bioavailability for cyanobacteria. Recent interpretations for the Macabu Formation, correlating to the BVF, indicate the deposits are chemical precipitates controlled by geochemistry of the waters (Herlinger et al., 2017).

The BVF and its correlations in other basins have been attributed to a set of depositional environments, from marine (Dias, 2005) to transitional i.e., continental to marine (Moreira et al., 2007; Carminatti et al., 2008; Gomes et al., 2009). However, the absence of marine fossils (e.g., miliolid foraminifera) and early sulphate minerals (gypsum, anhydrite) along the presence of ostracods with a wide salinity tolerance excludes a marine influence on the deposits of this formation (Wright and Barnett, 2015; Muniz and Bosence, 2015; Tedeschi, 2017; Pietzsch et al., 2018).

A lacustrine carbonate platform deposition model (Buckley et al., 2015; Faria et al., 2017) is also controversial based on seismic, isotopic and petrographic data, as the seismic geometries are acquisition artefacts for some authors (cf. Wright and Barnett, 2017). $^{86}Sr/^{87}Sr$ data supports the idea of a lacustrine depositional environment that would have evolved completely disconnected from the sea for a long time (Tedeschi, 2017), along (hyper)alkaline waters (e.g., Wright and Barnett, 2015, 2017, 2020; Herlinger et al., 2017; Lima and De Ros, 2019; Pietzsch et al., 2020; Carramal et al., 2022). Lacustrine carbonate environments are extremely dynamic and sensitive systems where low and high frequency changes in climate, water chemistry, and bathymetry lead to significant changes of litho- and biofacies and their patterns of distribution both horizontally and vertically (Flügel and Munnecke, 2010). Biogenic mediated sedimentation, abiotic-chemical precipitation, variable carbonate clastic input and eolian supply control a complex interaction of depositional processes managed by environmental fluctuations (Gierlowski-Kordesch, 2010).

# 3 MATERIAL AND METHODS

## 3.1 Structural restoration to evaluate rift evolution

Structural restoration seeks to revert the deformation interpreted in the present to a less deformed condition of the past (Wickham and Moeckel, 1997). Its application allows quantification of the intensity of deformation in geological units and evaluation of the viability of an interpretation or models taken as reference (e.g., Durand-Riard et al., 2010; Masini et al., 2011; Fiduk and Rowan, 2012; Giles and Rowan, 2012). A structure may be incoherent or geologically impossible if a restored section does not exhibit a good fit of the structural elements under geometric conservation conditions (Dahlstrom, 1969).

A balanced section must fit the available data and the recognized geometries in place or in analogous areas and may also be reconstructed into a pre-deformational geometry in which the balancing is based on some defined property (e.g., layer length or area; Dahlstrom, 1969; Elliott, 1983). When tectonic transport is three-dimensionally complex, the application of the assumptions related to conservation of matter loses its meaning, since its principal direction is parallel to the section (Hossack, 1979).

Section restoration has established itself as a standard tool in petroleum exploration, which has gradually incorporated more complex methods for restoration and quantification of deformation (e.g., Hossack, 1979; Woodward et al., 1986; Schultz-Ela, 1992; Wickham and Moeckel, 1997). Theoretical models of subsidence on passive margins and aulacogens could be correlated with stretching using analytical predictive capability in restoration (Gibbs, 1984).

The restoration of sedimentary horizons with preservation of local areas, thicknesses, and volume, as if they were multiple sections in synchrony along the main direction of tectonic transport, allowed the evolution of restoration from sections to surfaces (Massot, 2002; Galera et al., 2003). Thus, structural restoration techniques have evolved from investigating sections (2D), maps (surfaces), to volumes (3D) (Titeux, 2009). The RECON package (PETROBRAS/TECGRAF-PUCRJ) has been used in several studies (e.g., Santi, 2002; Fetter, 2009; Melo Garcia, 2012; Carvalho, 2023) and is one tool along the Move Suite (PE Limited) (Figure 12).

The replacement of traditional geometric techniques by computational and vectorial treatment of geomechanical concepts marked the evolution towards volumetric restoration, which is truly considered 3D (e.g., Santi et al., 2002; Maerten and Maerten, 2006; Moretti et al., 2006; Moretti, 2008). 3D techniques can be robust and predictive for small-scale structures (e.g., faults and fractures), enhancing the representation of petroleum reservoirs (Maerten, 2007). Currently, they are applied as exploration advances into more complex and difficult-to-characterize areas, such as the pre-salt of the Brazilian margin, with a focus on identifying structural features that can influence fluid flow.

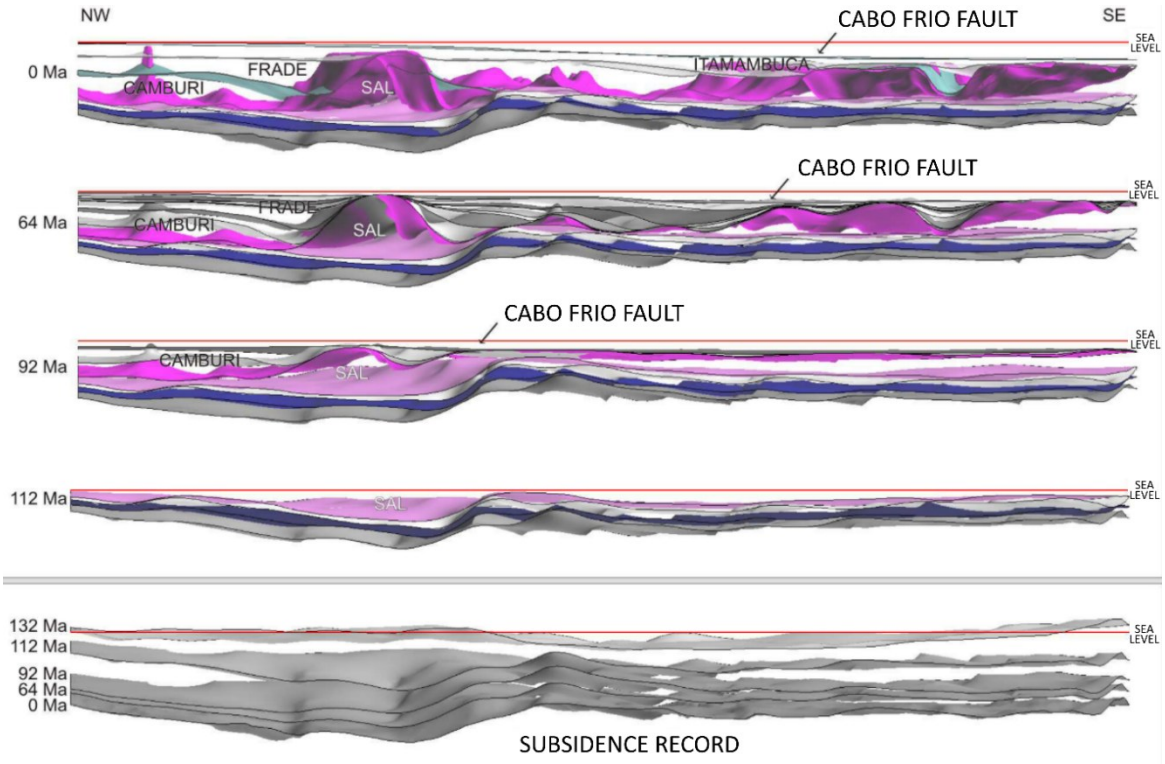


Figure 12 – Restoration palinspastic sequence for 0, 64, 92 and 112 Ma ago. The basement restored subsidence is superimposed from the past to the present day in the lower part of the figure (modified from Melo-Garcia, 2012).

Kinematic methods, which aim to represent how the geometry of a structure evolves according to the propagation of deformation, reach their limits in providing this type of information. Thus, while geometric results validate kinematics, geomechanical methods are designed to replicate the mechanics of the deformation process by identifying the history of stresses and strains that the study area has been subjected to (Caumon and Muron, 2006; Fossen, 2010). Kinematic models, however, are still needed in the representation of geologic deformation to coherently reconstruct the evolution of structures in time and space (Groshong, 2006).

Thus, modeling is performed in reverse, progressively and iteratively removing deformation, reconstructing shape and position (geometry and kinematics), and analyzing probable imposed natural stresses (dynamic origin). The area and length methods demonstrate the evolution of the geometry from the deformed to the pre-deformed state, without specifying the intermediate steps. As compaction processes occur, either tectonically, as shortening of parallel layers, or as a result of burial, the assumption that layer thickness and area remain constant during deformation is questioned (Mitra, 1994; Sans et al., 1999; Roure et al., 2005). In addition, non-competent rocks, which can flow according to viscous (e.g., salt) or plastic-viscous laws (e.g., shales) can impact these assumptions (Weijermars et al., 1993).

Backstripping, a form of isostatic restoration, is employed to describe the subsidence history of a basin. This process involves systematically removing sedimentary sequences and corresponding isostatic adjustments (Figure 13). While one-dimensional backstripping adheres to the Airy model of isostasy, the two- and three-dimensional counterparts consider lateral variations in load influence, applying flexural isostasy (Fossen, 2010).

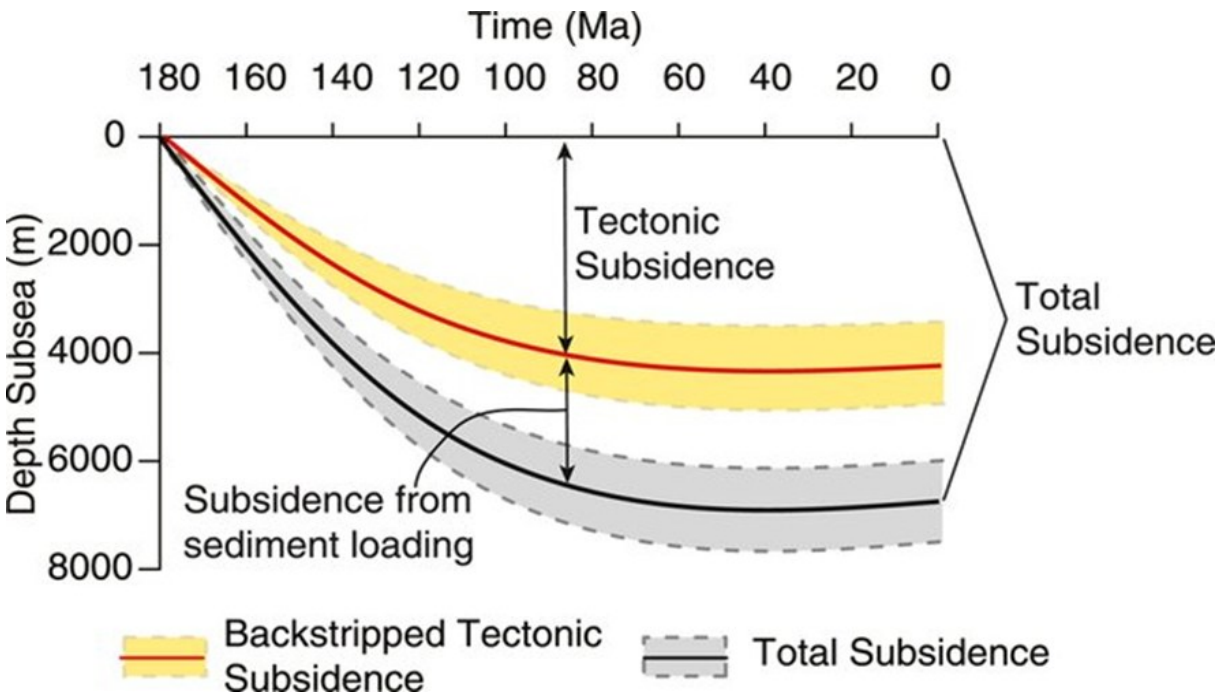


Figure 13 – Conceptual geohistory representation of backstripped tectonic subsidence (red/yellow) and total basin subsidence (black/gray curve). The component of subsidence due to sedimentary loading is the difference between the tectonic subsidence and total subsidence curves (from VanderLeest et al. (2022), after Van Hinte, 1978). Uncertainty bands represent the range of calculated subsidence values for the range of paleo sea-depth estimates.

The orientation of the restored sections should be taken into consideration, since it requires alignment with the direction of tectonic transport and insurance of flat deformation (Elliott, 1983; Woodcock and Fischer, 1986). In the pre-salt geological context, the orientation of fractures is often influenced by the structural setting, and their prevalence is intricately linked to their proximity to fault zones (Wennberg et al., 2021). The faults in the Iracema High follow three main orientations: NE-SW (predominant in the Tupi High), N–S and NW-SE (Adriano et al., 2022). Sections parallel to faults serve the purpose of connecting others and simplifying map construction.

A conventional active petroleum system comprises the synchronous existence and operation of four elements (mature source rocks, reservoir rocks, sealing rocks, and traps) and two time-dependent geological processes (migration and synchronism) (Magoon and Dow, 1994; Milani et al., 2000). Geochemical modeling (Chang et al., 2008) indicates that hydrocarbon generation in the continental shelf and slope area peaked between the Campanian and Maastrichtian (70-90 Ma). Additionally, there is a remarkable change in position through time of the post-salt structures in connection with the pre-salt structures (Guerra and Underhill, 2012).

The pre-salt section in the Santos Basin consists of organic-rich lacustrine shales of the Piçarras and Itapema formations as source rocks. The reservoirs are carbonate, composed of microbialites, stromatolites, and coquinas, from the Barra Velha and Itapema formations, respectively (Moreira et al., 2007). The beginning of the rift phase generated the main traps (basement structural highs) and the migration conduits (faults) from which the oil percolated (Papaterra, 2010). The seal consists of the evaporitic package of the Ariri Formation, which is up to 2,000 m thick, where heat is transferred from the top of the reservoirs to shallower portions, delaying the thermal cracking of hydrocarbons at great depths in the basin (Mello et al., 1995). Table 1 summarizes these units in the pre-salt, including the Camboriú Formation, tholeiitic basaltic flows often considered part of the economic basement (Chang et al., 2008) and discriminated here for the section restoration. Although Alkmim et al. (2025) present new depositional ages for the Barra Velha and Itapema formations, these are not suitable for application here since it is necessary to have that information for all the stratigraphic units involved.

| Evolutionary phase | Package | Age | Stratigraphic units |
|---|---|---|---|
| Drift | **Post-salt** | 112 Ma - | Camburi Gr. |
| Post-rift | **Salt** | 113 – 112 Ma | Ariri Fm. |
| | **Sag** | 117 – 113 Ma | Upper Barra Velha Fm. |
| Rift | **Rift II** | 130 – 117 Ma | Lower Barra Velha, Itapema and Piçarras Fms. |
| | **Rift I** | 137 – 130 Ma | Camboriú Fm. |

Table 1 – Definition of packages for seismic interpretation in this example, based on evolutionary phases, and age of stratigraphic units after Moreira et al. (2007), Buckley et al. (2015), Barnett et al. (2018) and Farias et al. (2019). The water column and basement are light blue and red in the models, respectively.

Interpretation of the section being restored is essential for defining parameters used in the software and tools, considering both structures and chronostratigraphic information (Figure 14). In this case, seismic profiles are selected following previous criteria, since they satisfactorily allow interpreters to understand the properties of rocks in subsurface and, therefore, classify them. Faults are the main structures observed, mostly recognizable once seismic horizons are discontinuous. These features can even disappear in a section, indicating a change in the geological record, mainly by erosion or a hiatus. If a reasonable number of horizons and faults in profiles are interpreted, isopach maps can be interpolated for each horizon, along with fault distribution in the area and trend analysis.

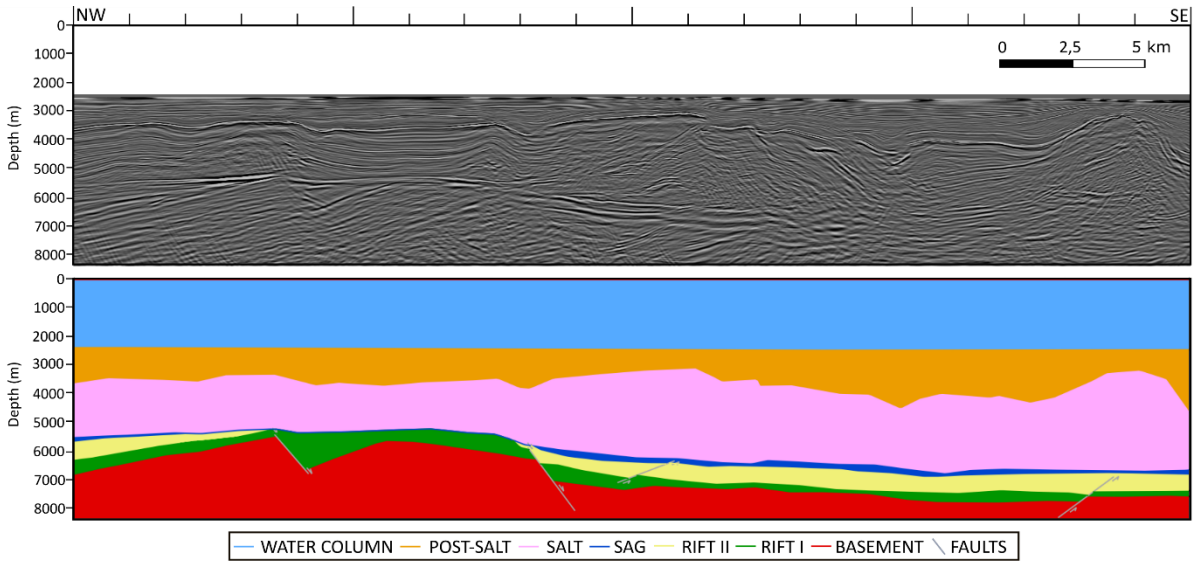


Figure 14 – Non-interpreted and interpreted profile for the Tupi High in the Santos Basin in different packages.

The first step to a simple-shear restoration is selecting the reference horizon to be flattened. The definition of the individual elements to be displaced works on the assumption that, in this technique, small-scale deformation is irrelevant. Thus, it can be treated as ductile deformation, where the continuity of the layer is preserved, and is below the resolution of the study section (Fossen, 2010). Restoration of the cross section by shifting the elements vertically until the reference horizon is horizontal also assumes that the fault geometry does not change during deformation. Fault displacement can then be removed by translation parallel to the regional along with the displacement parallel to the shear direction (Groshong, 2006).

Discrepancies may arise from minor imperfections in the cross section, an inaccurate selection of the shear angle, or the inadequacy of the simple-shear model in precisely capturing the deformation mechanism. It is anticipated that minor variations may occur even with an accurate cross section. The optimal shear angle for restoration is typically determined through a process of trial and error (Rowan and Kligfield, 1989).

The restoration of the Pre-salt interval operates independently of the deformation occurring in the overlying units. This decoupling of deformation is attributed to the plastic behavior exhibited by the salt interval (Hudec and Jackson, 2007), which undergoes deformation along with the overlying post-salt strata without necessarily inducing deformation in the pre-salt layer. Salt is subject to dissolution losses that become difficult to estimate, and even area conservation is not considered by most authors (e.g., Rowan, 1993). Although the viscosity of the salt exerts strong control over the rate and style of halokinetic deformation, where the interaction with the overburden is relatively more ductile at the beginning and more brittle at the end, salt is assumed to be homogeneous or uniform in time and space in most models (e.g., Vendeville and Jackson, 1993). The workflow for structural restoration in the NW-SE section in the Tupi field is represented in Figure 15, following the steps from Carvalho et al. (2024).

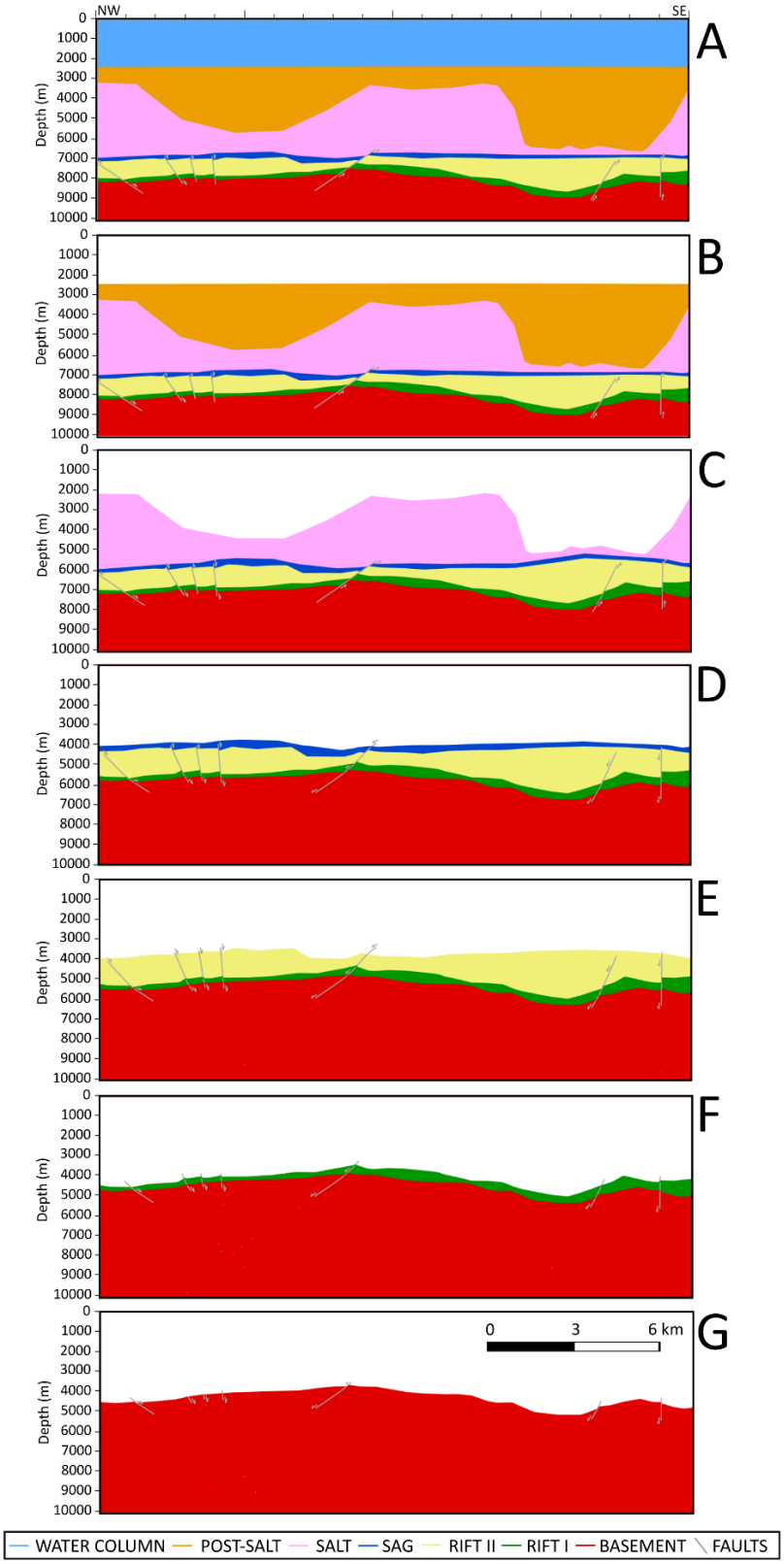


Figure 15 – Structural restoration performed on MOVE for the entire pre-salt layer. The workflow consists of (A) digitalization of horizons and faults of interest; (B) removal of the water column; (C) decompaction of the post-salt interval; (D) decompaction of the salt layer and fault restoration in the SAG interval; (E) decompaction of the SAG interval and fault restoration in the rift II interval; (F) decompaction of the rift II interval and fault restoration in the rift I interval; (G) decompaction of the rift I interval. During the restoration, data such as layer-parallel shortening (LPS), average vertical thickness and sediment rate are obtained.

All the faults are restored by moving the modules to join beds, respecting the interpreted offsets, using the simple-shear process on the fault entity (e.g., Carvalho, 2023). Table 2 lists some of the parameters defined for structural restoration. Default values are mostly applied for isostatic parameters.

| **Parameters** | **Packages** | | | | |
|---|---|---|---|---|---|
| | **Post-Salt** | **Salt** | **Sag** | **Rift II** | **Rift I** |
| **Porosity** | 0.56 | 0.00 | 0.41 | 0.56 | 0.50 |
| **Depth Coefficient ($km^{-1}$)** | 0.39 | - | 0.40 | 0.39 | 0.05 |
| **Density ($g/cm^3$)** | 2.68 | 2.20 | 2.71 | 2.68 | 2.85 |
| **Young Modulus (Mpa)** | 23750 | 5810 | 45000 | 23750 | 25000 |
| **Poisson Ratio** | 0.3 | 0.4 | 0.22 | 0.3 | 0.3 |

Table 2 – Parameters for structural restoration applied to each package in the Santos Basin. Porosity of a rock is a measure of its ability to hold a fluid, where 1 is the highest value. Depth Coefficient indicates how much the porosity diminishes per km. Density in rocks is a function of the densities of the individual grains, the porosity, and the fluid filling the pores. Young's modulus measures the ability of a material to withstand changes in length when under lengthwise tension or compression. Poisson's ratio measures the deformation in the material in a direction perpendicular to the direction of the applied force.

### 3.1.1 Iracema region

In the study area, restoration was performed in different stratigraphic units (Table 3), following the same parameters for Table 4 as those presented before. In Figure 16, the surface of the Upper Barra Velha Formation was restored for further analysis.

| **Evolutionary phase** | **Age** | **Stratigraphic units** |
|---|---|---|
| Drift | 112 Ma - | Camburi, Frade and Itamambuca Groups (Post-salt) |
| Post-rift | 113 – 112 Ma | Ariri Formation (Salt) |
| | 117 – 113 Ma | Upper Barra Velha Formation |
| Rift | 123 – 117 Ma | Lower Barra Velha Formation |
| | 126 – 123 Ma | Itapema Formation |
| | 130 – 126 Ma | Piçarras Formation |
| | 137 – 130 Ma | **Camboriú Formation*** |

Table 3 – Evolutionary phases and age of stratigraphic units after Moreira et al. (2007), Buckley et al. (2015), Barnett et al. (2018) and Farias et al. (2019) used for seismic interpretation in Iracema. The Camboriú Formation here is not separated from the crystalline basement and, therefore, not included in the restoration.

| Parameters | Stratigraphic units | | | | | |
|---|---|---|---|---|---|---|
| | Post-Salt | Salt | Upper Barra Velha | Lower Barra Velha | Itapema | Piçarras |
| **Porosity** | 0.56 | 0.00 | 0.41 | | | 0.56 |
| **Depth Coefficient ($km^{-1}$)** | 0.39 | - | 0.40 | | | 0.39 |
| **Density ($g/cm^3$)** | 2.68 | 2.20 | 2.71 | | | 2.68 |
| **Young Modulus (Mpa)** | 23750 | 5810 | 45000 | | | 23750 |
| **Poisson Ratio** | 0.3 | 0.4 | 0.22 | | | 0.3 |

Table 4 – Parameters for structural restoration applied to each stratigraphic unit in Iracema.

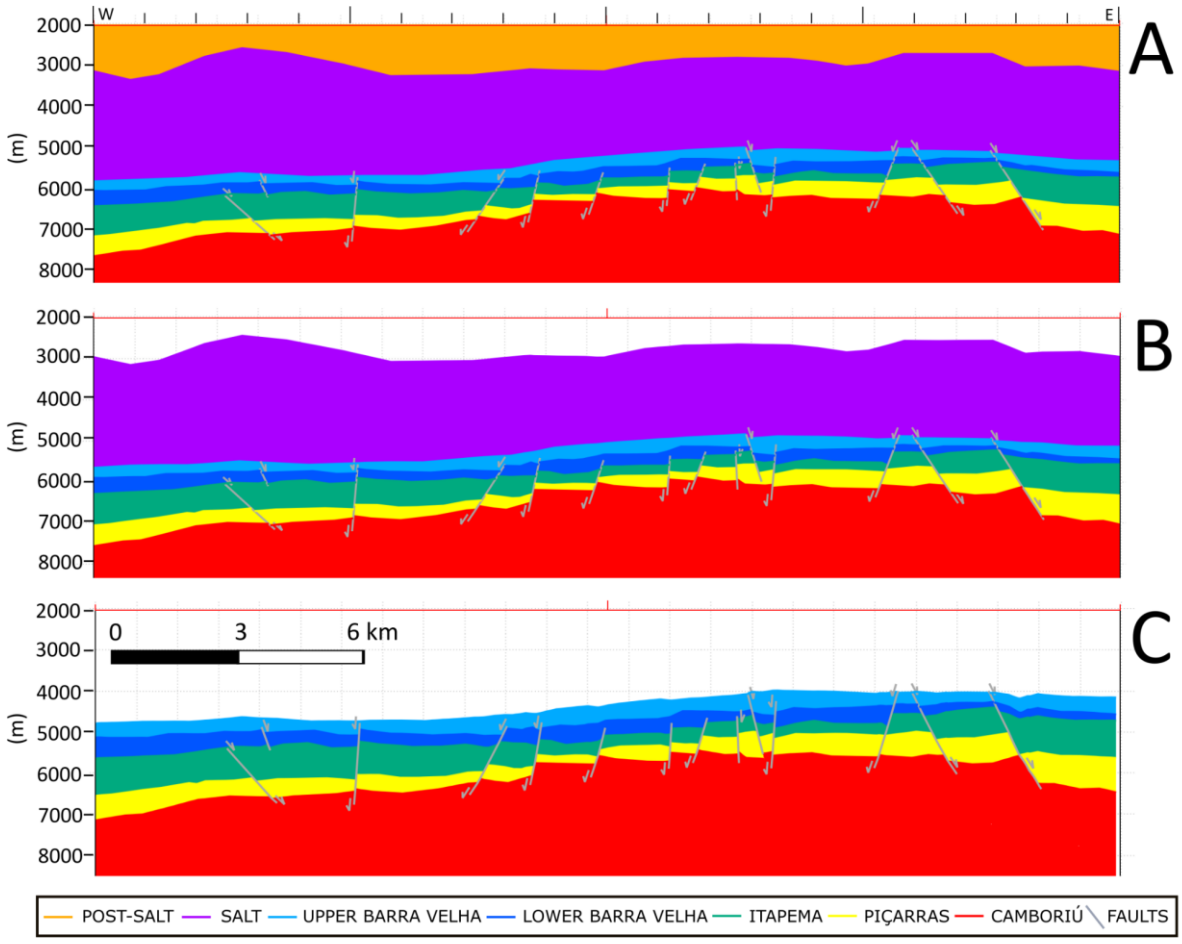


Figure 16 – Original interpretation in (A), with decompaction of the post-salt layer in (B), followed by decompaction of the salt layer and section restoration for the Upper Barra Velha Formation in (C).

## 3.2 Diagenetic processes and isotopic applications

A set of physical, chemical, and biological processes operating under relatively low temperature and pressure to convert sediments into sedimentary rocks and subsequently alter them defines the term diagenesis (Tucker and Dias-Brito, 2017). It is referred to as early diagenesis if it occurs right after deposition of particles or is associated with this process and, if it occurs after deposition, it is called late diagenesis. Water chemistry, particularly the Mg/Ca ratio, and temperature control primary mineralogy which has implications for diagenesis and secondary porosity development (Della Porta, 2015).

Post-depositional processes (e.g., dolomite cementation, dolomitization, silicification and dissolution) play a crucial role in determining the final porosity, since they can enlarge, modify, or destroy it (Basso et al., 2020). Dissolution occurs when pore fluids are subsaturated relative to the carbonate mineralogy and the secondary porosity it generates can give rise to great reservoirs (Tucker and Dias-Brito, 2017). The matrix dissolution associated with facies dominated by crystal shrubs with preserved and/or enhanced growth framework porosity and reworked spherulites/intraclasts that presented the best reservoir characteristics (Basso et al., 2022).

In fact, the depositional environment and the associated diagenetic alterations condition the reservoir quality in the Campos and Santos basins, where most of the porosity is of secondary origin (Herlinger et al., 2017). Diagenetic processes impacting on the evolution of porosity and permeability may be associated with the flow of hydrothermal fluids in some locations of the basin (Lima and De Ros, 2019; Lima et al., 2020, Sartorato et al., 2020).

Diagenesis in the Barra Velha Formation starts with an initial stage of dissolution, which occurs alongside or is followed by the precipitation of early diagenetic products dominated by either dolomite, calcite, or silica cementation (Lawson et al., 2022). Subsequently, saddle dolomite, equant calcite, and/or mega quartz precipitate, sometimes simultaneously with minerals such as metal sulfides, dawsonite, and APS, indicators of high temperature diagenesis or direct precipitation from hydrothermal fluids (Dill, 2001).

Early diagenesis is mainly related to the dissolution of Mg-clay substrates and its replacement by calcite spherulites, dolomite and silica on the evolution of the deposits (Wright and Barnett, 2015, 2020; Herlinger et al., 2017; Farias et al., 2019; Lima and De Ros, 2019). In the pre-salt succession, kerolite i.e., hydrated form of talc and stevensite are predominant (Sabato Ceraldi and Green, 2016). Stevensite is an authigenic clay mineral indicative of magnesium-rich waters, which has been reported in modern and ancient marine and lacustrine settings, commonly associated with alkaline evaporitic conditions, magmatism, hydrothermal action, and/or microbial metabolism (e.g., Tosca et al., 2011; Calvo and Pozo, 2015; Pozo and Calvo, 2018). Reorganization of basinal fluids and/or amplified thermal energy are reported to have destabilized stevensite in late diagenesis for dolomite precipitation (e.g., Tosca and Wright, 2018).

Stevensite plays a prominent role in comprehending the processes of the BVF and its correlations (Sabato Ceraldi and Green, 2016; Saller et al., 2016). Its presence or dissolution is an imperative detail for determining the permo-porous quality of the reservoirs. It is believed that the pre-salt lacustrine environments of the Santos and Campos basins showed high alkalinity, high concentrations of Mg/Si and low $pCO_2$ given the extensive occurrence of stevensite (Tosca and Masterson, 2014). The supply of abundant dissolved Ca, Mg and $SiO_2$ from recurrent basalt floods and hydrothermal activity in the rift allowed the deposition of authigenic Mg-rich clays and non-marine carbonates in shallow water depths (Gierlowski-Kordesch, 2010; Della Porta, 2015). The continuous contribution of Ca into the evaporating brines during salt deposition resulted in thick tachyhydrite layers at the end of considerable evaporite cycles (Leite et al., 2020).

The effects of temperature changes in response to cooling of hydrothermal fluids can also significantly impact the massive silica precipitation in the Pre-salt lakes (Alvarenga et al., 2016). Density differences can be triggered by a subsurface hydrothermal cell circulation relatable to the rift-sag tectonic scenarios. Since leakage to underlying aquifers can occur in topographically closed lakes with insufficient hydraulic pressure gradients during low-stand periods, Mercedes-Martín et al. (2019) conclude that such mechanisms have played a crucial but underestimated role in the chemical evolution of the Pre-salt alkaline lakes.

The rate of alterations in carbonate compositions is influenced by several factors, including the elemental concentration ratio between carbonate and fluid, the distinction between open- and closed-system behavior, porosity, and distribution coefficients identified in earlier modeling studies on water-rock interaction (Banner et al., 1988; Banner and Hanson, 1990; Wang and Cerling, 1994; Maliva, 1998). Parameters such as recrystallization rate and groundwater discharge rate are also parameterized and found to be significant contributors to the alterations in carbonate compositions (Zhao et al., 2020). From a practical perspective, the groundwater discharge rate in the reactive transport model is linked to the concept of open vs. closed system behavior in the water-rock interaction model, where a high groundwater discharge rate corresponds to 'open systems,' and vice versa.

Carbonates deposited in lacustrine environments, typically freshwater, exhibit wide isotopic variation. This variation depends primarily on the isotopic composition of rainfall in the watershed area, its quantity and seasonality, temperature, evaporation rate, relative humidity, and biological productivity (Farias, 2018). However, several natural environments and experimental studies have demonstrated that significant deviations in fractionation, predicted from equilibrium conditions, occur as the rate of mineral precipitation and influence of $CO_2$ degassing in solutions enriched in this gas, as well as solution pH, affects the carbonic species dissolved (Beck et al., 2005; Kele et al., 2011; Watkins et al., 2013, 2014).

The $\delta^{18}O$ and $\delta^{13}C$ of lacustrine biogenic carbonates depend on the isotopic composition of the sources of oxygen i.e., water and carbon i.e., dissolved inorganic carbon (DIC), respectively. DIC presents a cyclical record in the carbonates and the hypotheses to explain its primary source contemplate contemporaneous magmatism and volcanism in the basin and its variability in response to lake water dynamics due to lake level oscillation or to atmospheric $pCO_2$ change (Pietzsch et al., 2020). Interpretations of lacustrine $\delta^{18}O$ and $\delta^{13}C$ signals obtained from bulk material can be compromised if the occurrence of diagenetic carbonates (e.g., dolomite, siderite) coexisting with primary surface water precipitates (e.g., aragonite, calcite) is not recognized (Lacey et al., 2015; McCormack et al., 2018). The correlation between $\delta^{18}O$ and $\delta^{13}C$ is increased and their values lowered once the isotopes are homogenized from some diagenetic processes such as meteoric exposure (e.g., Christ et al., 2018). High isotopic values from both isotopes may indicate a minor diagenetic alteration,

once $\delta^{18}O$ values tend to decrease due to diagenesis (Lima and De Ros, 2019), and it can also suggest evaporitic conditions (Talbot, 1990; Farias et al., 2019).

Talbot (1990) provided a summary of the primary environmental influences on covariance trends in lakes of diverse morphologies and geographical locations, outlining the following key points: (i) Increasing evaporation or residence time leads to a positive evolution in $\delta^{18}O$ isotopic values; (ii) Higher latitude, altitude, or continentality shifts the origin towards more negative $\delta^{18}O$ values; (iii) Short residence times and abundant vegetation favor more negative $\delta^{13}C$ values; (iv) Lakes with drier impoundments exhibit a tendency to covary with more positive values for $\delta^{13}C$; (v) The primary production of organic matter and the release of carbon into the atmosphere, attributed to the rising rate of water evaporation, contribute to more positive values of $\delta^{13}C$ (Talbot and Kelts, 1990).

Moreover, other isotopes are fundamental for the pre-salt study. The application of the isotopic ratio of $^{87}Sr/^{86}Sr$ technique should be integrated with additional information and data (e.g., petrographic and elemental geochemical) and considered in the context of the regional and local geological environment. The $^{87}Sr/^{86}Sr$ ratios of marine carbonates from the Phanerozoic era are distinctly determined by the data presented by Peterman et al (1970). In contrast, non-marine carbonates exhibit $^{87}Sr/^{86}Sr$ ratios that reflect the origin of the strontium, allowing for values within broad limits, both exceeding and falling below the contemporaneous seawater value (Figure 17).

Furthermore, insights into the age or Rb/Sr ratio of rocks within the drainage basin can be inferred from the $^{87}Sr/^{86}Sr$ ratios of non-marine carbonates formed during deposition. When these ratios are examined within a stratigraphic context, variations in the ratio also indicate changes in the geology of the watershed, offering valuable information about its geological history (Faure and Barrett, 1973). Radiogenic Sr isotopes can provide a record of weathering and/or regional drainage patterns and be used as a dependable tracer of fluid sources (Pietzsch et al., 2018). Lately, they have been successfully applied to the study of marine and continental (e.g., lacustrine) carbonate successions for stratigraphic correlation and paleoenvironmental reconstruction (e.g., Rhodes et al., 2002; Gierlowski-Kordesch et al., 2008).

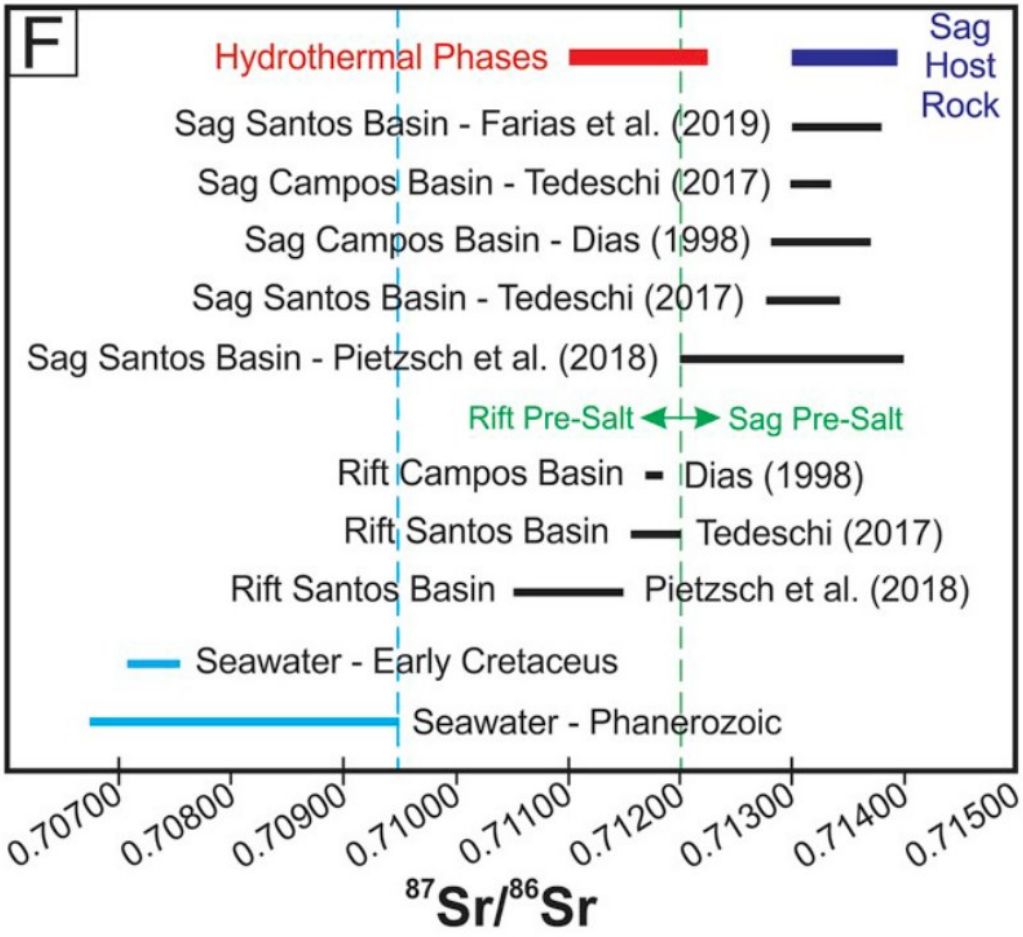


Figure 17 – $^{87}Sr/^{86}Sr$ values obtained in the hydrothermal phases and sag host rocks compared to Early Cretaceous and Phanerozoic seawater (Jenkyns et al., 1995; McArthur et al., 2012; Yamamoto et al., 2013; Bodin et al., 2015; Ando, 2015) and Pre-Salt carbonate (Dias, 1998; Tedeschi, 2017; Pietzsch et al., 2018; Farias et al., 2019) (from Lima et al., 2020).

$^{87}Sr/^{86}Sr$ geochemistry has been increasingly employed in lacustrine deposits lacking diagnostic age indicators to provide chronostratigraphic correlation (Hart et al., 2004; Baddouh et al., 2017), since they can be exceptionally sensitive indicators of lacustrine evolution (Doebbert et al., 2014). Due to its long residence time, the $^{87}Sr/^{86}Sr$ ratio of seawater remains homogeneous at any given time (White, 2013). River discharge into the oceans enriches seawater with more radiogenic strontium ($^{87}Sr$) because rivers drain rocks predominantly composed of granite from the continental crust, which contains elevated strontium due to the radioactive decay of $^{87}Rb$ ($^{87}Sr/^{86}Sr \approx 0.7200 \pm 0.005$). An increase in the strontium content is interpreted as evidence of a shift from steady state to progressively more evaporitic conditions (Neat et al., 1979). Waters resulting from the percolation of mafic rocks or associated with hydrothermalism (mid-ocean ridges, oceanic islands, island arcs, and large lava flows on continents) have lower $^{87}Sr$ content, and consequently, a lower ratio ($^{87}Sr/^{86}Sr \approx 0.704 \pm 0.002$) compared to marine carbonates ($^{87}Sr/^{86}Sr \approx 0.7080 \pm 0.001$).

### 3.2.1 Geochemical analyses

Isotopic analyses of C, O and Sr were conducted in 27 samples (Figure 18A) of a 108 m sidewall carbonate core in the Upper Barra Velha Formation. Following the results, the shallowest sample was disregarded, leaving a 101 m column for analysis.

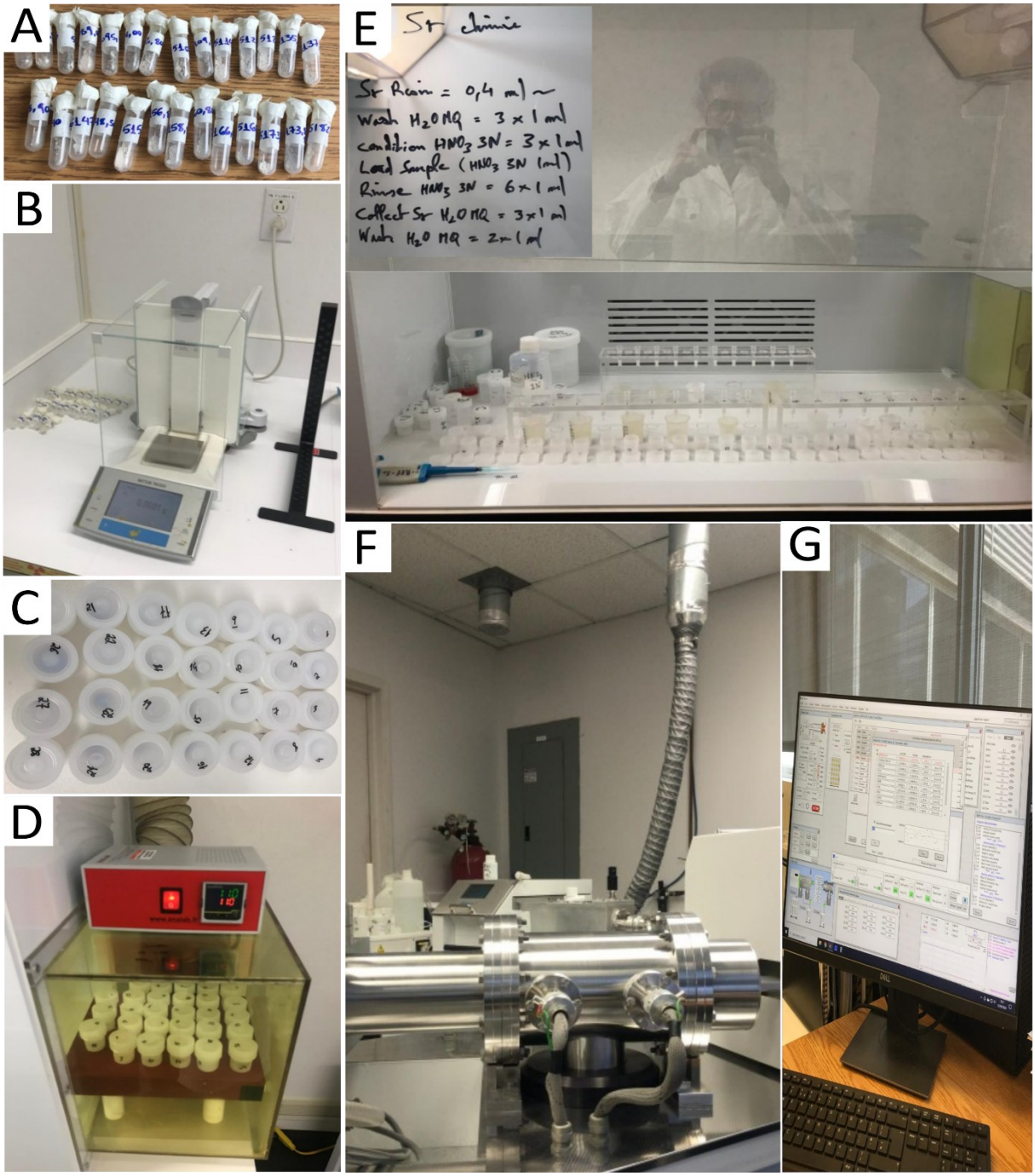


Figure 18 – Workflow of radiogenic Sr analysis. (A) Powder extracted from plugs; (B) precision balance; (C) samples after addition of $HNO_3$; (D) hot plate with samples at 110ºC; (E) tutorial for Sr chemistry and execution; (F) MC-ICP-MS; (G) operational system of the equipment.

The samples were collected at the Petrobras facility in Macaé (RJ), slabbed from drill core plugs perpendicular to laminations. Unaltered domains were micro-drilled to produce the powders that were used in isotopic analyses at the sample preparation laboratory at CPMTC/IGC – UFMG.

For Sr analysis, approximately 50 mg of each sample was weighed (Figure 18B), placed in a Teflon® beaker and then covered with 0.5 ml of $HNO_3$ (Figure 18C). The beakers were placed on a hot plate at 110 ºC for four days to ensure complete digestion. Afterward, the samples were opened and maintained at 80 ºC until complete evaporation (Figure 18D). To separate Rb from Sr, 0.4 ml of Sr-Spec resin was added to a Bio-Spin column. The column was washed with 3 ml of distilled $H_2O$, followed by conditioning with 3 ml of $HNO_3$ 3N. The samples, diluted in 1 ml of $HNO_3$ 3N, were then loaded onto the column.

Rinsing was performed with 6 ml of $HNO_3$ 3N, followed by an additional 3 ml of distilled $H_2O$, which allowed the collection of Sr. To adjust the sample back to 3N, 0.6 ml of $HNO_3$ 14N was added. The column was thereafter washed with 2 ml of distilled $H_2O$, and the entire process was repeated to ensure Sr purification (Figure 18E). Finally, the samples were evaporated before undergoing isotopic analysis.

Sr isotope ratios were analyzed by the Multi-Collector Inductively Coupled Plasma Mass Spectrometry (MC-ICP-MS) on a Nu Plasma 3 at the Radiogenic Isotope Geochemistry Laboratory at GEOTOP–UQAM (Figure 18F). The equipment was calibrated, and each sample analysis took approximately 5 minutes, with a standard analyzed every five samples. All data were corrected for internal mass bias using $^{86}Sr/^{88}Sr = 0.1194$. Repeated measurements of the SRM 987 standard yielded a long-term mean of 0.710214 ± 0.000013 (n = 7) (Figure 18G).

Carbon and oxygen isotope ratios were measured using a Nu Instruments Perspective Isotope Ratio Mass Spectrometry (IRMS) at the Stable Isotopes Laboratory at GEOTOP–McGill University in Montréal, Canada (Figure 19A). Circa 150 µg of each powdered sample was weighed in glass vials. They were placed in the equipment along with eight standards after it reached 70 ºC and then reacted individually with $H_3PO_4$ after heating to 90 ºC for 1 h (Figure 19B). The released $CO_2$ was collected through cold-finger distillation and analyzed against an in-house reference gas. Samples were calibrated to VPDB (Vienna Pee Dee Belemnite) using standards

referenced to NBS-19 (NCM and UQ6). Errors based on long-term repeated analysis of standards are better than 0.05‰ (1σ) for both $\delta^{13}C$ and $\delta^{18}O$ (Figure 19C).

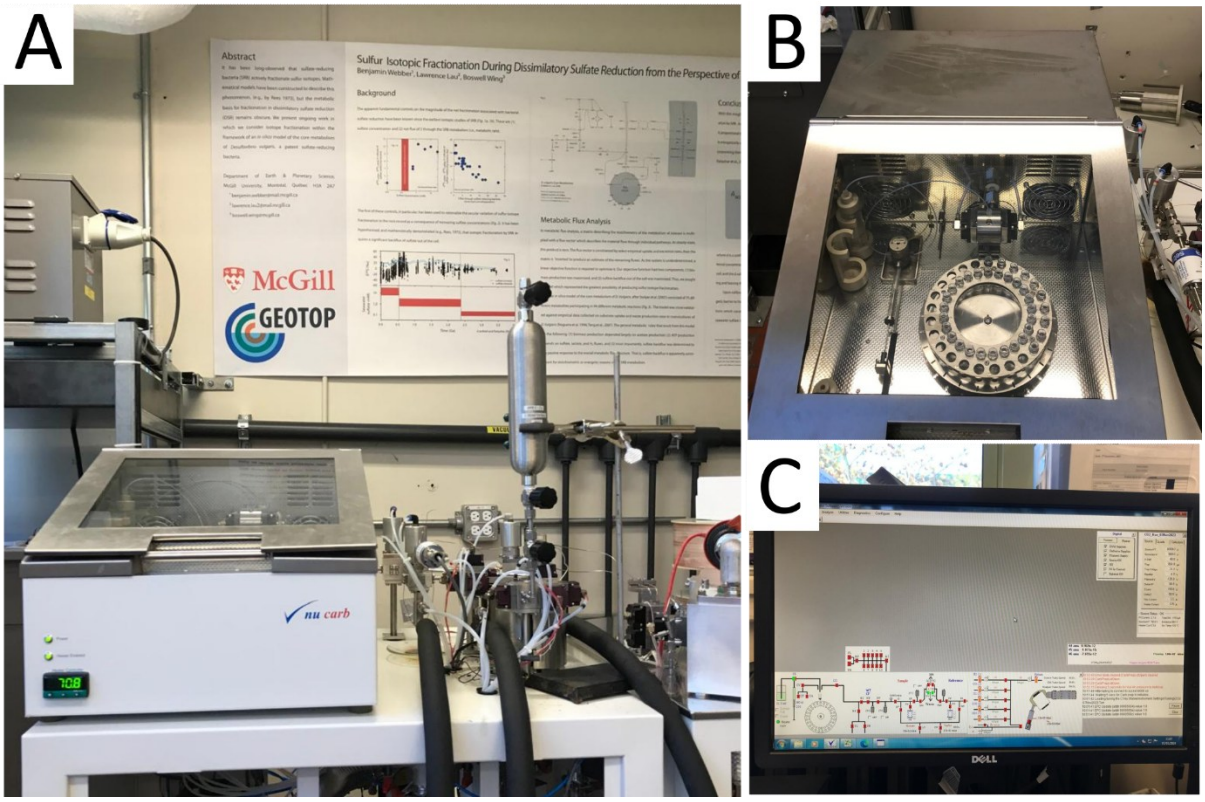


Figure 19 – Equipage used for C and O stable isotopic analyses. (A) IRMS; (B) closer look running the samples; (C) operational system of the equipment.

The concentration of elements, such as Ca, Mg, Sr, Rb, Fe and Mn was measured using iCAP 6000 Series Inductively Coupled Plasma Optical Emission Spectroscopy (ICP-OES) at GEOTOP–McGill University (Figure 20A). Sample preparation focused on mass (m), and the first step was to weigh a microcentrifuge tube on a balance ($m_1$). Approximately 10 mg of the sample was then weighed into the same tube ($m_2$). Following this, 1 mL of $HNO_3$ 2% was added using a pipette ($m_3$). The mixture was allowed to react with the cap open for 15 minutes, after which the tube was capped and shaken thoroughly. Subsequently, the cap was gently opened, and the tube was left to sit for an additional 15 minutes, repeating this process until no new bubbles were observed (Figure 20B).

After the reaction was complete, the tube was capped and centrifuged for 5 minutes. Following centrifugation, 0.5 mL of the clear solution was pipetted into a 15 mL centrifuge tube ($m_4$). Finally, approximately 9.5 mL of 2% nitric acid was added to achieve a total volume of about 10 mL ($m_5$) preparing the sample for analysis.

To operate the equipment, calibration solutions were required. A stock solution was prepared in a 50 mL centrifuge tube, by adding standard solutions according to the target concentrations (Pietzsch et al., 2018; Farias et al., 2019) and $HNO_3$ 2% to complete 50 mL. The solution was diluted by factors of 2, 4, 8, 16, 32, and 64 times. The concentrations of each new solution were recorded to be applied during the analysis. The final concentration in ppm was calculated via $\mathbf{c_2 = (c_1 \times v_1) / v_2}$, where $c_1$ corresponds to the concentration found; $v_1$ equals $m_4 + m_5$ and, $v_2$, represents $m_2$ (see Appendix A).

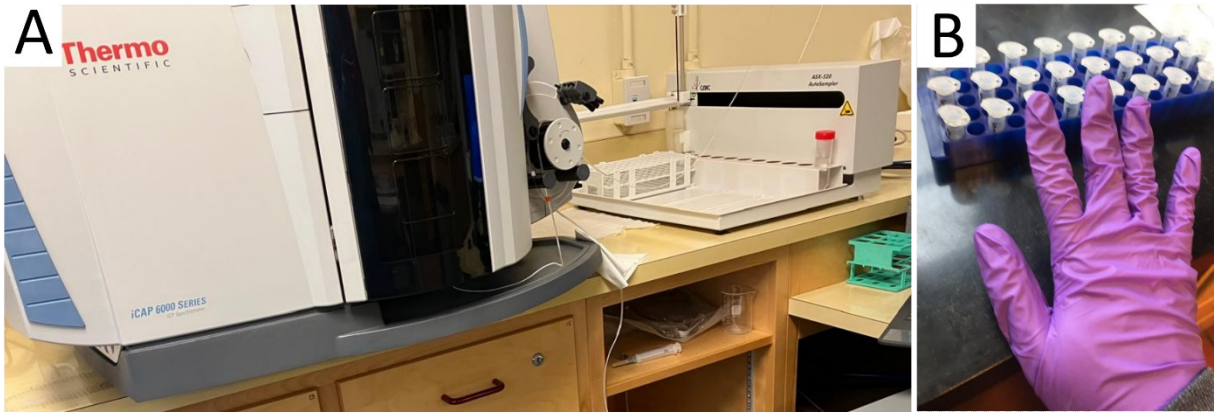


Figure 20 – Equipment utilized to obtain major elements concentration. (A) ICP-OES; (B) clear solution before addition of $HNO_3$.

# 4 STRUCTURAL CONTROL ON THE GEOCHEMISTRY OF PRE-SALT LACUSTRINE CARBONATES IN THE TUPI FIELD, SANTOS BASIN

Deniro Costa[a,b*]; Tiago Novo[a]; Ross Stevenson[b]; Galen Halverson[c], Tobias Fonte-Boa[a]; Humberto Reis[a,d]

[a] Universidade Federal de Minas Gerais, Programa de Pós-graduação em Geologia, Instituto de Geociências, Departamento de Geologia, CPMTC-IGC. Avenida Pres. Antônio Carlos, 6627, Belo Horizonte, MG 31270-901, Brasil.

[b] Département des sciences de la Terre et de l'atmosphère/Geotop, Université du Québec à Montréal, Montréal, Québec H2X 3Y7, Canada

[c] Department of Earth and Planetary Sciences/Geotop, McGill University, Montréal, Québec H3A 0E8, Canada

[d] HR Consulting Energy and Geosciences Ltda, Santo Antônio, Belo Horizonte, MG, Brazil

Abstract:

Lacustrine carbonate deposits from pre-salt reservoirs in the offshore basins of Southeastern Brazil are key contributors to the country's oil production. This study examines the structural and geochemical properties of the Barra Velha Formation, the main hydrocarbon reservoir in the Santos Basin. The influence of local and regional tectonic evolution on the deposition of the Barra Velha Formation was investigated using 2D seismic sections and structural restoration. Major element concentrations, stable isotope analyses (C, O) and radiogenic Sr isotope ratios were conducted on carbonate samples from a sidewall borehole from the Iracema region of the Tupi oil field, allowing the evaluation of diagenetic influences and structural controls on element distribution. $\delta^{13}C$ and $\delta^{18}O$ values are consistent with those found in previous studies of the Santos Basin, indicating that primary seawater isotopic signals may have been largely preserved. Additional observations support minimal alteration, such as high Ca/Mg in most samples and low concentrations of Mn and Fe. High $^{87}Sr/^{86}Sr$ values may indicate a significant contribution of Sr from continental erosion or terrestrial sources with a minor input from less radiogenic sources, possibly volcanic. During diagenesis, Rb can be incorporated into secondary mineral phases or associated with clay materials. Results indicate that the mapped fault structures may

have contributed to local diagenetic alteration, as the fault system likely acted as a conduit for Rb and Sr transport while simultaneously promoting the deposition of Mg-clays in the area. There is low evidence of hydrothermal overprinting when compared to produced fields in the pre-salt context.

Keywords: pre-salt carbonates; Sr isotopes; C and O isotopes; fault activity; oil field; Santos Basin.

## 4.1 Introduction

The Brazilian Atlantic margin encompasses the main sedimentary basins (Santos and Campos), where petroleum exploration is currently concentrated. Located below prominent Aptian salt deposits, petroleum production from pre-salt reservoirs in 2023 accounted for 76.07% of Brazil's total oil production, with the Tupi field alone accounting for 25.04% of the production (ANP, 2023). The giant 'pre-salt' offshore reservoirs in the Santos Basin are distributed primarily in the carbonates of the Barra Velha Formation (BVF) (Moreira et al., 2007) and their tectonic, stratigraphic, and sedimentological evolution has been extensively studied (e.g., Muniz and Bosence, 2015; Wright and Barnett, 2015; Sabato Ceraldi and Green, 2016; Herlinger et al., 2016, 2017; Pietzsch et al., 2018; Lima and De Ros, 2019; Farias et al., 2019). However, despite numerous studies, the relationship between structural controls on fault generation and/or reactivation and elemental distribution remains poorly understood. Sr enrichment or occurrence of calcite over dolomite and vice-versa are debatable in the context of sources and displacement during and after deposition.

In this study, we analyzed the carbonate sedimentation in the Santos basin using rocks obtained from a continuous drill core over 100 m long in the BVF at the Iracema area, in the northwestern sector of the Tupi field (Figure 1). We integrated the seismic interpretation with detailed geochemical analysis of major elements, carbon, oxygen and strontium isotopes and compare it with correlative units of the neighboring Campos basins. In addition to providing a broader understanding of the major environmental conditions leading to the formation of the studied deposits within the context of the Brazilian Atlantic Margin, our analysis revealed the role of faulting in their deposition. The achieved results provide key insights into the Cretaceous evolution of the Santos

Basin and correlative depocenters, as well as important processes controlling the petroleum system of the Brazilian pre-salt.

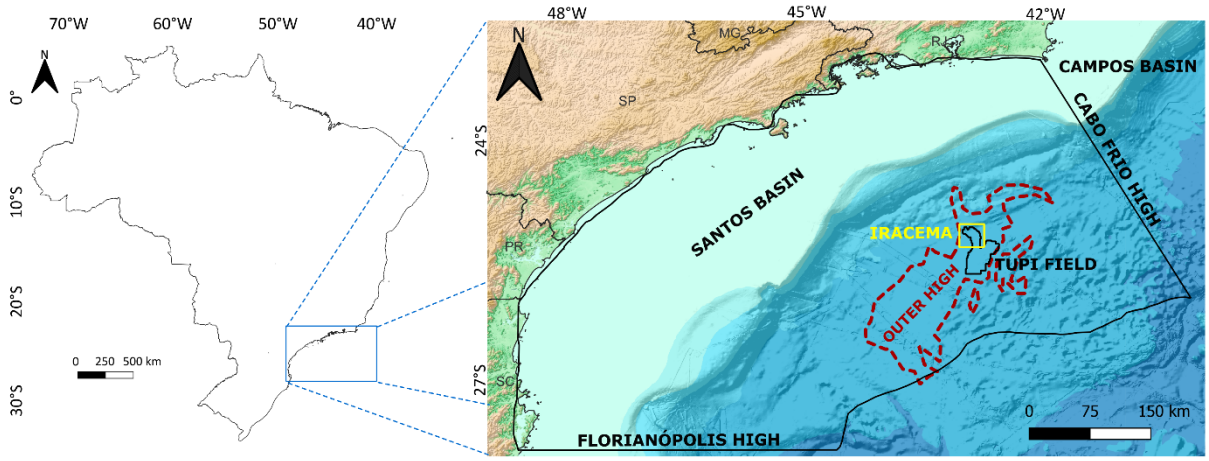


Figure 1 – Map of Brazil, highlighting the Santos Basin and the study area. The Outer High limit was based on Ysaccis et al. (2019). Topographic map from GEBCO_2023 (https://download.gebco.net/).

## 4.2 Geological setting

The marginal basins that comprise the Brazilian South Atlantic margin share a common tectono-sedimentary evolutionary history (Figure 2) (Karner and Driscoll, 1999; Mohriak, 2001; Quirk et al., 2013). Rifting initiation along the central segment of the South Atlantic dates to the Berriasian (~140 Ma) (França et al., 2007; Moreira et al., 2007; Winter et al., 2007) and led to the intrusion of widespread igneous rocks, as well as the nucleation of faults, rotated blocks and associated grabens containing thick sedimentary successions (Milani et al., 2007). The major NE- to NNE-trending normal faults were developed dominantly parallel to the present-day southeastern Brazilian coast, under a WNW-ESE extensional regime (Macedo, 1989; Chang et al., 1992; Karner, 2000; Meisling et al., 2001). This rifting architecture currently defines the regional trend of the Espírito Santo, Campos and Santos offshore basins (Ojeda, 1982; Chang et al., 1992). The rifting episode was followed by the sag phase, during which carbonate-rich successions were deposited and afterwards covered by evaporite strata. The deposition of thick, siliciclastic-dominated Late Cretaceous to Cenozoic strata describes the post-salt successions (Moreira et al., 2007; Chang et al., 2008; Dias et al., 2008; Buckley et al., 2015).

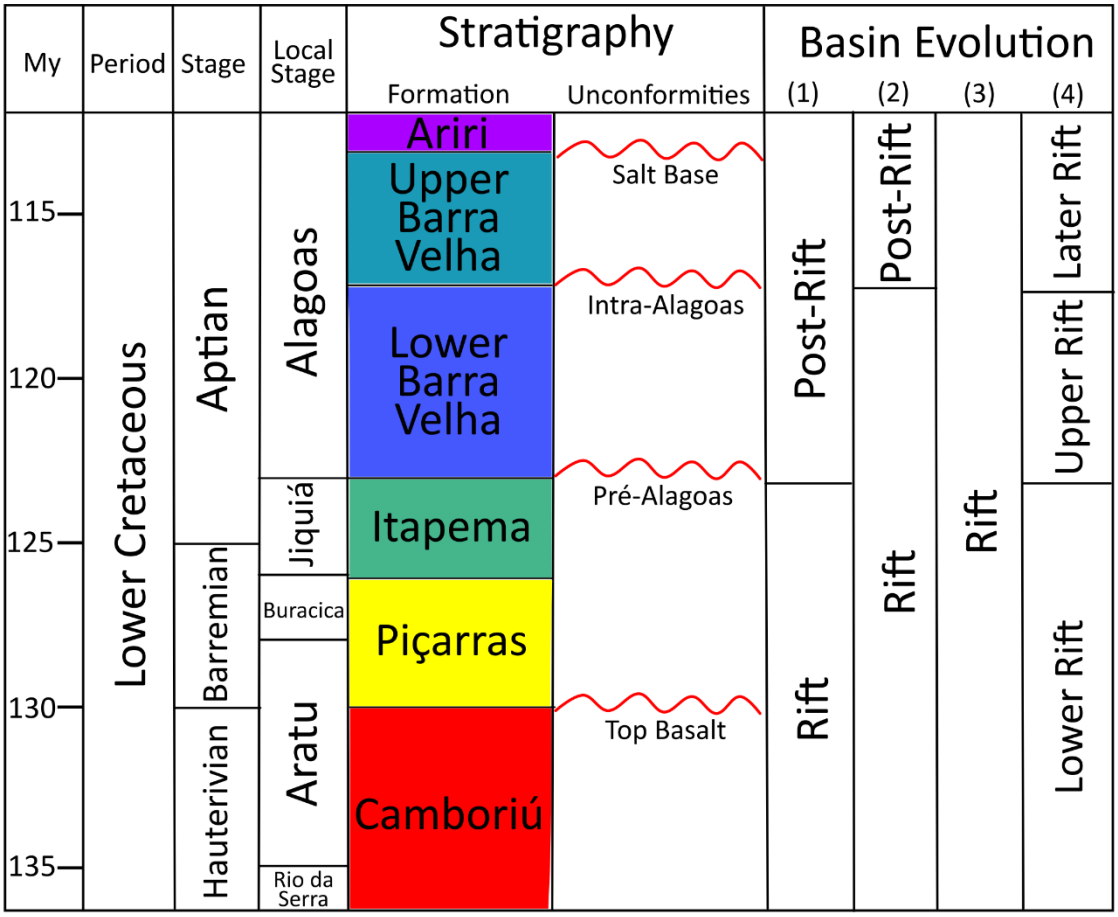


Figure 2 – Lower Cretaceous stratigraphic chart for Santos Basin. Stratigraphy description from Wright and Barnett (2015). Basin evolution suggest by (1) Moreira et al. (2007) (drift phase was omitted as it is not part of the studied interval); (2) Buckley et al. (2015), Barnett et al. (2018) and Farias et al. (2019); (3) Karner and Gambôa (2007), Torsvik et al. (2009) and Moulin et al. (2013); (4) Adriano et al. (2022).

The Santos Basin covers an area of ~350,000 km$^2$ in Southeastern Brazil and is bounded to the south and to the north, respectively, by the Florianópolis and Cabo Frio Highs, with numerous structural features (Ojeda, 1982). During the Hauterivian to Early Aptian rift phase, the basin was affected by NE-trending normal faults that are locally associated with NW-striking transfer faults and partially contemporaneous with the emplacement of the tholeiitic basaltic rocks of the Camboriú Formation (Chang et al., 2008; Cainelli and Mohriak, 1999b; Moreira et al., 2007; Zalán et al., 2011). Afterward, the basin received the siliciclastic-dominated Piçarras Formation and the carbonate-dominated Itapema Formation, respectively.

The deposition of the Barra Velha Formation (BVF), which unconformably overlies the Itapema Formation, occurs during the Alagoas stage, transitioning into a post-rift phase from the clastic/carbonate sedimentary sequence to an evaporitic environment (Moreira et al., 2007; Chang et al., 2008; Carminatti et al., 2009; Buckley et al., 2015). Wright and Barnett (2015) divided the BVF into two units separated by the Intra-

Alagoas unconformity: the Eoaptian Lower Barra Velha (upper rift), and the overlying Neoaptian Upper Barra Velha (sag). The lower BVF is composed of limestones, stromatolites and laminites that were deposited in shallow lacustrine settings contemporaneously with distal shales, whereas the upper BVF comprises limestones intercalated with shales. Proximal to the basin-bounding faults, the BVF is composed of sandstones and conglomerates deposited in alluvial fans (Moreira et al., 2007).

The sag phase represented the evolution of the strain softening process into lithospheric rifting, with the development of a broad, laterally continuous, sag-like depression, characterized by a transitional environment from continental to shallow marine (Chang et al., 2008). Although the sag phase is generally described as a period of tectonic quiescence, the more distal parts of the rift remained locally active, generating normal faulting (Karner and Gamboa, 2007). The reactivation of the pre-existing faults propagated to the base of the evaporites, indicating that extensional deformation persisted until the Upper Aptian (Faria et al., 2017).

Different authors still debate and argue that the sag lacustrine settings developed periodically isolated from the open ocean and under extremely high alkaline conditions (e.g., Wright and Barnett, 2015, 2017, 2020; Herlinger et al., 2017; Lima and De Ros, 2019). This led to the deposition of fluvio-deltaic and lacustrine carbonate successions showing little to no influence from marine waters (Braccini et al., 1997; Harris, 2000; Gomes et al., 2009). Sporadic marine incursions of the south (across the São Paulo Ridge) and an increased evaporation rate relative to the water influx (Mio et al., 2005) resulted in the deposition of the ~ 2 km thick and widespread Neoaptian evaporite deposits of the Ariri Formation (Mohriak, 2003; Moreira et al., 2007; Dias, 2008; Mohriak et al., 2012).

Alkmim et al. (2025) (and references therein) revised the depositional ages of the Itapema and Barra Velha formations, including carbonate cementation events. They carried out in situ U-Pb LA-ICP-MS geochronological determinations on calcite and dolomite phases and obtained: (1) 126.9 ± 4.7 Ma as the minimum age of the Itapema Formation; (2) age of deposition of the BVF lacustrine carbonates between the Late Hauterivian and Lower Aptian, during the 126.2–120.0 Ma interval; (3) three main phases of cementation at c. 119.6, 116.4 and 110.7 Ma. These results implicate changes of interpretation for carbonate deposition and alteration, that may include a structural factor.

## 4.3 Materials and methods

### 4.3.1 Seismic interpretation and structural restoration

For this work, we selected 2D sections from a 3D seismic depth-converted volume (R0282-Santos Cluster) containing the Iracema area (700 km²), along with information from wells in the region to aid in seismic interpretation. These wells include composite and geophysical well logs and lithostratigraphic description. The identification of faults and five representative seismic horizons followed the seismic facies characterization of Adriano et al. (2022) in a regular interval of 365 m along the 72 inlines, in order to cover the entire area of study. 40 crosslines were interpreted for quality control and to allow interpolation of the horizons and integration with faults to generate isopach maps.

In Figure 3, horizon A represents the top of Camboriú Formation, consisting of a high amplitude positive reflector, usually faulted, which accounts for its good to medium lateral continuity. Horizon B corresponds to the top of Piçarras Formation, presenting itself as a medium amplitude negative reflector with some variations in the structural high, where lateral continuity goes from medium to low, to high. Horizon C indicates the top of Itapema Formation, characterized by a low amplitude positive reflector with similar features to the previous horizon. Horizon D consists of the top of Lower Barra Velha Formation, i.e., Intra-Alagoas unconformity (Moreira et al., 2007). Despite its high positive amplitude, this erosional surface is not evident as the lateral continuity is medium to low in the structural high, where interpretation is made at zero-crossing between reflector terminations of different seismic sequences (Adriano et al., 2022). Finally, Horizon E is equivalent to the top of Upper Barra Velha Formation, with a strong amplitude positive reflector and good lateral continuity, containing some fault occurrences as seen in Figure 3.

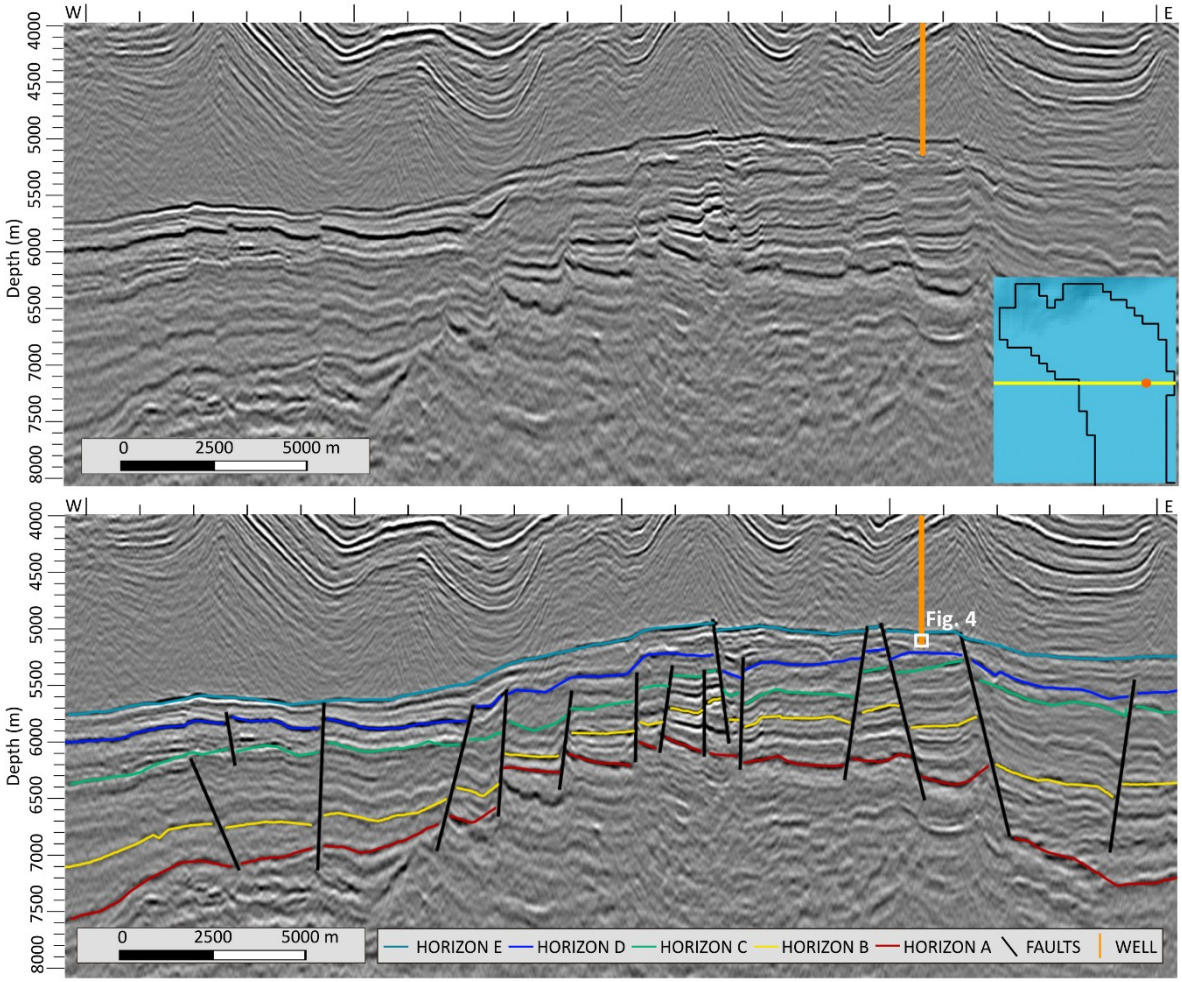


Figure 3 – Non-interpreted and interpreted seismic profiles. Horizon A (red), Horizon B (yellow), Horizon C (green), Horizon D (dark blue) and Horizon E (light blue) represent, respectively, top of Camboriú, Piçarras, Itapema, Lower Barra Velha and Upper Barra Velha Formations. Well (orange) corresponds to 7-LL-83D-RJS.

Structural restoration seeks to revert the deformation interpreted in the present to a less deformed condition of the past (Wickham and Moeckel, 1997). As the transfer zone shifts trends in the Iracema region, structural restoration was performed in three sectors where change was visible, from north to south. Workflow here follows Carvalho et al. (2024), with decompaction of the post-salt (Figure 4A) and salt intervals (Figure 4B), followed by the reconstruction of the Upper Barra Velha Formation (Figure 4C). Age of stratigraphic units followed Moreira et al. (2007), Buckley et al. (2015), Barnett et al. (2018) and Farias et al. (2019). All the analyses were performed in MOVE 2022 software, with parameters such as depth coefficient ($km^{-1}$), Young Modulus (Mpa) and Poisson Ratio with default values, whereas porosity and density ($g/cm^3$) were modified according to the data obtained for the area.

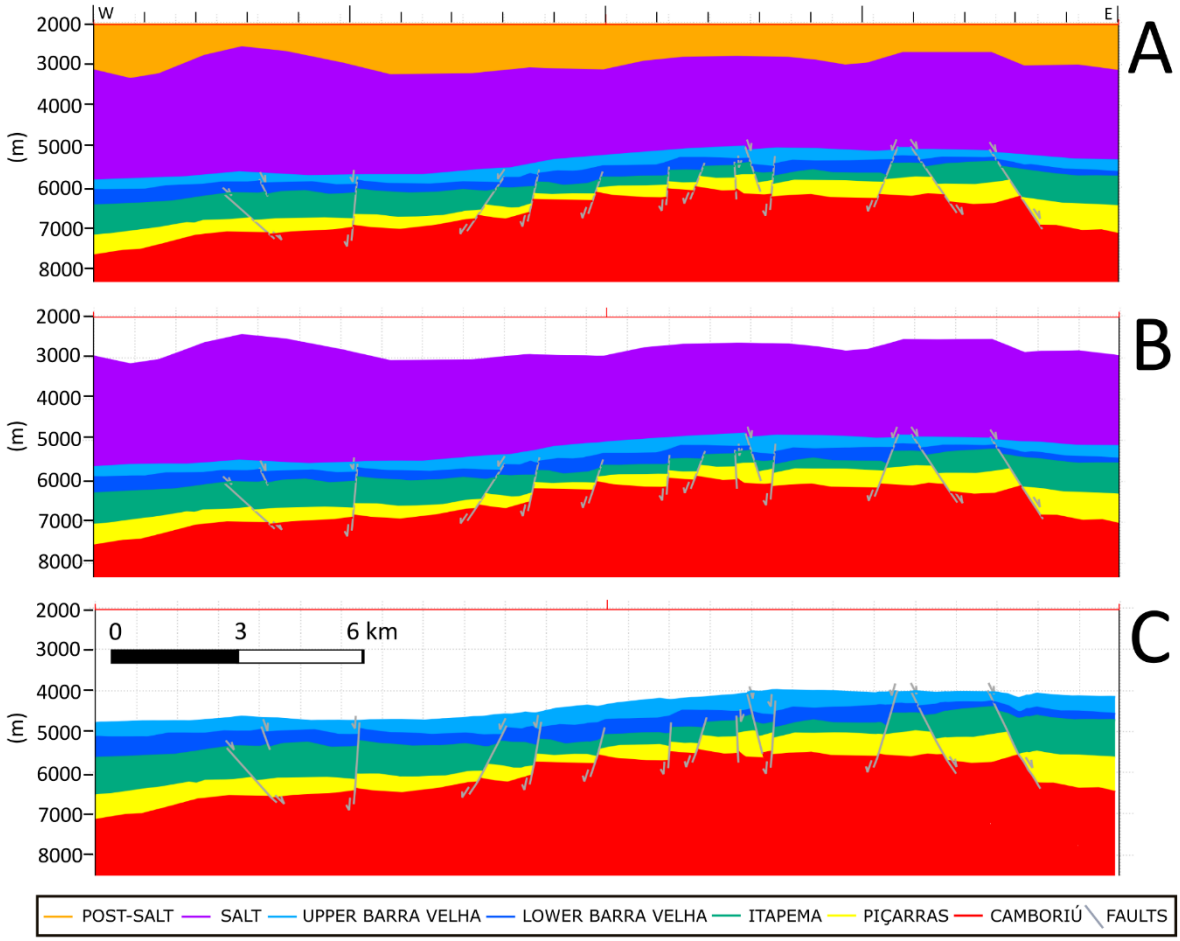


Figure 4 – Structural restoration for the W-E section containing the studied well. Original interpretation in (A), with decompaction of the post-salt layer (Itamambuca, Frade and Camburi Groups) in (B), followed by decompaction of the salt layer (Ariri Formation) and section restoration for the Upper Barra Velha Formation in (C). Scale in (B) and (C) is used to indicate the vertical dislocation of the pre-salt layers.

### 4.3.2 Geochemical data

This study is based on data from 26 samples of a 101 m sidewall carbonate core situated in the upper portion of the Barra Velha Formation. The selected well is located in the middle of the Iracema transfer zone, in an interesting spot for correlation to structural features. The samples were collected and slabbed from plugs of the drill core perpendicular to laminations. Unaltered domains in the portions available were micro-drilled to produce the powders for isotopic analyses.

Carbon and oxygen isotope ratios (Table 1) were measured using a Nu Instruments Perspective Isotope Ratio Mass Spectrometry (IRMS) in the Stable Isotopes Laboratory at McGill University/GEOTOP in Montréal, Canada. Circa 150 µg of each powdered sample was weighed into glass vials and reacted individually with $H_3PO_4$

after heating to 90 ºC for 1 hour. The released $CO_2$ was collected through cold-finger distillation and analyzed against an in-house reference gas. Samples were referenced to the VPDB using in-house standards calibrated to NBS-19. Errors based on long-term repeat analysis of standards are better than 0.05‰ (1σ) for both $^{13}C$ and $^{18}O$.

Sr isotope ratios were analyzed by the Multi Collector Inductively Coupled Plasma Mass Spectrometer (MC-ICP-MS) on a Nu Plasma 3 at the Université du Québec à Montréal/GEOTOP Radiogenic Isotope Geochemistry Laboratory. Approximately 50 mg of each sample were subject to acid attack, which was followed by separation of Sr from Rb in Bio-Spin columns filled with Sr Spec resin twice to ensure Sr purification (Moore and Wade, 2013; Stevenson et al., 2014). All data were corrected for internal mass bias using $^{86}Sr/^{88}Sr = 0.1194$. Repeated measurements of the SRM 987 standard yielded a long-term average of 0.710214 ± 0.000013 (n = 7) (Table 1).

| DEPTH (m) | $^{87}Sr/^{86}Sr$ | $\delta^{18}O$ (‰ VPDB) | $\delta^{13}C$ (‰ VPDB) |
|---|---|---|---|
| 5081.5 | 0.71302 | 1.76 | 0.94 |
| 5085.9 | 0.71312 | -0.25 | 1.87 |
| 5089 | 0.71311 | 0.18 | 2.65 |
| 5095.1 | 0.71326 | -1.22 | 3.00 |
| 5098 | 0.71332 | 2.12 | 1.29 |
| 5102.8 | 0.71347 | 1.44 | 2.27 |
| 5107.3 | 0.71324 | 1.38 | 2.80 |
| 5109.4 | 0.71353 | 0.87 | 2.94 |
| 5114.3 | 0.71363 | 1.15 | 2.30 |
| 5114.4 | 0.71347 | -0.52 | 3.16 |
| 5122.6 | 0.71373 | 1.67 | 3.09 |
| 5124 | 0.71382 | 2.05 | 0.79 |
| 5135.7 | 0.71345 | 1.06 | 2.69 |
| 5137 | 0.71353 | 2.44 | 2.75 |
| 5138.9 | 0.71346 | 1.33 | 2.03 |
| 5147 | 0.71366 | -0.62 | 1.55 |
| 5148.5 | 0.71340 | 2.53 | 1.46 |
| 5151.8 | 0.71334 | 0.20 | 2.05 |
| 5156.8 | 0.71303 | 0.48 | 2.08 |
| 5158.8 | 0.71352 | 0.12 | 2.42 |
| 5160.3 | 0.71311 | 1.91 | 2.31 |
| 5166 | 0.71360 | 0.04 | 1.58 |
| 5168.3 | 0.71354 | 1.12 | 2.79 |
| 5173.3 | 0.71378 | 2.96 | 2.37 |
| 5173.4 | 0.71367 | 2.66 | 2.44 |
| 5182.8 | 0.71436 | 3.86 | 2.03 |

Table 1 – Isotopic data for $^{87}Sr/^{86}Sr$, $\delta^{18}O$, $\delta^{13}C$ from carbonate rocks in the Barra Velha Formation.

The concentrations of Ca, Mg, Sr, Rb, Fe and Mn (Table 2) was measured using an iCAP 6000 Series Inductively Coupled Plasma Optical Emission Spectroscopy (ICP-OES) at GEOTOP–McGill University. Solutions were prepared using 1 ml of 2% $HNO_3$ to digest 10 mg of each sample, after which 0.5 ml of the solution was added to 9.5 ml

of $HNO_3$ 2% for analysis. Five calibration standards were made to bracket the target concentrations (Pietzsch et al., 2018; Farias et al., 2019).

| DEPTH (m) | Ca (ppm) | Mg (ppm) | Sr (ppm) | Rb (ppm) | Mn (ppm) | Fe (ppm) |
|---|---|---|---|---|---|---|
| 5081.5 | 110483 | 39203 | 1319 | 251 | 362 | 288 |
| 5085.9 | 154493 | 27787 | 1255 | 356 | 806 | 399 |
| 5089 | 175384 | 10977 | 1120 | 412 | 423 | 328 |
| 5095.1 | 178021 | 11720 | 1502 | 410 | 238 | 76 |
| 5098 | 86332 | 41602 | 785 | 199 | 241 | 241 |
| 5102.8 | 161475 | 33380 | 1628 | 370 | 103 | 276 |
| 5107.3 | 140435 | 16511 | 1284 | 321 | 166 | 122 |
| 5109.4 | 161767 | 14975 | 1757 | 363 | 181 | 125 |
| 5114.3 | 166985 | 8477 | 1324 | 372 | 93 | 93 |
| 5114.4 | 157524 | 11872 | 1143 | 359 | 111 | 120 |
| 5122.6 | 169759 | 22867 | 1490 | 375 | 77 | 145 |
| 5124 | 119490 | 55233 | 772 | 268 | 64 | 193 |
| 5135.7 | 121751 | 32736 | 1154 | 272 | 84 | 197 |
| 5137 | 140794 | 34352 | 1261 | 330 | 136 | 182 |
| 5138.9 | 167354 | 18259 | 1054 | 395 | 226 | 273 |
| 5147 | 88199 | 43790 | 893 | 210 | 199 | 1268 |
| 5148.5 | 144417 | 27751 | 1124 | 341 | 375 | 283 |
| 5151.8 | 178637 | 9799 | 1083 | 423 | 144 | 499 |
| 5156.8 | 167867 | 15035 | 1351 | 400 | 240 | 196 |
| 5158.8 | 134339 | 8907 | 714 | 322 | 122 | 3326 |
| 5160.3 | 158603 | 26331 | 1370 | 377 | 160 | 731 |
| 5166 | 74245 | 22204 | 461 | 172 | 21 | 204 |
| 5168.3 | 117554 | 8127 | 1048 | 276 | 44 | 121 |
| 5173.3 | 159914 | 11784 | 1443 | 377 | 57 | 132 |
| 5173.4 | 136109 | 30519 | 1658 | 320 | 66 | 198 |
| 5182.8 | 126942 | 42999 | 1756 | 281 | 132 | 492 |

Table 2 – Major elements data from carbonate rocks in the Barra Velha Formation.

## 4.4 Results

### 4.4.1 Seismic interpretation and structural restoration

After seismic analysis, the surfaces of the top of each Formation of the pre-salt (Upper and Lower Barra Velha, Itapema, Piçarras and Camboriú) were elaborated and represented in isopach maps (Figure 5). The greatest depth was close to 7,500 m, whereas the shallowest point was around 4,700 m. Faults were identified in discontinuities of reflectors and were not well distributed in the region.

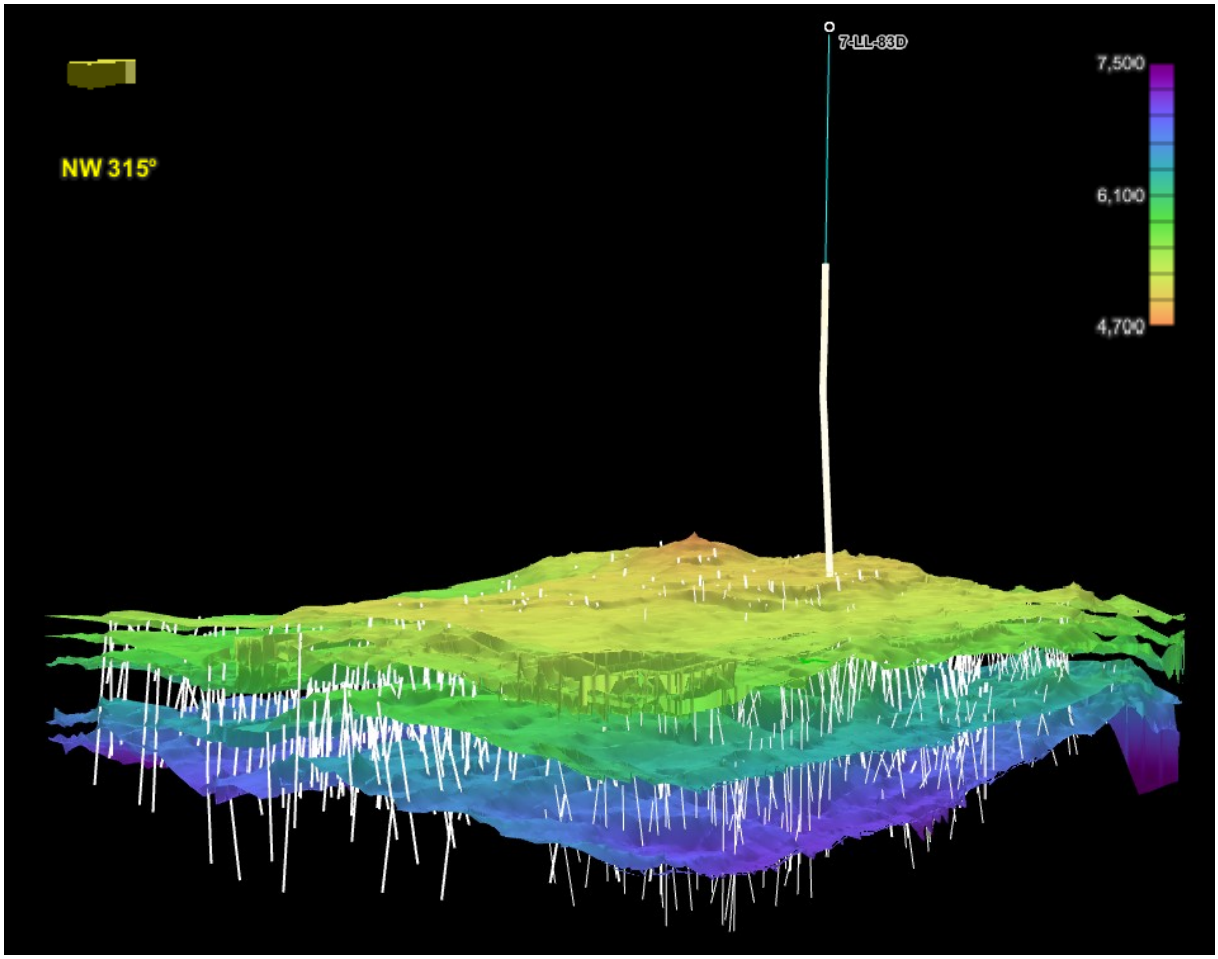


Figure 5 – Representation of the isopach maps for the pre-salt formations.

Structural restoration was conducted in three sectors with distinct fault orientations: the northern sector (faults trending NW-SE), the central sector, which includes the studied well (faults trending N-S), and the southern sector (faults trending NE-SW). Layer-parallel shortening (LPS), typically associated with the formation of folds and thrust faults (e.g., Şengör and Bozkurt, 2013), can also occur in transfer zones, as it reflects deformation in regions of progressive strain. For the Upper BVF, LPS values varied across the area, with -16% in the northern sector, 40% in the central sector (near the studied well), and 8% in the southern sector, indicating significant shortening concentrated in the central region. Sedimentation rates (m/Ma) decrease progressively from north to south, from 96 to 88, and finally to 81. Similarly, the average vertical thickness of sedimentary layers (m) decreases from 385 in the north, to 351 in the center, and 322 in the south.

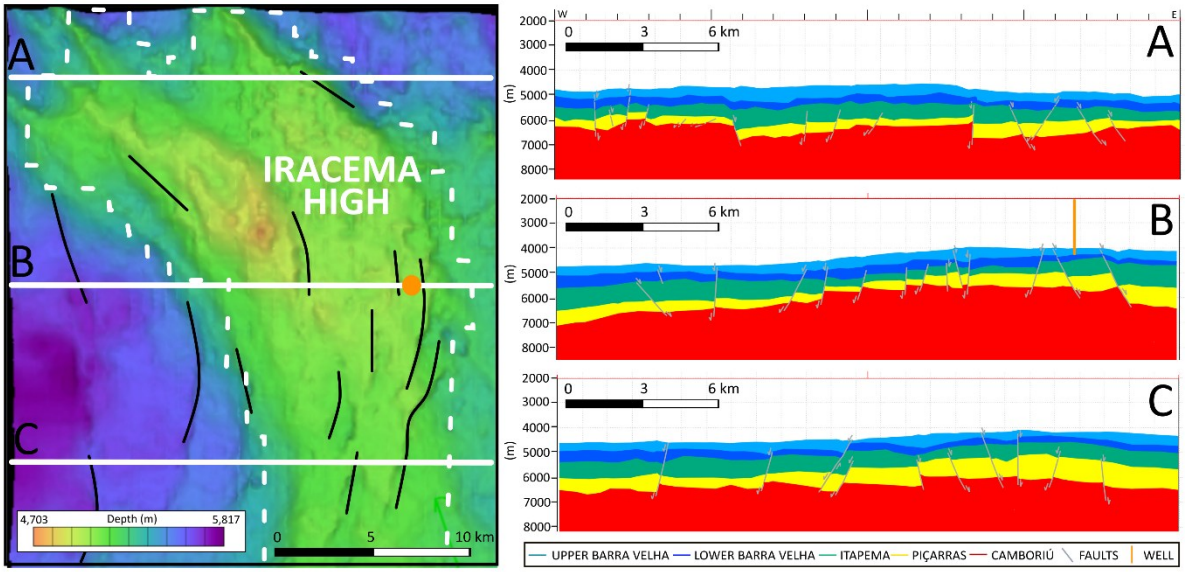


Figure 6 – Structural contour and isopach map of the top of the Upper Barra Velha Formation in the Iracema region. Normal faults follow NE-SW, N-S and NW-SE trends. Structural restoration was performed for sections in the (A) north, (B) center (including the studied well), and (C) south of the studied area. Scale in meters only indicates the vertical dislocation of layers after decompaction of post-salt and salt.

Sedimentation rates are stable during the last stage of the rift phase in the Lower Barra Velha Formation (Wright and Barnett, 2015) whereas there is an increase during the sag phase from south to north. Fig. 6A shows a lack of faults reaching the top of the BVF, with a negative LPS (-16%) that could suggest extension or more likely the effect of tectonic accommodation with active subsidence, with higher sedimentation rates. Meanwhile, Fig. 6B presents the profile where the studied well is located, with a high LPS (40%) that indicates greater tectonic deformation, as the (re)activation of normal faults and the differential movement of the block accommodate this shortening due to the removal of burial charge. Indeed, the section contains a considerable amount of faulting that cuts through the entire pre-salt package. Adriano et al. (2022) identified some faults that were active throughout all rifting phases and suggest that NE-SW trending faults are syn-tectonic with Upper Barra Velha Formation deposition. Determining whether a structure is syn- or post-depositional depends on observing a change in the thickness of the layers in the restoration. In this case, we were able to identify structures near the studied well that were either reactivated or generated in the post-rift phase. Fig. 6C shows that the minor LPS (8%) corresponds to a region of greater tectonic stability outside the transfer zone, despite some faults reaching the base of the salt layer.

### 4.4.2 Geochemical data

The 26 samples collected from well 7-LL-83D-RJS (Fig. 3) were classified according to the facies scheme used by Farias et al. (2019). Petrographic descriptions along with porosity and permeability information allowed us to identify the following carbonate facies: laminite, calcirudite, recrystallized limestone, spherulitestone and shrubby spherulitestone (Fig. 7).

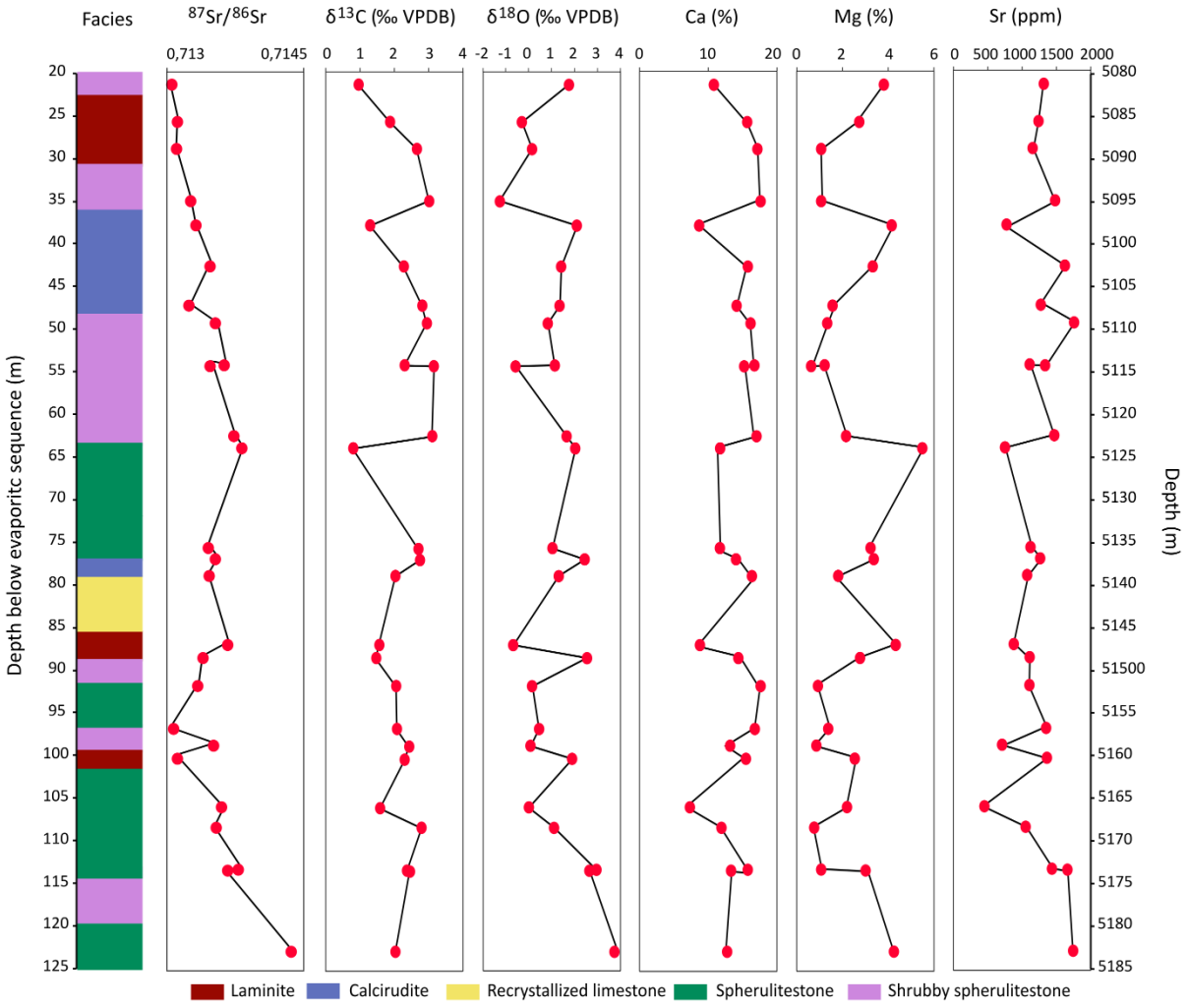


Figure 7 – Profiles of $\delta^{13}C$, $\delta^{18}O$ and $^{87}Sr/^{86}Sr$ isotopic values and concentration of Ca, Mg and Sr in the samples of the studied well, presented in the real depth and relative depth below the evaporitic sequence. Facies distribution is inferred beyond the points of sampling.

Silicified cement was mainly found in the spherulitestones, while Mg-clays were associated with calcirudites. The wells nearby also present some of these features, as well as intense silicification and recurrent dolomite formation. $\delta^{13}C$ values range from + 0.79 to + 3.16‰, with an average of + 2.22‰. The values of $\delta^{18}O$ vary from - 1.22 to + 3.86‰, with average values of +1.18‰. $^{87}Sr/^{86}Sr$ values range from 0.7130 at the

top of the section to 0.7144 at the bottom, with an average of 0.7135, similar to the results reported by Pietzsch et al. (2018). The negative correlation between Ca and Mg reflects their competitive substitution in carbonates. Values for Sr compare well with those of Pietzsch et al. (2018) and Lawson et al. (2022) but are much less than those presented by Farias et al. (2019).

Although no consistent correlations are observed between the Sr, O and C isotope compositions of the different carbonate facies (Figure 8), the laminites are predominantly associated with $\delta^{18}O$ values ≤ 0 and the shrubby spherulitestones yield some of the highest $\delta^{13}C$ values. Overall, the samples collected from the greatest depths, near the boundary between the Upper and Lower Barra Velha Formation, exhibit significantly higher values of $\delta^{18}O$ and $^{87}Sr/^{86}Sr$.

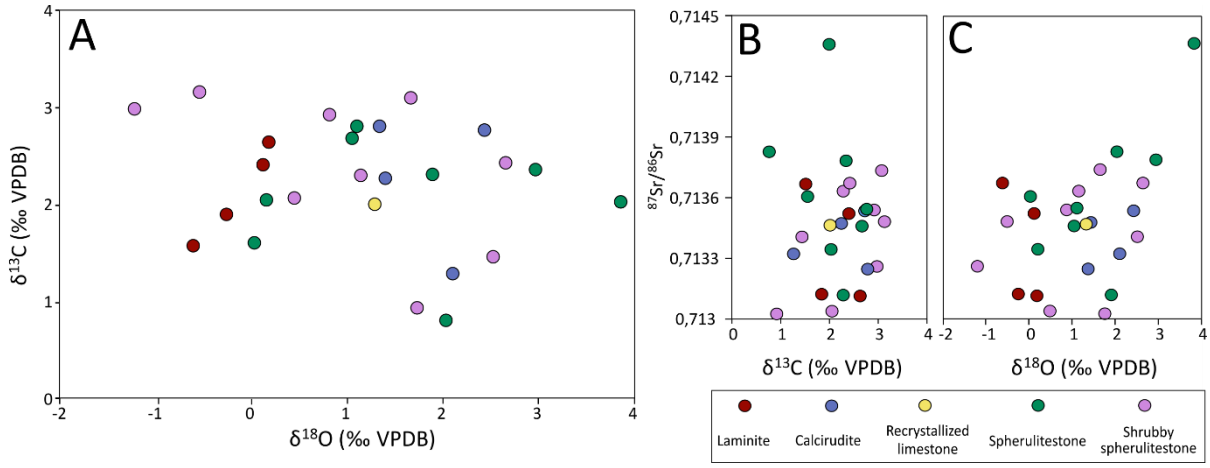


Figure 8 – Scatter plots for (A) $\delta^{18}O$ vs. $\delta^{13}C$; (B) $\delta^{13}C$ vs. $^{87}Sr/^{86}Sr$; and (C) $\delta^{18}O$ vs. $^{87}Sr/^{86}Sr$. Facies are represented in colored circles. Note that no correlation can be observed in the data.

## 4.5 Discussion

### 4.5.1 Influence of diagenetic processes

The depositional environments of the Southeastern Brazilian Atlantic pre-salt lacustrine carbonates are linked to significant temporal changes in lake water chemistry and structural positions within the basins (Sabato Ceraldi and Green, 2016; Saller et al, 2016). The extent of diagenetic alteration in carbonate compositions is influenced by factors such as the difference in elemental concentrations between carbonate and fluid, whether the system remained open or closed, the degree of porosity, and distribution coefficients identified in earlier modeling studies of water-rock interaction (Banner et al., 1988; Banner and Hanson, 1990; Wang and Cerling, 1994;

Maliva, 1998). Positive $\delta^{13}C$ and $\delta^{18}O$ values (Fig. 5A) are typically interpreted to reflect the evaporation conditions of the environment (Talbot and Kelts, 1990), whereas negative $\delta^{18}O$ values close to zero reflect negligible diagenetic alteration of the lacustrine carbonates. Shifts in the values of $\delta^{18}O$ towards lighter compositions can also be produced by recrystallization processes (Lima and De Ros, 2019).

The degree of preservation of the original chemical composition of the carbonates versus the degree of alteration due to diagenetic processes or tectono-structural factors are investigated with the aid of Figure 9. In carbonates formed in lacustrine environments (such as in the pre-salt), the replacement of Ca by Mg during dolomitization can result in lower Sr levels, since dolomite incorporates less Sr than calcite. However, the amount of Sr in the samples is still high (Figure 7) (exceeding 500 ppm in all but one sample), and dolomitic phases were not identified in the samples analyzed, although there may be some indication of partial dolomitization from sidewall rocks that were not totally recovered from the well.

The positive correlation between Ca and Sr (Figure 9A) may indicate diagenetic alteration by Sr-enriched fluids. Alternatively, rising salinity and temperature within the shallowing basin could lead to increased concentrations of these elements, favoring the precipitation of Mg-rich dolomite and/or calcite, which is consistent with pre-salt depositional conditions (e.g. Wright and Barnett, 2015, 2017, 2020; Herlinger et al., 2017; Lima and De Ros, 2019; Pietzsch et al., 2020; Almeida Carvalho et al., 2022; Carramal et al., 2022). This is supported by the Mg concentrations in the samples (2,3% on average) (Figure 9B) which are consistent with Mg-calcite (e.g., Farias et al., 2019) rather than dolomite compositions. This suggests that diagenetic alteration was negligible in these samples, although the analyzed carbonates likely include both primary and altered compositions. Carbonates with high Mg/Ca ratios may reflect alteration due to diagenetic processes (e.g. dolomitization), whereas high Ca/Mg ratios suggest preserved original compositions, similar to higher $\delta^{18}O$ values, since shifts towards lighter compositions are also a product of processes such as recrystallization (Figure 9C) (Lima and De Ros, 2019).

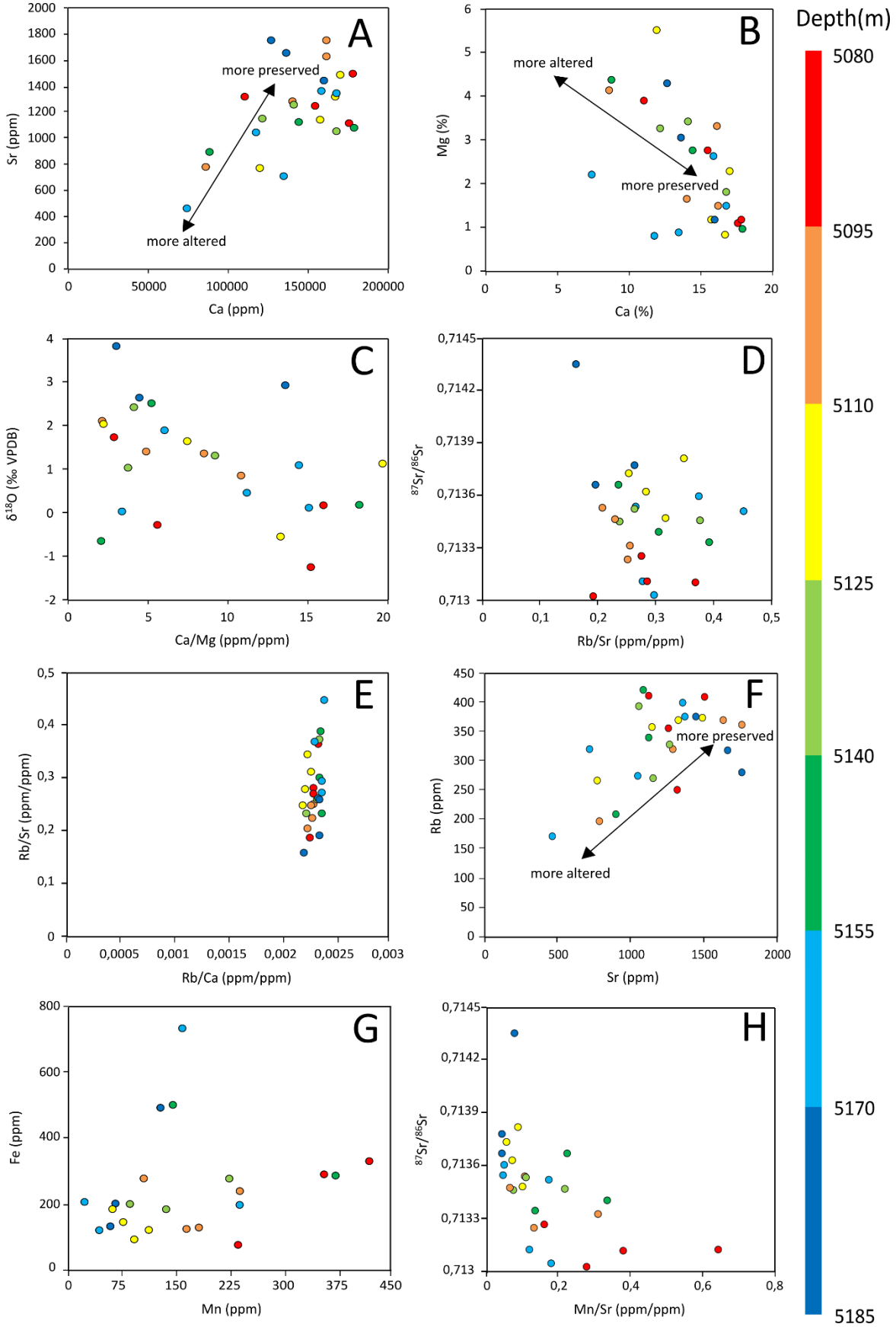


Figure 9 – Scatter plots of (A) Ca vs. Sr; (B) Ca vs. Mg; (C) Ca/Mg vs. $\delta^{18}O$; (D) Rb/Sr vs. $^{87}Sr/^{86}Sr$; (E) Rb/Ca vs. Rb/Sr; (F) Sr vs. Rb; (G) Mn vs. Fe; and (H) Mn/Sr vs. $^{87}Sr/^{86}Sr$. Colors of the samples indicate their depth in the well.

The deposition of Mg-rich authigenic shales, travertines, stromatolites, grainstones, spherulitic packstones and mudstones in the Brazilian marginal basins during the Aptian are related to the extrusion of the Mg-rich Paraná basalts (Szatmari and Milani, 2016). The Sr in the carbonates is too radiogenic to have been derived solely from the erosion of continental flood basalts in the Santos Basin region. Thus, volcanic sources were likely not the only contributors to the lake waters (Pietzsch et al., 2018). Indeed, Pietzsch et al. (2018) state that their mass-balance calculations show a felsic end-member as a significant source of water, Sr and other ions to the paleo-lake, likely contributing up to four orders of magnitude more Sr than the mafic source. Felsic basement rocks and/or alluvial detritus could have provided the underground water with elements and compounds such as Ca, Mg, and $SiO_2$ (Tedeschi, 2017; Farias et al., 2019). However, the granitic-gneissic basement is not a suitable source for the large quantities of Ca and Mg that precipitated in the sag phase rocks (Lima et al., 2020).

The lack of correlation between Rb/Sr and $^{87}Sr/^{86}Sr$ indicates a negligible contribution of radiogenic Sr from Rb-rich silicates (clays, K-feldspar) in the samples (Figure 9D). Thus, the $^{87}Sr/^{86}Sr$ ratios of the carbonates reflect those of the water from which they precipitated and any subsequent diagenetic alteration. The radiogenic $^{87}Sr/^{86}Sr$ ratios could reflect waters sourced from aquifers within acidic bedrock, where prolonged residence times led to high Ca and Mg concentrations (e.g., East Africa; Ojiambo et al., 2003). Regardless of the exact nature of the crustal source, our data is consistent with the interpretation that the $^{87}Sr/^{86}Sr$ ratios of the carbonates reflect a mixture of mafic and felsic sources with the latter being dominant (Pietzsch et al., 2018). On one hand, we have a felsic end-member, likely derived from crustal/fluvial sources, with high $^{87}Sr/^{86}Sr$, $\delta^{18}O$ and low Rb, Mn and Fe, presenting values consistent with the Alagoas stage from Pietzsch et al., 2018. On the other hand, a diagenetic end-member would be comparable to the Jiquiá stage from the same work, with lower $^{87}Sr/^{86}Sr$, $\delta^{18}O$ and higher Rb, Mn and Fe.

The specific correlation between Rb/Ca and Rb/Sr (Figure 9E) may indicate that the initial incorporation of Rb reflected environmental conditions rather than intense diagenetic processes, as the Rb is mobilized or incorporated in the carbonates proportionally to Sr and Ca. Moreover, it was expected that Rb and Sr would correlate negatively, since they behave differently during alteration processes and diagenetic

evolution. However, in Figure 9F, it is seen that they tend to correlate positively. During diagenesis, while Sr replaces Ca, Rb may be incorporated into secondary mineral phases or associated with clay materials.

In the context of the Santos Basin, Mg-clays are most commonly found in the Tupi field (e.g., Carramal et al., 2022). Mg-silicates can precipitate directly from marine or lacustrine waters, or from diagenetic pore fluids (i.e., neoformation or by alteration of precursor phases; Galán and Pozo, 2011). Parameters such as salinity, pH and Mg/Si ratio of the fluids control their stability, favoring certain species over others (Jones, 1986; Tosca and Masterson, 2014; Tutolo and Tosca, 2018). In the adjacent fields to Tupi, Mg-silicates are not as abundant as their diagenetic alteration products, turning this field into an adequate area for the study of this occurrence (Carramal et al., 2022). The distinct structural framework and geometries across the basin (Carlotto et al., 2017; Ysaccis et al., 2019) were an important control on the development of Mg-silicates. The preservation of Mg-clays suggests that the structural environment played a pivotal role in governing the diagenetic modifications, with more pronounced transformations occurring in regions featuring structural elevations and fault zones (Almeida Carvalho et al., 2022).

Although there are some outliers for Fe and Mn concentration (Figure 9G), the observed values are consistent with mild diagenetic alteration, indicating preservation of the depositional signal and does not indicate detrital influence in the results. One sample worth mentioning is the one with the highest $^{87}Sr/^{86}Sr$ value. It represents an outlier and coincidently reflects the interface of the Upper Barra Velha (sag phase) and the Lower Barra Velha Formation (rift phase). A high value of Mn/Sr (Figure 9H) would suggest conditions with higher hydrothermal activity, responsible for introducing these elements into the system. However, there is a lack of sufficient data from further discussion, including microscopic analyses that would help identify more complex components in the diagenetic and hydrothermal sphere. Moreover, it cannot be ruled out the remobilization of some elements in post depositional processes.

### 4.5.2 Structural component and isotopic comparison with producing fields

Early faulting in the pre-salt reservoirs coincides with syn-depositional tectonic deformation (e.g., Farias et al., 2019) and gravitational instability caused by local

processes at edges of the shelf (Nolting et al., 2018). Burial faults are associated with gradual loading and increasing confining stresses within a context of late-stage faulting and heightened lithostatic pressure. The development of such structures during carbonate deposition and subsequent exposure to meteoric or burial diagenesis increases the complexity of characterizing and modeling faults in the subsurface, as they are often long-lived, widely distributed, and act as pathways for fluid migration (e.g., Budd et al., 2013). Even if only segments of faults may be reactivated during tectonic evolution, it is essential to determine the scale at which this occurs (Le Pichon et al., 2014; Şengör, 2016). The structures may be resurrected (e.g., thrust fault is reactivated), replacement (e.g., thrust fault reactivating a normal fault; Cohen, 1982) or revolutionary (i.e., entirely independent of pre-existing fabric; Şengör et al., 1985).

Figure 6 presents an isopach map showing fault occurrences at the top of the BVF at Iracema in an isopach map. The faults in the Iracema High are oriented in three main directions: NE-SW (predominant in the Tupi High), N–S and NW-SE (Adriano et al., 2022). Rifting is inferred to have been active during the deposition of all pre-salt lithologies, coinciding with the formation of the Iracema transfer zone. Although the NE-SW trend of the main fracture was inherited from basement structures, continued rifting induced an NW-SE inflection, forming an S-shaped feature (Magnavita, 2021). It is noted that most of the faults mapped follow a N-S direction, with some trending NW-SE in the north and NE-SW in the south. These structures are important in the evolution of the lacustrine carbonates, as they aid in identifying the input of essential elements.

The different oil fields of the Brazilian Atlantic Margin exhibit numerous common reservoir characteristics, but have demonstrated differences, necessitating thorough scrutiny, especially when significant structural events, magmatic intrusions, or hydrothermal systems have overprinted the initial features, extending beyond the typical influences of burial diagenesis (Araújo et al., 2022). This is illustrated by a comparison of isotopic data from fields within the Santos and Campos Basins (Figure 10B). Some of the previous studies use information from one well (Farias et al., 2019; Pietzsch et al., 2020), four wells (Lima et al., 2020; Lawson et al., 2022) or 21 wells (Almeida Carvalho et al., 2022) (Figure 10C). In the latter study, data from more different wells were averaged according to a given facies. Only data for the Upper

Barra Velha Formation are depicted in Figure 10C with the addition of data from the Macabu Formation that is correlated to the BVF (Lima et al., 2020).

Figure 10C illustrates a progressive increase in the $\delta^{18}O$ and $\delta^{13}C$ isotope values from the Macabu to the Upper Barra Velha Formation. Although this increase could be interpreted as a product of diagenetic alteration (Lima and De Ros, 2019), it can also suggest evaporitic conditions (Talbot, 1990; Farias et al., 2019). This latter interpretation is supported by the presence of Mg-clays that are deposited in evaporitic environments (Galán and Pozo, 2011; Pozo and Calvo, 2018). We note that the highest $\delta^{18}O$ values are associated with the intervals with high Mg-clay content. The majority of the results from the Upper Barra Velha Formation in the Santos Basin yield overlapping positive $\delta^{13}C$ and $\delta^{18}O$ values. Sporadic negative $\delta^{18}O$ values correspond to silicified or extensively dolomitized matrix associated with calcite spherulites (Farias et al., 2019; Pietzsch et al., 2020). Lawson et al. (2022) use the $\delta^{18}O$ data to calculate the $\delta^{18}O_{fluid}$ of the water in the ancient lakes and found values similar to those estimated for the time-equivalent conjugate pre-salt lakes from the Kwanza Basin of Angola. Farias et al. (2019) does not address the origin of the negative $\delta^{13}C$ values in their study. Pietzsch et al. (2020) suggests that the largely positive $\delta^{13}C$ of the Upper Barra Velha Formation reflect equilibration with atmospheric $CO_2$.

Almeida Carvalho et al. (2022) studied the relationship between the location of the isotopic data and their structural location and found that the distribution of the $\delta^{13}C$ and $\delta^{18}O$ values depends on the location of the wells on their depositional profile in the Tupi field. For example, samples located in a lower area within a structural high have relatively constant the $\delta^{13}C$ values, whereas a change in the $\delta^{13}C$ values is observed on a higher structural position. As noted above, although the $\delta^{18}O$ values present significant differences between units, the highest values are associated with the intervals with high Mg-clay content. This suggests that hydrothermal activity contributed only locally to the alteration of the pre-salt carbonates and to the precipitation of specific mineral assemblages that include the Mg-clays (Almeida Carvalho et al., 2022). In contrast, in the northern Campos Basin, Lima et al. (2020) concluded that more negative $\delta^{18}O$ values may have been produced by a fault-focused hydrothermal system that involved mixing of fluids derived from several sources such as the granitic-gneissic basement, the rift sedimentary succession, Late Cretaceous

and Paleogene magmatism, and possibly fluids derived from the rising and exhumation of the asthenosphere.

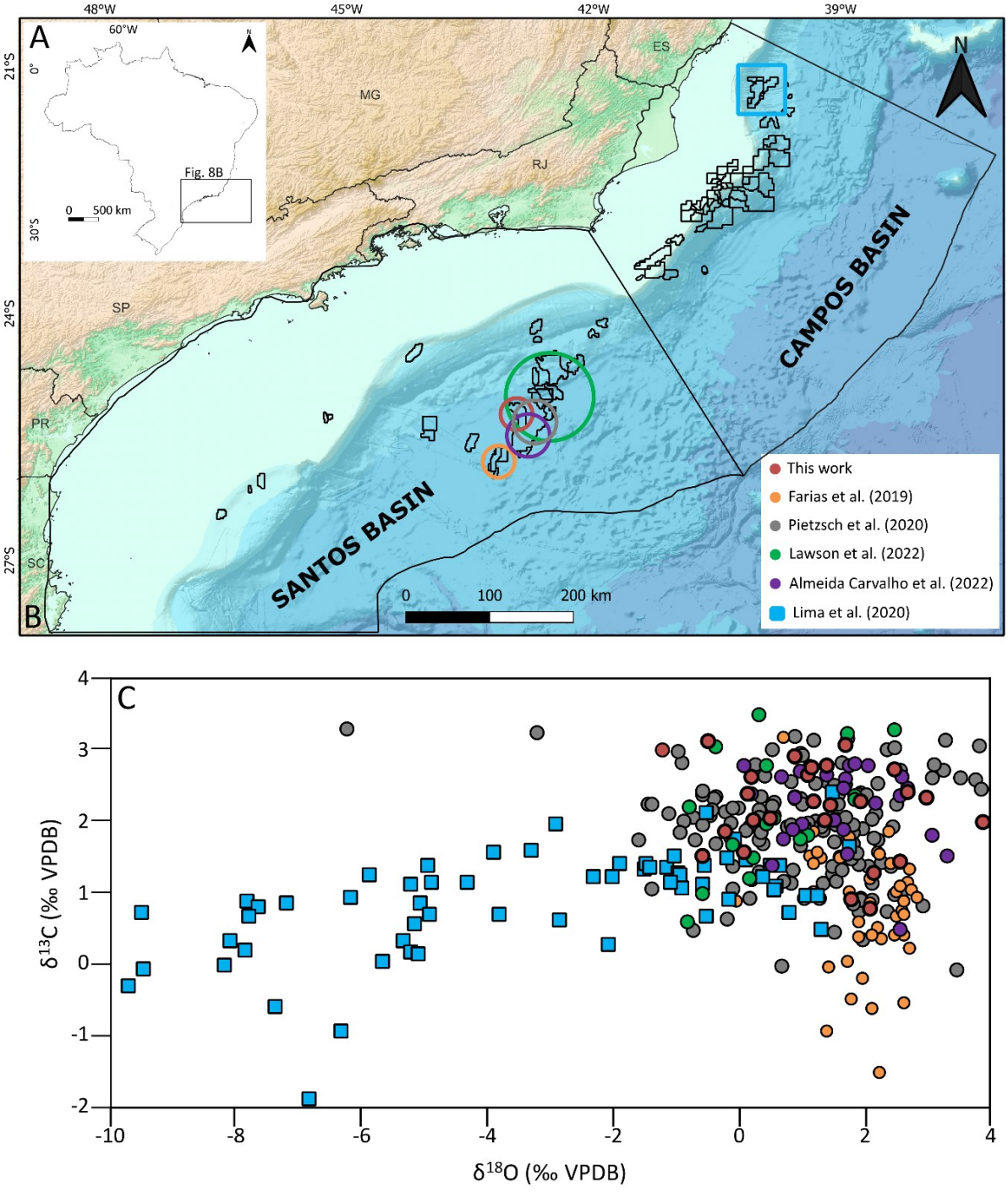


Figure 10 – (A) Map of Brazil, highlighting the Santos and Campos basins. (B) Map of estimated location of samples from Farias et al. (2019) (orange), Pietzsch et al. (2020) (gray), Lawson et al. (2022) (green), Almeida Carvalho et al. (2022) (purple) and Lima et al. (2020) (blue) within the production fields. Topographic map from GEBCO_2023 (https://download.gebco.net/). (C) Scatter plot of $\delta^{18}O$ vs. $\delta^{13}C$ isotopes for the Santos (circles) and Campos basins (squares).

## 4.6 Conclusion

The overall geological and geochemical framework, combined with the structural component and comparison between basins allowed us to recognize that the pre-salt carbonates analyzed at the Iracema area have been through slightly diagenetic alteration, although they are still close to the original composition. Fault activity in the area, whether the structures were burial related or reactivated, did not implicate intense hydrothermal processes around the studied well. The fault system may have been responsible for transporting Rb and Sr and allowing the deposition of Mg-clays in the area, also leading to a variation in deformation from north to south. In future work, it would be important to correlate the occurrence of Mg-clays and fault networks, while building a geological model for Iracema that aggregates data from other wells. This study demonstrates the importance of structural and geochemical assessments in distinguishing the evolution of the different oil fields, and the role of these assessments in determining the degree of preservation of original carbonate compositions.

## 4.7 Acknowledgements

This study was financed in part by the Coordenação de Aperfeiçoamento de Pessoal de Nível Superior – Brasil (CAPES) – Finance Code 001. Samples acquisition was carried by Petrobras through the project entitled “Inteligência artificial aplicada à exploração de petróleo na camada pré-sal” (nº 28184). DFGC was supported by the ELAP (Emerging Leaders in the Americas Program) of the Canadian Bureau for International Education/Foreign Affairs and International Trade Canada during his stay at the GEOTOP Research Center, Montréal, Canada. The assistance of lab technicians Thi Hao Bui (McGill University) and Julien Gogot (UQAM), as well as André Poirier (UQAM) with the MC-ICP-MS is highly appreciated. The authors especially thank ANP for providing the seismic data and samples used in this work, the DUG company for the DUG Insight academic license applied for seismic visualization, interpretation, analysis, and PE Limited (Petex) for the MOVE application used for fault analysis and structural restoration. The support and discussion with members of the SÍSMICA research group, mainly Mariana Leite, Fernanda Moura Costa, Maria José Oliveira and Caique Pinheiro de Carvalho is also appreciated. Finally, the authors thank Felipe Farias from Petrobras for his suggestions and constant support.

# 5 CONCLUSIONS

Inheritance and faults are some of the key themes in rifted margin research considered high priority targets, as reactivation of fractures is a critical step for the development of major faults. The Brazilian Atlantic margin is extremely asymmetric and lithospheric inherited NE-SW features control the deformation in the Santos Basin proximal domain, with a series of NE-SW to NNE-SSW-trending normal faults. In the Outer High, the inflection in the NW portion of the Tupi field, in the Iracema High, is due to the NW-SE-trending transfer zones. It is suggested that rifting was active during the deposition of all pre-salt lithologies, while the Iracema transfer zone was generated.

The reactivation of the pre-existing faults propagates to the base of the evaporites, indicating that syn-depositional tectonic deformation of the Upper Barra Velha Formation coincides with early faulting in the pre-salt reservoirs. Structural restoration was able to determine the syn- or post-depositional character of structures close to the studied well, whether they were reactivated or generated in the post-rift phase. Most of the faults mapped follow a N-S direction, with some trending NW-SE in the north and NE-SW in the south, up to the top of the Upper Barra Velha Formation.

The degree of alteration due to diagenetic process or tectono-structural factors versus the degree of preservation of the original chemical composition of the carbonates was investigated. Post-depositional processes (e.g., dolomite cementation, dolomitization, silicification and dissolution) and parameters such as recrystallization rate and groundwater discharge rate are found to be significant contributors to the alterations in carbonate compositions. Considering the carbonate facies described – laminite, calcirudite, recrystallized limestone, spherulitestone and shrubby spherulitestone –, silicified cement was mainly found in the spherulitestones, and Mg-clays were associated with calcirudites. Even though wells nearby presented recurrence of dolomite, dolomitic phases were not identified in the samples analyzed, although there may be some indication of partial dolomitization from sidewall rocks that were not totally recovered from the well. Along with a positive correlation between Ca and Sr, high amount of Sr in the samples and high Ca/Mg ratios and $\delta^{18}O$, it is understood that the carbonate samples of this study likely include both primary and altered compositions.

The radiogenic $^{87}Sr/^{86}Sr$ ratios are consistent with data available for the basin and could reflect waters derived from aquifers within acidic bedrock that acquired high Ca and Mg concentrations due to long residence times (e.g., East Africa). Regardless of the exact nature of the crustal source, data from this work is consistent with the interpretation that the $^{87}Sr/^{86}Sr$ ratios of the carbonates reflect a mixture of mafic and felsic sources, with the latter being the dominant source. On one hand, we have a felsic end-member, likely derived from crustal/fluvial sources, with high $^{87}Sr/^{86}Sr$, $\delta^{18}O$ and low Rb, Mn and Fe. The reorganization of preexisting drainage patterns (e.g., Paraíba do Sul River) may have occurred during the uplift of onshore features (e.g., Serra do Mar and Serra da Mantiqueira), facilitating the total denudation of topographic highs and sedimentation in topographic lows to act uninterruptedly. Offshore subsidence may have occurred due to the deposition of sediments transported by river networks, which continuously shape rifted margins (e.g., Santos Basin). On the other hand, a diagenetic end-member, with lower $^{87}Sr/^{86}Sr$, $\delta^{18}O$ and higher Rb, Mn and Fe.

There are structural features that can influence fluid flow migration (e.g., burial faults, often long lived and presented in a wide distribution) and, when overlapped, geochemical and structural data indicate that these faults may have acted as conduits for the transport of elements during diagenesis (e.g., Rb and Sr) but hydrothermalism is negligible in the area. As a matter of fact, since the distribution of the $\delta^{13}C$ and $\delta^{18}O$ values depends on the location of the wells on their depositional profile in the Tupi field, this suggests that hydrothermal activity contributed only locally to the alteration of the pre-salt carbonates and to the precipitation of specific mineral assemblages that include the Mg-clays. In contrast, in the northern Campos Basin, it was concluded by other authors that more negative $\delta^{18}O$ values may have been produced by a fault-focused hydrothermal system that involved mixing of fluids derived from several sources.

It is relevant to consider further research into the Outer High and the fields within it. A broader study including geochemistry of rocks from several wells and dating techniques (e.g., U-Pb in carbonates) would be more consistent and relatable to the exploration of hydrocarbons in the Santos Basin.

# REFERENCES


Adriano M.S., Figueiredo, J.P., Coelho, P.H.G.R., Borghi, L., 2022. Tectonic and stratigraphic evolution of the Santos Basin rift phase: New insights from seismic interpretation on Tupi oil field area, **Journal of South American Earth Sciences**, Volume 116, 103842, ISSN 0895-9811, https://doi.org/10.1016/j.jsames.2022.103842.

Agostini, A., Corti, G., Zeoli, A., Mulugeta, G., 2009. Evolution, pattern, and partitioning of deformation during oblique continental rifting: Inferences from lithospheric-scale centrifuge models, **Geochem. Geophys. Geosyst.**, 10, Q11015, doi:10.1029/2009GC002676.

Alkmim F.F., Lana C.C., Silva M.A.L., Dias-Filho D.C., Mendonça K.R.N., Zambonato E.E., Carvalho B.R.B.M., 2025. U-Pb ages of pre- to post-salt carbonates, Santos and Campos basins, SE Brazil: Implications for the evolution of the South Atlantic, **Marine and Petroleum Geology**, Volume 171, 107192, ISSN 0264-8172, https://doi.org/10.1016/j.marpetgeo.2024.107192.

Allen, P.A., Allen, J.R., 2005. Basins in their plate tectonic environment. In: Allen, P.A., Allen, J.R. (Eds.), **Basin Analysis**: Principles and Applications. Blackwell Publishing, pp. 3-19. ISBN 0-632-05207-4.

Almeida, F.F.M., 1986. Distribuição regional e relações tectônicas do magmatismo pós-paleozóico do Brasil. **Revista Brasileira de Geociências**, v. 16, p. 325-349.

Almeida, F.F.M., Carneiro, C.D.R., 1998. Origem e evolução da Serra do Mar. **Revista Brasileira de Geociências**, 28, (2), 135-150 doi:10.25249/0375-7536.1998135150 .

Almeida, J., Dios, F., Mohriak, W., Valeriano, C., Heilbron, M., Eirado, L., Tomazzoli, E., 2013. Pre-rift tectonic scenario of the Eo-Cretaceous Gondwana break-up along SE Brazil-SW Africa: insights from tholeiitic mafic dyke swarms. **Geological Society London Special Publications**. 369. 11. 10.1144/SP369/24.

Almeida Carvalho, A.M., Hamon, Y., Souza Jr, O.G., Carramal, N.G., Collard, N., 2022. Facies and diagenesis distribution in an Aptian pre-salt carbonate reservoir of the Santos Basin, offshore Brazil: A comprehensive quantitative approach, **Marine and Petroleum Geology**, Volume 141, 105708, ISSN 0264-8172, https://doi.org/10.1016/j.marpetgeo.2022.105708.

Alvarenga, R.S., Iacopini, D., Kuchle, J., Scherer, C.M.S., Goldberg, K., 2016. Seismic characteristics and distribution of hydrothermal vent complexes in the Cretaceous offshore rift section of the Campos Basin, offshore Brazil. **Marine and Petroleum Geology**, 74, 12-25.

Alves, E.C., 1981. Estruturas da Margem Continental Sul Brasileira e das Áreas Oceânicas Continentais Adjacentes. **Recursos Minerais (Relatório Final)**. Rio de Janeiro: PETROBRAS/CENPES/DINTEP. Série Projeto REMAC, 9.

Alves, E.C., 2002. **Zonas de Fraturas Oceânicas e suas Relações com a Compartimentação Tectônica do Sudeste do Brasil.** Tese de Doutorado. Departamento de Geologia da Universidade Federa do Rio de Janeiro, 247 p.

Amante, C., Eakins, B.W., 2009. ETOPO1 1 Arc-minute Global Relief Model: Procedures, **Data Sources and Analysis**, NOAA Technical Memorandum NESDIS NGDC-24. https://doi.org/10.1594/PANGAEA.769615.

Ando, A., 2015. Intersite discrepancy in the amplitude of marine negative $\delta^{13}C$ excursion at the onset of early Aptian oceanic anoxic event 1a: reconciliation through Sr isotopic screening of peculiar diagenetic overprint on the Pacific reference section (Deep Sea Drilling Project Site 463). In: Neal, C.R., Sager, W.W., Sano, T., Erba, E. (Eds.), Environmental Consequences of Ontong Java Plateau and Kerguelen Plateau Volcanism. **Geological Society of America Special Paper** 511. The Geological Society of America, Boulder, USA, pp. 329–339.

ANP – Agência Nacional do Petróleo, Gás Natural e Biocombustível, 2023. **Boletim da Produção de Petróleo e Gás Natural.** Available in: https://www.gov.br/anp/pt-br/centrais-de-conteudo/publicacoes/boletins-anp/boletins/arquivos-bmppgn/2023/encarte-boletim-dezembro.pdf Access: Sep. 2024.

Araújo, C.C., Madrucci, V., Homewood, P., Mettraux, M., Ramnani, C.W., Spadini, A.R., 2022. Stratigraphic and sedimentary constraints on presalt carbonate reservoirs of the South Atlantic Margin, Santos Basin, offshore Brazil. **AAPG Bulletin**, vol. 106, issue 12, pp. 2513-2546. 10.1306/08082219218.

Araujo, M.N., Pérez-Gussinyé, M., Muldashev, I., 2023. Oceanward rift migration during formation of Santos–Benguela ultra-wide rifted margins. **Geological Society, London, Special Publications**, Volume 524, Pages 65 – 91. https://doi.org/10.1144/SP524-2021-123

Arienti, L.M., Souza, R.S., Viana, S., Cuglieri, M.A., Silva, R.P., Tonietto, S., Paula, L., Gil, J.A., 2018. Facies association, depositional systems, and paleophysiographic models of the Barra Velha Formation, pre-salt sequence – Santos Basin, Brazil. In: **AAPG Annual Convention & Exhibition 2018**, Salt Lake City, Utah.

Aslanian, D., Moulin, M., Olivet, J.-L., Unternehr, P., Matias, L., Bache, F., Rabineau, M., Nouzé, H., Klingelhoefer, F., Contrucci, I., Labails, C., 2009. Brazilian and African passive margins of the central segment of the south Atlantic Ocean: kinematic constraints. **Tectonophysics (Special Issue: role of magmatism)** 468, 98–112.

Asmus, H.E., 1982. Geotectonic significance of Mesozoic-Cenozoic magmatic rocks in the Brazilian continental margin and adjoining emerged area. In: **Congresso Latino-Americano de Geologia.** Servicio Geologico Nacional, Buenos Aires, pp. 761–779.

Asmus H.E., 1984. Geologia da margem continental brasileira. In: C. Schobbenhaus, D. A. Campos, G. R. Derze, H. E. Asmus (eds.) **Geologia do Brasil**: texto explicativo do mapa geológico do Brasil e da área oceânica adjacente, incluindo depósitos minerais, DNPM, p.: 443-472.

Autin, J., Leroy, S., Beslier, M.O., d'Acremont, E., Razin, P., Ribodetti, A., Bellahsen, N., Robin, C., Al Toubiet, K., 2010. Continental break-up history of a deep magma-

poor margin based on seismic reflection data (northeastern Gulf of Aden margin, offshore Oman). **Geophys. J. Int.** 180, 501–519. doi: 10.1111/j.1365-246X.2009.04424.x

Azevedo, R.L.M., 2004. Paleoceanografia e a evolução do Atlântico Sul no Albiano. **Boletim de Geociências da Petrobras**, [s. l.], v. 12, n. 2, p. 231-249.

Baddouh, M., Carroll, A.R., Meyers, S.R., Beard, B.L., Johnson, C.M., 2017. Chronostratigraphic Correlation of Lacustrine Deposits Using $^{87}Sr/^{86}Sr$ Ratios, Eocene Green River Formation, Wyoming, U.S.A. **Journal of Sedimentary Research**, 87, (4): 406–423. https://doi.org/10.2110/jsr.2017.27.

Banner, J.L., Hanson, G.N., Meyers, W.J., 1988. Water-Rock Interaction History of Regionally Extensive Dolomites of the Burlington-Keokuk Formation (Mississippian): **Isotopic Evidence**. https://doi.org/10.2110/pec.88.43.0097.

Banner, J.L., Hanson, G.N., 1990. Calculation of simultaneous isotopic and trace element variations during water-rock interaction with applications to carbonate diagenesis, **Geochimica et Cosmochimica Acta**, Volume 54, Issue 11, Pages 3123-3137, ISSN 0016-7037, https://doi.org/10.1016/0016-7037(90)90128-8.

Barnett, A.J., Obermaier, M., Amthot, J., Juk, K., Camara, R., Sharafodin, M., Bolton, M., 2018. Origin and significance of thick carbonate grainstone packages in non-marine successions: a case study from the Barra Velha Formation, Santos Basin. In: **AAPG ACE 2018**.

Basso, M., Belila, A.M.P., Chinelatto, G.F., Souza, J.P.P., Vidal, A.C., 2020. Sedimentology and petrophysical analysis of pre-salt lacustrine carbonate reservoir from the Santos Basin, southeast Brazil. **Int. J. Earth Sci.** 110, 2573–2595.

Basso, M., Souza, J.P.P., Honório, B.C.Z., Melani, L.H., Chinelatto, G.F., Belila, A.M.P., Vidal, A.C., 2022. Acoustic image log facies and well log petrophysical evaluation of the Barra Velha Formation carbonate reservoir from the Santos Basin, offshore Brazil. **Carbonates and Evaporites**, 37(3), 50.

Beck, W.C., Grossman, E.L., Morse, J.W., 2005. Experimental studies of oxygen isotope fractionation in the carbonic acid system at 15°, 25°, and 40° C. **Geochim. Cosmochim. Acta** 69, 3493–3503.

Belém, J., 2014. **Geoquímica, Geocronologia e contexto geotectônico do magmatismo máfico associado ao feixe de fraturas Colatina, Estado do Espírito Santo.** Tese de doutorado, Universidade Federal de Minas Gerias - Instituto de Geociências - Programa de Pós-Graduação em Geologia. p. 138 (in Portuguese).

Blaich, O.A., Faleide, J.I., Tsikalas, F., Franke, D., León, E., 2009. Crustal-scale architecture and segmentation of the Argentine margin and its conjugate off South Africa, **Geophysical Journal International**, Volume 178, Issue 1, Pages 85–105, https://doi.org/10.1111/j.1365-246X.2009.04171.x

Bodin, S., Meissner, P., Janssen, N.M.M., Steuber, T., Mutterlose, J., 2015. Large igneous provinces and organic carbon burial: controls on global temperature and continental weathering during the Early Cretaceous. **Glob. Planet. Chang.** 133, 238–253.

Braccini, E., Denison, J.R., Scheevel, P., Jeronimo, P., Orsolini, P., Barletta, V., 1997. A revised chrono-litho-stratigraphic framework for the pre-salt (Lower Cretaceous) in Cabinda, Angola. **Bulletin des Centres de Recherches Exploration-Production Elf-Aquitaine**, 21, 125–151.

Brune, S., Heine, C., Clift, P.D., Pérez-Gussinyé, M., 2017a. Rifted margin architecture and crustal rheology: reviewing iberia-newfoundland, central South Atlantic, and South China Sea. **Mar. Pet. Geol.** 79, 257–281. doi: 10.1016/j.marpetgeo.2016.10.018

Brune, S., Kolawole, F., Olive, J.-A., Stamps, D.S., Buck, W.R., Buiter, S.J.H., Furman, T., Shillington, D.J., 2023. Geodynamics of continental rift initiation and evolution **Nature Reviews Earth & Environment** volume 4, pages 235–253.

Buck, W.R., 2006. The role of magma in the development of the Afro-Arabian Rift System. **Geol. Soc. Lond. Spec. Publ.** 259, 43–54.

Buckley, J.P., Bosence, D., Elders, C., 2015. Tectonic setting and stratigraphic architecture of an Early Cretaceous lacustrine carbonate platform, Sugar Loaf High, Santos Basin, Brazil. In: BOSENCE, D. W. J. et al. (eds) Microbial Carbonates in Space and Time: Implications for Global Exploration and Production. **Geological Society, London, Special Publications,** 418, p.175–191.

Budd, D.A., Frost, E.L., Huntington, K.W., Allwardt, P.F., 2013. Syndepositional deformation features in high-relief carbonate platforms: long-lived conduits for diagenetic fluids. **Journal of Sedimentary Research**, 2013, v. 82, 12–36 Research Article DOI: 10.2110/jsr.2013.3.

Cainelli, C., Mohriak, W.U., 1998. Geology of Atlantic Eastern Brazilian basins. In: **AAPG, International Conference & Exhibition Short Course** – Brazilian Geology Part II, Rio de Janeiro, Brazil, 67p. + figures.

Cainelli, C., Mohriak, W. U., 1999b. Some remarks on the evolution of sedimentary basins along the Eastern Brazilian continental margin. **Episodes**, 22(3):206-216.

Calegari, S.S., Neves, M.A., Guadagnin, F., França, G.S., Vincentelli, M.G.C., 2016. The Alegre Lineament and its role over the tectonic evolution of the Campos Basin and adjacent continental margin, Southeastern Brazil. **J. S. Am. Earth Sci.** 69, 226–242.

Calvo, J.P., Pozo, M., 2015. Geology of magnesian clays in sedimentary and non-sedimentary environments. In: **Magnesian Clays**: Characterization, Origin and Applications; Pozo, M., Galán, E., Eds, 123-174.

Carlotto, M.A., Silva, R.C.B., Yamato, A.A., Trindade, W.L., Moreira, J.L.P., Fernandes, R. A.R., Ribeiro, O.J.S., 2017. Libra: a newborn giant in the Brazilian pre-salt province. In: Merrill, R.K., Sternbach, C.A. (Eds.), **Giant Fields of the Decade 2000–2010**. AAPG Memoir 113, Houston, Texas, pp. 165–176.

Carminatti, M., Wolff, B., Gamboa, L., 2008. New exploratory frontiers in Brazil. In: **19th World Petroleum Congress.** WPC Proceedings, Madrid, Spain, v. 1, p. 225-239.

Carminatti, M., Dias, J.L., Wolff, B., 2009. From turbidites to carbonates: breaking paradigms in deep waters: Houston, Texas. In: **Offshore Technology Conference**, 4–7 May, OTC 20124.

Carramal, N.G., Oliveira, D.N., Cacela, A.S.M., Cuglieri, M.A.A., Natasha, P., Rocha, N.P., Viana, S.M., Toledo, S.L.V., Pedrinha, S., De Ros, L.F., 2022. Paleoenvironmental insights from the deposition and diagenesis of aptian pre-salt magnesium silicates from lula field, Santos Basin, Brazil. **J. Sediment. Res.** 92, 12–31.

Carvalho, R.K., 2023. **Caracterização e restauração estrutural de uma área do Pré-sal da Bacia de Santos e o impacto da paleogeografia no controle da deposição das fácies no reservatório.** Master's thesis. Universidade Federal do Rio de Janeiro.

Carvalho, M.D., Praca, U.M., Silva-Telles, A. C., Jahnert, R. J., Dias, J. L., 2000. Bioclastic carbonate lacustrine facies models in the Campos Basin (Lower Cretaceous), Brazil. In: Gierlowski-Kordesch, E.H. & Kelts, K.R. (eds) **Lake Basins through Space and Time.** AAPG Studies in Geology, 46, 245–256.

Carvalho, R.K., Mello, C.L., Souza Junior, O.G. de., 2024. Caracterização e restauração estrutural de uma área do Pré-sal da Bacia de Santos e o impacto da paleogeografia no controle da deposição das fácies no reservatório. **Geologia USP.** Série Científica, 24(1), 51-72. https://doi.org/10.11606/issn.2316-9095.v24-200523

Castro, J.C., Azambuja Filho, N.C., 1981. Fácies, análise estratigráfica e reservatórios da Formação Lagoa Feia, Cretáceo Inferior da Bacia de Campos. **PETROBRAS/CENPES/LABOR**, Relatório interno, p. 110.

Caumon, G., Muron, P., 2006. Surface restoration as a mean to characterize transverse fault slip uncertainty. In: **Gocad Meeting**, 26, Nancy, Proceedings, 11 p.

Chang, H.K., Kowsmann, R.O., Figueiredo, A.M.F., Bender, A., 1992. Tectonics and stratigraphy of the east Brazil rift system: an overview, **Tectonophysics**, 213, 97–138.

Chang, H.K., Assine, M.L., Corrêa, F.S., Tinen, J.S., Vidal, A.C., Koike, L., 2008. Sistemas petrolíferos e modelos de acumulação de hidrocarbonetos na Bacia de Santos. **Brazilian Journal of Geology**, 38(2), 29-46.

Chenin, P., Manatschal, G., Ghienne, J., Chao, P., 2021. The syn-rift tectono-stratigraphic record of rifted margins (Part II): A new model to break through the proximal/distal interpretation frontier. **Basin Research** 00, 1–44. https://doi.org/10.1111/bre.12628.

Chinelatto, G.F., Belila, A.M.P., Basso, M., Souza, J.P.P., Campane Vidal, A., 2020. A taphofacies interpretation of shell concentrations and their relationship with petrophysics: A case study of Barremian-Aptian coquinas in the Itapema Formation, Santos Basin-Brazil, **Marine and Petroleum Geology**, Volume 116, 104317, ISSN 0264-8172, https://doi.org/10.1016/j.marpetgeo.2020.104317.

Christ, N., Maerz, S., Kutschera, E., Kwiecien, O., Mutti, M., 2018. Palaeoenvironmental and diagenetic reconstruction of a closed-lacustrine carbonate system – the challenging marginal setting of the Miocene Ries Crater Lake (Germany). **Sedimentology** 65, 235–262.

Cohen, C. R., 1982. Model for a passive to active continental margin transition: implications for hydrocarbon exploration. **American Association of Petroleum Geologists Bulletin**, 66, 708–718.

Corti, G., 2012. Evolution and Characteristics of Continental Rifting: Analog Modeling Inspired View and Comparison with Examples from the East African Rift System. **Tectonophysics**, 522-523, 1-33. http://dx.doi.org/10.1016/j.tecto.2011.06.010

Costa, D.F.G., 2022. **Late cretaceous exhumation of the Doce River Valley and the Colatina Fracture Zone, southeastern Brazil**: implications from apatite fission-track data. Monografia de graduação. Universidade Federal de Minas Gerais, Belo Horizonte, 62 p.

Costa, D.F.G., Fonseca, A., De Grave, J., Novo, T., 2024. Relating differential crustal architecture to passive margin evolution: A case study from the Colatina Fracture Zone (SE Brazil) using apatite fission-track thermochronology. **Geological Journal**, 59(10), 2789-2802.

Courtillot, V., Jaupart, C., Manighetti, I., Tapponnier, P., Besse, J., 1999. On causal links between flood basalts and continental breakup. **Earth Planet. Sci. Lett**. 166, 177–195.

Dahlstrom, C.D.A., 1969. Balanced cross sections. **Canadian Journal of Earth Sciences** 6, 743–757.

Davison, I., 2007. Geology and tectonics of the South Atlantic Brazilian salt basins. **Geological Society, London, Special Publications**, 272, 345-359. https://doi.org/10.1144/gsl.sp.2007.272.01.18

Davis, G.H., Reynolds, S.J., Kluth, C.F., 2011. **Structural geology of rocks and regions**. John Wiley & Sons.

Deckart, K., Feraud, G., Marques, L.S., Bertrand, H., 1998. New time constraints on dyke swarms related to the Paraná – Etendeka magmatic province, and subsequent South Atlantic opening, southeastern Brazil. **J. Volcan. Geotherm. Res**., 80, 67–83.

Della Porta, G., 2015. Carbonate build-ups in lacustrine, hydrothermal and fluvial settings: comparing depositional geometry, fabric types and geochemical signature. In: Bosence, D.W.J., Gibbons, K.A., Le Heron, D.P., Morgan, W.A., Pritchard, T., Vining, B.A. (Eds.), Microbial Carbonates in Space and Time: Implications for Global Exploration and Production. vol. 418. **Geological Society, London, Special Publications**, pp. 17–68.

Dias, J.L., 1998. **Análise sedimentológica e estratigráfica do Andar Aptiano em parte da margem leste do Brasil e no Platô das Malvinas** – considerações sobre as primeiras incursões e ingressões marinhas do oceano Atlantico Sul Meridional. PhD Thesis. Programa de Pós-Graduação em Geociências. Universidade Federal do Rio Grande do Sul, Porto Alegre, 411 p.

Dias, J.L., 2005. Tectônica, estratigrafia e sedimentação no Andar Aptiano da margem leste brasileira. **B. Geoci. Petrobras**, Rio de Janeiro, v. 13, n. 1, p. 7-25.

Dias, J.L., 2008. Estratigrafia e sedimentação dos evaporitos neo-aptianos na margem leste brasileira. In: W.U. Mohriak, P. Szatmari, S. Anjos (Orgs.). **Sal**:

Geologia e Tectónica. Exemplos nas Bacias Brasileiras (pp. 223-231). São Paulo: Beca Edições.

Dill, H.G., 2001. The geology of aluminium phosphates and sulphates of the alunite group minerals: a review. **Earth-Science Reviews**, 53(1-2), 35-93.

Direen, N.G., Borissova, I., Stagg, H.M.J., Colwell, J.B., Symonds, P.A., 2007. Nature of the continent–ocean transition zone along the southern Australian continental margin: A comparison of the Naturaliste Plateau, SW Australia, and the central Great Australian Bight sectors, in Karner, G.D., et al., eds., Imaging, Mapping and Modelling Continental Lithosphere Extension and Breakup: **Geological Society of London Special Publications**, v. 282, p. 239–264.

Doebbert, A., Johnson, C., Carroll, A., Beard, B., Pietras, J., Rhodes Carson, M., Norsted, B., Throckmorton, L., 2014. Controls on Sr isotopic evolution in lacustrine systems: Eocene green river formation, Wyoming. **Chemical Geology**. 380. 10.1016/j.chemgeo.2014.04.008.

Durand-Riard, P., Caumon, G., Muron, P., 2010. Balanced restoration of geological volumes with relaxed meshing constraints, **Computers & Geosciences**, Volume 36, Issue 4, Pages 441-452, ISSN 0098-3004, https://doi.org/10.1016/j.cageo.2009.07.007.

Ebinger, C., Scholz, C.A., 2012. Continental Rift Basins: The East African Perspective. In **Tectonics of Sedimentary Basins**: Recent Advances (pp. 183-208). John Wiley and Sons Inc. https://doi.org/10.1002/9781444347166.ch9.

Elliott, D., 1983. The construction of balanced cross sections. **Journal of Structural Geology** 5, 101.

Engelmann de Oliveira, C.H., Jelinek, A.R., Chemale Jr., F., Cupertino, J.A., 2016. Thermotectonic history of the southeastern Brazilian margin: evidence from apatite fission track data of the offshore Santos basin and continental basement. **Tectonophysics** 685, 21–34.

Faria, D.L.P, Reis, A.T., Souza Junior, O.S., 2017. Three-dimensional stratigraphic-sedimentological forward modelling of an Aptian carbonate reservoir deposited during the sag stage in the Santos basin, Brazil. **Mar. Pet. Geol.** 88, 676–695. https://doi.org/10.1016/j.marpetgeo.2017.09.013

Farias, F.A., 2018. **Petrogênese de carbonatos acamadados da Formação Barra Velha, Aptiano da Bacia de Santos**: M.Sc. thesis, Universidade Federal do Paraná.

Farias, F., Szatmari, P., Bahniuk, A., França, A. B., 2019. Evaporitic carbonates in the pre-salt of Santos Basin – genesis and tectonic implications. **Mar. Petrol. Geol.** 105, 251–272. https://doi.org/10.1016/j.marpetgeo.2019.04.020.

Faure, G., Barrett, P.J., 1973. Strontium isotope compositions of non-marine carbonate rocks from the Beacon Supergroup of the Transantarctic Mountains, **Journal of Sedimentary Research**, 43 (2): 447–457. https://doi.org/10.1306/74D72793-2B21-11D7-8648000102C1865D.

Ferreira, F.J.F., 1982. Geologia da Bacia do Paraná - Alinhamentos estruturais-magnéticos da região centro-oriental da Bacia do Paraná e seu significado tectônico. In: Paulipetro - Consórcio CESP/IPT (ed.) **Bacia do Paraná**: reavaliação da

potencialidade e prospectividade em hidrocarbonetos. IPT, publicações especiais, 12, 143-166.

Fetter, M., 2009. The role of basement tectonic reactivation on the structural evolution of Campos Basin, offshore Brazil: evidence from 3D seismic analysis and section restoration. **Mar. Pet. Geol.** 26, 873-886. https://doi.org/10.1016/j.marpetgeo.2008.06.005.

Fiduk, J.C., Rowan, M.G., 2012. Analysis of folding and deformation within layered evaporites in Blocks BM--S--8 & --9, Santos Basin, Brazil. **Geological Society, London, Special Publications,** 363, 471–-487. https://doi.org/10.1144/sp363.22

Flügel, E., Munnecke, A., 2010. **Microfacies of carbonate rocks**: analysis, interpretation and application (Vol. 976, p. 2004). Berlin: Springer.

Fodor, R.V., McKee, E.H., Asmus, H.E., 1984. K-Ar ages and the opening of the South Atlantic Ocean: Basaltic rock from the Brazilian margin, **Marine Geology**, Volume 54, Issues 1–2, Pages M1-M8, ISSN 0025-3227, https://doi.org/10.1016/0025-3227(83)90002-6.

Fonte-Boa, T.M.R., Peifer, D., Fonseca, A.C.L., Novo, T.A., 2022. The southeast Brazilian rifted continental margin is not a single, continuous upwarp: Variations in morphology and denudation patterns along the continental drainage divide. **Earth-Science Reviews**, Volume 231, 2022, 104091, ISSN 0012-8252, https://doi.org/10.1016/j.earscirev.2022.104091.

Fossen, H., 2010. **Structural Geology**. Cambridge University Press, Cambridge, 463. https://doi.org/10.1017/CBO9780511777806

França, R.L., Del Rey, A.C., Tagliari, C.V., Brandão, J.R., De Rossi Fontanelli, P., 2007. Bacia do Espírito Santo. **Bol. Geociências Petrobras** 15, 501-509 (in Portuguese).

Franke, D., Barckhausen, U., Baristeas, N., Engels, M., Ladage, S., Lutz, R., Montano, J., Pellejera, N., Ramos, E.G., Schnabel, M., 2011. The continenteocean transition at the southeastern margin of the South China Sea. **Marine and Petroleum Geology.**

Franke, D., 2012. Rifting, lithosphere breakup and volcanism: Comparison of magma-poor and volcanic rifted margins, **Marine and Petroleum Geology**, doi: 10.1016/ j.marpetgeo.2012.11.003.

Fulfaro, V.I., 1974. Tectônica do alinhamento estrutural do Paranapanerna**. Bol. Inst . Geoc.**, Uni!'. São Paulo, S 129-138.

Funck, T., Jackson, H.R., Louden, K.E., Dehler, S.A., Wu, Y., 2004. Crustal structure of the northern Nova Scotia rifted continental margin (eastern Canada). **Journal of Geophysical Research and Solid Earth**, 109.

Galán, E., Pozo, M., 2011. Palygorskite and sepiolite deposits in continental environments. Description, genetic patterns and sedimentary settings. In: **Developments in Clay Science**, vol. 3. Elsevier, pp. 125–173.

Galera, C., Bennis, C., Moretti, I., Mallet, J.L., 2003. Construction of coherent 3D geological blocks. **Computers & Geosciences**, 29(8):971-984.

Gamboa, L.A.P., Machado, M.A.P., Silveira, D.P., Freitas, J.T.R., Silva, S.R.P., 2008. Evaporitos estratificados no Atlântico Sul. In: Mohriak, W.U., Szatmari, P., Anjos, S. (Org.) **Sal geologia e tectônica**: exemplos nas bacias brasileiras. Beca Edições Ltda., p.: 91-163.

Gibbs, A.D., 1984. Structural evolution of extensional basin margins, vol. 141. **Journal of the Geological Society**, London. 609–620.

Gierlowski-Kordesch, E.H., 2010. Lacustrine carbonates. **Developments in sedimentology**, 61, 1-101.

Gierlowski-Kordesch, E.H., Jacobson, A.D., Blum, J.D., Valero Garćes, B.L., 2008. Watershed reconstruction of a Paleocene–Eocene Lake basin using Sr isotopes in carbonate rocks. **GSA Bulletin**; 120 (1-2): 85–95. doi: https://doi.org/10.1130/B26070.1.

Giles, K.A., Rowan, M., 2012. Concepts in halokinetic-sequence deformation and stratigraphy. **Geological Society London Special Publications** 363(1):7-31 DOI: 10.1144/SP363.2.

Gomes, P.O., Kilsdonk, B., Minken, J., Grow, T., Barragan, R., 2008. The outer high of the Santos Basin, Southern São Paulo Plateau, Brazil: pre-salt exploration outbreak, paleogeographic setting, and evolution of the syn-rift structures. In: **American Association of Petroleum Geologists International Conference and Exhibition**, Cape Town, South Africa, October 26-29, 2008, Abstracts CD, 6p.

Gomes, P.O., Kilsdonk, B., Minken, J., Grow, T., Barragan, R., 2009. The Outer High of the Santos Basin, southern São Paulo Plateau, Brazil: pre-salt exploration outbreak, paleogeographic setting, and evolution of the syn-rift structures. In: **AAPG Search and Discovery** Article #10193.

Gomes, P.O., Kildonk, B., Grow, T., Minken, J., Barragan, R., 2012. Tectonic evolution of the outer high of Santos basin, southern Sao Paulo Plateau, Brazil, and implications for hydrocarbon exploration. In: **Tectonics and sedimentation**: Implications for petroleum systems, 100, pp. 125–142. AAPG Memoir.

Gomes, J.P., Bunevich, R.B., Tedeschi, L.R., Tucker, M.E., Whitaker, F.F., 2020. Facies classification and patterns of lacustrine carbonate deposition of the Barra Velha Formation, Santos Basin, Brazilian Pre-salt. **Marine and Petroleum Geology**, v. 113, p. 104-176.

Graça, M.C., Kusznir, N., Stanton, N.S.G., 2019. Crustal thickness mapping of the central South Atlantic and the geodynamic development of the Rio Grande Rise and Walvis Ridge. **Marine and Petroleum Geology**, 101, 230-242.

Groshong, R.H., 2006. 3-D Structural geology: a practical guide to quantitative surface and surface map interpretation. **Springer-Verlag Berlin**, Heidelberg, 400 pp.

Guerra, M.C.M., Underhill, J.R., 2012. Role of halokinesis in controlling structural styles and sediment dispersal in the Santos Basin, offshore Brazil. In: G.I. Alsop, S.G. Archer, A.J. Hartley, N.T Grant, R. Hodgkinson (eds.) Salt tectonics, sediments and prospectivity. **Geological Society, London, Special Publications**, 363, p.: 175-206.

Harris, P.M., 2000. Toca Carbonate, Congo Basin: response to an evolving rift lake. In: Mello, M.R., Katz, B.J. (Eds.), **Petroleum Systems of South Atlantic Margins**. vol. 73. AAPG Memoir, pp. 341–360.

Harris, P.M., Ellis, J., Purkis, S.J., 2013. Assessing the extent of carbonate deposition in early rift settings. **AAPG bulletin**, 97(1), 27-60.

Hart, W.S., Quade, J., Madsen, D.B., Kaufman, D.S., Oviatt, C.G., 2004. The 87Sr/86Sr ratios of lacustrine carbonates and lake-level history of the Bonneville paleolake system. **Geological Society of America Bulletin**, 116(9-10), 1107-1119.

Hasui, Y, Carneiro, C.D.R., Coimbra, A.M., 1975. The Ribeira Folded Belt. **Revista Brasileira de Geociências** 5,257-266.

Hasui Y., Mioto, J.A., 1992. **Geologia Estrutural Aplicada**. ABGE/Votorantim, 462 pp.

Hawkesworth, C.J., Blake, S., Evans, P., Hughes, R., Macdonald, R., Thomas, L.E., Turner, S. P., Zellmer, G., 2000. Time Scales of Crystal Fractionation in Magma Chambers—Integrating Physical, Isotopic and Geochemical Perspectives, **Journal of Petrology**, Volume 41, Issue 7, Pages 991–1006, https://doi.org/10.1093/petrology/41.7.991.

Heilbron, M., Mohriak, W.U., Valeriano, C.M., Milani, E.J., Almeida, J., Tupinambá, M., 2000. From collision to extension: The roots of the southeastern continental margin of Brazil. In **Atlantic rifts and continental margins** (pp. 1–-32). American Geophysical Union. https://doi.org/10.1029/gm115 p0001.

Heilbron, M., Valeriano, C.M., Tassinari, C.C.G., Almeida, J., Tupinambá, M., Siga, O., Trouw, R., 2008. Correlation of Neoproterozoic terranes between the Ribeira Belt, SE Brazil and its African counterpart: comparative tectonic evolution and open questions, in: **Geological Society, London, Special Publications**. pp. 211–237. https://doi.org/10.1144/SP294.12.

Heine, C., Zoethout, J., and Müller, R.D., 2013. Kinematics of the South Atlantic rift, **Solid Earth**, 4, 215–253, https://doi.org/10.5194/se-4-215-2013.

Henry, C.D., Faulds, J.E., dePolo, C.M., 2007. Geometry and timing of strike-slip and normal faults in the northern Walker Lane, northwestern Nevada and northeastern California: Strain partitioning or sequential extensional and strike-slip deformation?, in: S.M. Roeske, A.B. Till, D.A. Foster, J.C. Sample (eds.) **Exhumation Associated with Continental Strike-Slip Fault Systems**.

Herlinger Jr., R., 2016. **Controles deposicionais e diagenéticos das propriedades petrofísicas dos reservatórios Aptianos/Barremianos do Grupo Lagoa Feia no norte da Bacia de Campos**: M.S. thesis, Universidade Federal do Rio Grande do Sul.

Herlinger, R.J., Zambonato, E.E., De Ros, L.F., 2017. Influence of diagenesis on the quality on the quality of lower Cretaceous Pre-Salt lacustrine carbonate reservoirs from northern Campos Basin, offshore Brasil. **J. Sediment. Res.** 87, 1285–1313. https://doi.org/10.2110/jsr.2017.70.

Hossack, J.R., 1979. The use of balanced cross-sections in the calculation of orogenic contraction: A review **Journal of the Geological Society**, 136(6): 705-711.

Hudec, M.R., Jackson, M.P.A., 2007. "Terra infirma: Understanding salt tectonics". **Earth-Science Reviews**, 82 (1–2):1– 28, 2007. doi:10.1016/j.earscirev.2007.01.001. ISSN 0012-8252.

Huismans, R.S., Beaumont, C., 2008. Complex rifted continental margins explained by dynamical models of depth-dependent lithospheric extension. **Geology**; 36 (2): 163–166. doi: https://doi.org/10.1130/G24231A.1

Huismans, R.S., Beaumont, C., 2014. Rifted continental margins: The case for depth-dependent extension, **Earth and Planetary Science Letters**, Volume 407, Pages 148-162, ISSN 0012-821X, https://doi.org/10.1016/j.epsl.2014.09.032.

Ingersoll, R.V., 2011. Tectonics of sedimentary basins, with revised nomenclature. In **Tectonics of Sedimentary basins**: Recent advances. Hoboken, NJ: Wiley, pp. 1–43.

Ingersoll, R.V., Busby, C.J., 1995. Tectonics of sedimentary basins, in Busby, C.J., and Ingersoll, R.V., eds., **Tectonics of sedimentary basins**. Oxford, Blackwell Science, 1–51.

Japsen, P., Bonow, J.M., Green, P.F., Cobbold, P.R., Chiossi, D., Lilletveit, R., Magnavita, L.P., Pedreira, A., 2012. Episodic burial and exhumation in NE Brazil after opening of the South Atlantic. **Bull. Geol. Soc. Am**. 124, 800–816. https://doi.org/10.1130/B30515.1.

Jelinek, A., Chemale Jr., F., van der Beek, P., Guadagnin, F., Cupertino, J., Viana, A., 2014. Denudation history and landscape evolution of the northern east-Brazilian continental margin from apatite fission-track thermochronology. **J. S. Am. Earth Sci.** 54, 158–181.

Jenkyns, H.C., Paull, C.K., Cummins, D.I., Fullagar, P.D., 1995. Strontium isotope stratigraphy of lower cretaceous atoll carbonates in the mid-pacific mountains. In: Winterer, E.L., Sager, W.W., Firth, J.V., Sinton, J.M. (Eds.), **Proceedings of the Ocean Drilling Program, Scientific Results** 143. Texas A & M University, Ocean Drilling Program, College Station, USA, pp. 89–97.

Jones, B.F., 1986. Clay minerals diagenesis in lacustrine sediments. **US Geological Survey Bulletin**, 1578, 291–300.

Jones, B.F., Naftz, D.L., Spencer, R.J., Oviatt, C.G., 2009. Geochemical evolution of great salt lake, Utah, USA. **Aquatic Geochemistry**, 15, 95-121.

Karner G.D., 2000. Rifts of the Campos and Santos Basins, Southeastern Brazil: distribution and timing. In: M.R. Mello & B.J. Kats (eds.) **Petroleum systems of South Atlantic margins**. AAPG Memoir, 73, p.:301-315.

Karner, G.D., Driscoll, N.W., 1999. Tectonic and stratigraphic development of the West African and eastern Brazilian margins: insights from quantitative basin modelling. In: CAMERON, N.R.; BATE, R.H.; CLURE, V.S. The oil and gas habitats of the South Atlantic. **London: Geological Society, Special Publications**, v. 153, p. 11-40.

Karner, G.D., Gamboa, L.A.P., 2007. Timing and origin of the South Atlantic pre-salt sag basins and their capping evaporites. **Geol. Soc. Lond. Spec. Publ.** 285 (1), 15–35.

Kele, S., Özkul, M., Fórizs, I., Gökgöz, Baykara, M.O., Alçiçek, M.C., Németh, T., 2011. Stable isotope geochemical study of Pamukkale travertines: new evidences of low temperature non-equilibrium calcite-water fractionation. **Sediment. Geol**. 238, 191–212.

Kinabo, B.D., Atekwana, E.A., Hogan, J.P., Modisi, M.P., Wheaton, D.D., Kampunzu, A.B., 2007. Early structural development of the Okavango rift zone, NW Botswana. **Journal of African Earth Sciences**, 48(2-3), 125-136.

Kirstein, L.A., Kelley, S., Hawkesworth, C., Turner, S., Mantovani, M., Wijbrans, J., 2001. Protracted felsic magmatic activity associated with the opening of the South Atlantic. **Journal of the Geological Society**, 158(4), 583-592.

Kowsmann, R.O., Costa, M.P.A., Boa Hora, M.P., Guimarães, P.P., 1982. Geologia estrutural do platô de São Paulo. **32o Cong. Bras. Geol..,** Salvador, BA. Anais, SBG, 4, 1558-1569.

Kukla, P.A., Strozyk, F., Mohriak, W.U., 2018. South Atlantic salt basins – Witnesses of complex passive margin evolution. **Gondwana Research**, 53, 41–-57. https://doi.org/10.1016/j.gr.2017.03.012.

Kumar N., Gamboa L.A.P., 1979. Evolution of the São Paulo plateau (southeastern Brazilian margin) and implications for the early history of South Atlantic. **Geol. Soc. Am. Bull.,** 90:281–293.

Lacey, J.H., Leng, M.J., Francke, A., Sloane, H.J., Milodowski, A., Vogel, H., Baumgarten, H., Wagner, B., 2015. Mediterranean climate since the Middle Pleistocene: a 640 ka stable isotope record from Lake Ohrid (Albania/Macedonia). **Biogeosci. Discuss.** 12 (16), 13427–13481. https://doi.org/10.5194/bgd-12-13427-2015.

Lavier, L.L., Manatshal, G., 2006. A mechanism to thin the continental lithosphere at magma-poor margins. **Nature**, 440:324-328.

Lawson, M., Sitgreaves, J., Rasbury, T., Wooton, K., Esch, W., Marcon, V., Eiler, J., 2022. New age and lake chemistry constraints on the Aptian pre-salt carbonates of the central South Atlantic. **Bulletin**, 135(3-4), 595-607.

Le Pichon, X., İmren, C., Rangin, C., Şengör, A.M.C., Siyako, M., 2014. The South Marmara Fault. **International Journal of Earth Sciences (Geologische Rundschau),** 103, 219–231, http://doi.org/10.1007/s00531-013-0950-0.

Lima, B.E., De Ros, L.F., 2019. Deposition, diagenetic and hydrothermal processes in the Aptian Pre-Salt lacustrine carbonate reservoirs of the northern Campos Basin, offshore Brazil. **Sediment. Geol.** 383, 55–81. https://doi.org/10.1016/j.sedgeo.2019.01.006.

Lima, B.E., Tedeschi, L.R., Pestilho, A.L.S., Santos, R.V., Vasquez, J.C., Guzzo, J.V.P., De Ros, L.F., 2020. Deep-burial hydrothermal alteration of the Pre-Salt carbonate reservoirs from northern Campos Basin, offshore Brazil: evidence from petrography, fluid inclusions, Sr, C and O isotopes. **Mar. Petrol. Geol.** 113.

Lister, G.S., Etheridge, M.A., Symonds, P.A., 1991. Detachment models for the formation of passive continental margins. **Tectonics**, 10(5), 1038-1064.

Lourenço, F.S., Alkmim, F.F., Araujo, M.N.C., Romeiro, M.A.T., Matos, G.C., Crósta,

A.P., 2016. The Piúma lineament, southern Espírito Santo: Structural expression and tectonic significance. **Brazilian Journal of Geology**. 46. 531-546.

Lúcio, T.D.G., Souza, I.A., Vicentelli, M.G.C., 2011. Projeção dos lineamentos Paranapanema e Tietê desde o embasamento aflorante até a bacia submersa – Bacia de Santos. **SBGf - Sociedade Brasileira de Geofísica.**

Macedo J.M., 1987. **Evolução estrutural da Bacia de Santos e áreas continentais adjacentes.** Tese de Doutorado. Universidade Federal de Ouro Preto, 165 p

Macedo J.M., 1989. Evolução tectônica da Bacia de Santos e áreas continentais adjacentes (Tectonic evolution of the Santos Basin and adjacent continental areas). **Bol. Geoc. Petrobras**, 3:159-173.

Maerten, L., Maerten, F., 2006. Chronologic modeling of faulted and fractured reservoirs using geomechanically based restoration: technique and industry applications. **American Association of Petroleum Geologists Bulletin** 90, 1201–1226.

Maerten, L, 2007. Geomechanics to solve structure related issues in petroleum reservoirs. **AAPG European Region Newsletter** 2, 2–3.

Magnavita, L., 2021. **Arquitetura tectônica e cinemática do rifte do SE (com ênfase em Santos).** Webinar Luciano Magnavita. Available in: https://youtu.be/gLY9Ernt7zE Access: sep. 2023.

Magoon, L.B., Dow, W.G., 1994. **The petroleum system**: chapter 1: Part I. Introduction.

Maliva, R.G., 1998. Skeletal aragonite neomorphism — quantitative modelling of a two-water diagenetic system, **Sedimentary Geology**, Volume 121, Issues 3–4, Pages 179-190, ISSN 0037-0738, https://doi.org/10.1016/S0037-0738(98)00080-3.

Manatschal, G., 2004. New models for evolution of magma-poor rifted margins based on a review of data and concepts from West Iberia and the Alps. **International Journal of Earth Sciences**, 93, 432-466.

Maniatis, G., Kurfeß, D., Hampel, A., Heidbach, O., 2009. Slip acceleration on normal faults due to erosion and sedimentation - Results from a new three-dimensional numerical model coupling tectonics and landscape evolution: **Earth and Planetary Science Letters**, v. 284, p. 570–582, https://doi.org/10.1016/j.epsl.2009.05.024.

Mascle, J.R., Renard, V., 1976. The marginal São Paulo Plateau, comparison with the southern Angolan margin. **An. Acad. Bras. Cienc**., 48:179-190.

Masini, M., Bigi, S., Poblet, J., Bulnes, M., Di Cuia, R., Casabianca, D., 2011. Kinematic evolution and strain simulation based on cross-section restoration of the Maiella Mountain: an analogue for oil fields in the Apennines (Italy). In: J. Poblet & R.J. Lisle (eds.) Kinematic evolution and structural styles of fold and trust belts. **Geological Society, London, Special Publications**, 349, p.: 25-44.

Massot, J., 2002. **Implémentation de méthodes de restauration équilibrée**. Tese de doutorado, Institut National Polytechnique de Lorraine, Nancy, France, 157 p.

McArthur, J.M., Howarth, R.J., Shields, G.A., 2012. Chapter 7 – strontium isotope stratigraphy. In: Gradstein, F.M., Ogg, J.G., Schmitz, M.D., Ogg, G.M. (Eds.), **The Geologic Time Scale**. Elsevier, Boston, USA, pp. 127–144.

McCormack, J., Bontognali, T.R.R., Immenhauser, A., Kwiecien, O., 2018. Controls on cyclic formation of Quaternary early diagenetic dolomite. **Geophys. Res. Lett.** 45 (8), 3625–3634. https://doi.org/10.1002/2018GL077344.

McKenzie, D., 1978. Some Remarks on the Development of Sedimentary Basins. **Earth and Planetary Science Letters**, 40:25-32.

Meeuws, F.J., Holford, S.P., Foden, J.D., Schofield, N., 2016. Distribution, chronology and causes of Cretaceous–Cenozoic magmatism along the magma-poor rifted southern Australian margin: Links between mantle melting and basin formation. **Marine and Petroleum Geology**, 73, 271-298.

Meisling, K.E., Cobbold, P.R., Mount, V.S., 2001. Segmentation of an obliquely rifted margin, Campos and Santos basins, southeastern Brazil. **AAPG Bull.** 85 (11), 1903–1924.

Mello, U.T., Karner, G.D., Anderson, R.A., 1995. Role of salt in restraining the maturation of subsalt source rock. **Marine and Petroleum Geology**, 12:697-716.

Melo-Garcia, S.F.D., 2012. **Restauração estrutural da halotectônica na porção central da bacia de Santos e implicações para os sistemas petrolíferos**. Universidade Federal de Ouro Preto.

Mercedes-Martín, R., Rogerson, M.R., Brasier, A.T., Vonhof, H.B., Prior, T.J., Fellows, S.M., Reijmer, J.J.G., Billing, I., Pedley, H.M., 2016. Growing spherulitic calcite grains in saline, hyperalkaline lakes: experimental evaluation of the effects of Mg-clays and organic acids. **Sedimentary Geology**, 335, 93-102.

Mercedes-Martín, R., Ayora, C., Tritlla, J., Sánchez-Román, M., 2019. The hydrochemical evolution of alkaline volcanic lakes: a model to understand the South Atlantic Pre-salt mineral assemblages. **Earth-Science Reviews**, 198, 102938.

Milani, E.J., Brandão, J.A.S.L., Zalán, P.V., Gamboa, L.A.P., 2000. Petróleo na margem continental brasileira: geologia, exploração, resultados e perspectivas. **Revista Brasileira de Geofísica**, 18, 352-396.

Milani, E.J., Rangel, H.D., Bueno, G.V., Stica, J.M., Winter, W.R., Caixeta, J.M., Neto, O.C.P., 2007. Bacias sedimentares brasileiras: cartas estratigráficas – Introdução. **Bol. Geociências Petrobras** 15 (2), 183–198.

Mio, E.D., 2005. **Modelagem crustal da Bacia de Santos pela integração de métodos geofísicos**. Instituto de Geociências da Universidade Estadual Paulista, Rio Claro, São Paulo, p. 94. Thesis (Master).

Mitra, S., 1994. Strain variation in thrust sheets across the Sevier fold and thrust belt (Idaho Utah Wyoming): implications for section restoration and wedge taper evolution. **Journal of Structural Geology** 16, 585-602.

Modica, C.J., Brush, E.R., 2004. Postrift sequence stratigraphy, paleogeography, and fill history of the deep-water Santos Basin, offshore southeast Brazil. **AAPG Bulletin**, [s. l.], v. 88, n. 7, p. 923-945.

Mohn, G., Manatschal, G., Müntener, O., Beltrando, M., Masini, E., 2010. Unravelling the interaction between tectonic and sedimentary processes during lithospheric thinning in the Alpine Tethys margins, **Int. J. Earth Sci**., 99, 75–101, doi:10.1007/s00531-010-0566-6.

Mohriak, W.U., 2001. South Atlantic Ocean Salt Tectonics, Volcanic Centers, Fracture Zones and their relationship with the origin and evolution of the South Atlantic Ocean: geophysical evidence in the Brazilian and West African margins. In: **7th International Congress of the Brazilian Geophysical Society**.

Mohriak, W.U., 2003. Bacias Sedimentares da Margem Continental Brasileira, in: Bizzi, L.A., Schobbenhaus, C., Vidotti, R.M., Gonçalves, J.H. (Eds.), **Geologia, tectônica e recursos minerais do Brasil:** texto, mapas e SIG. Serviço Geológico do Brasil - CPRM, 692p.

Mohriak, W.U., 2004. Recursos energéticos associados à ativação tectônica mesozóico-cenozóica da América do Sul. In: MANTESSO NETO, V. et al. **Geologia do continente sul-americano:** evolução da obra de Fernando Flávio Marques de Almeida. São Paulo: Beca Produções Culturais. Chapter XVIII, p. 293-318.

Mohriak, W.U., Szatmari, P., Anjos, S., 2012. Salt: geology and tectonics of selected Brazilian basins in their global context. In: Alsop, G.I., Archer, S.G., Hartley, A.J., Grant, N.T., Hodgkinson, R. (Eds.), Salt, Tectonics, Sediments and Prospectivity. **Geol. Soc. London Spec. Publ** 363. pp. 131–158.

Mohriak W.U., Paula O.B., 2005. Major tectonic features in the southeastern Brazilian margin. In: **SBGf**, International Congress, 9, Expanded Abstracts, SBGf174.

Mohriak, W.U., Hobbs, R., Dewey, J.F., 1990b. Basin-forming processes and the deep structure of the Campos Basin, offshore Brazil. **Marine and Petroleum Geology**, 7(2):94-122.

Mohriak W.U., Macedo J.M., Castellani R.T., Rangel H.D., Barros A.Z.N, Latgé M.A.L., Ricci J.A., Mizusaki A.M.P., Szatmari P., Demercian L.S., Rizzo J.G. and Aires J.R., 1995. Salt tectonics and structural styles in the deep-water province of the Cabo Frio region, Rio de Janeiro, Brazil. In: M.P.A. Jackson, D.G. Roberts, S. Snelson (eds.) **Salt tectonics**: a global perspective. AAPG Memoir, 65, p.: 273–304.

Mohriak, W.U., Nóbrega, M., Odegard, M.E., Gomes, B.S., Dickson, W.G., 2010. **Geological and geophysical interpretation of the Rio Grande Rise, south-eastern Brazilian margin**: extensional tectonics and rifting of continental and oceanic crusts.

Moreira J.L.P., Carminatti M., 2004. Sistemas deposicionais de talude e bacia no Eoceno da bacia de Santos. **Boletim de Geociências da Petrobras**, 12(1):73-87.

Moreira, J., Madeira, C., Gil, J., Machado, M., 2007. Bacia de Santos. **B. Geoci. Petrobras** 2 (15), 531–549.

Moretti, I., 2008. Working in complex areas: new restoration workflow based on quality control, 2D and 3D restorations. **Marine and Petroleum Geology** 25 (3), 205 -218.

Moretti, I., Lepage, F., Guiton, M., 2006. KINE3D: a new 3D restoration method based on a mixed approach linking geometry and geomechanics. **Oil and Gas Science and Technology** 61 (2), 277-289.

Moulin, M., Aslanian, D., Unternehr, P., 2010. A new starting point for the history of the Equatorial and South Atlantic. **Earth Sci. Rev.** 98, 1–37.

Moulin, M., Aslanian, D., Rabeneau, M., Patriat, M., Matias, L., 2013. Kinematic keys of the Santos–Namibe basins. **Geol. Soc., Lond., Spec. Publ.** 369 (1), 91–107.

Muniz, M.C., Bosence, D.W.J., 2015. Pre-salt microbialites from the Campos Basin (offshore Brazil): image log facies, facies model and cyclicity in lacustrine carbonates. In: Bosence, D.W.J., Gibbons, K.A., Le Heron, D.P., Morgan, W.A., Pritchard, T., Vining, B.A. (Eds.), Microbial Carbonates in Space and Time: Implications for Global Exploration and Production, vol. 418. **Geological Society of London, Special Publication**, pp. 221–242. https://doi.org/10.1144/SP418.10.

Naliboff, J.B., Buiter, S.J.H., Péron-Pinvidic, G., Osmundsen, P.T., Tetreault, J., 2017. Complex fault interaction controls continental rifting. **Nat. Commun.** 8:1179. doi: 10.1038/s41467-017-00904-x

Neat, P.L., Faure, G., Pegram, W.J., 1979. The isotopic composition of strontium in non-marine carbonate rocks: The Flagstaff Formation of Utah. **Sedimentology** 26: 271–282

Neuharth, D., Brune, S., Wrona, T., Glerum, A., Braun, J., Yuan, X., 2022. Evolution of rift systems and their fault networks in response to surface processes. **Tectonics**, 41(3), e2021TC007166.

Nolting, A., Zahm, C.K., Kerans, C., Nikolinakou, M.A., 2018. Effect of carbonate platform morphology on syndepositional deformation: Insights from numerical modeling. **Journal of Structural Geology**, 115, 91-102.

Novais, L.C.C., Teixeira, L.B., Neves, M.T., Rodarte, J.B.M., Almeida, J.C.H., Valeriano, C.M., 2004. Novas ocorrências de diques de diabásio na faixa Colatina – ES: estruturas rúpteis associadas e implicações tectônicas para as bacias de Campos e do Espírito Santo. **Boletim de Geociências da Petrobras**, 12(1):191-194.

Ojeda, H.A.O., 1982. Structural framework, stratigraphy and evolution of Brazilian marginal basins. **Am. Assoc. Petrol. Geol. Bull**. 66, 732-749.

Ojiambo, S.B., Lyons, W.B., Welch, K.A., Poreda, R.J., Johannesson, K.H., 2003. Strontium isotopes and rare earth elements as tracers of groundwater–lake water interactions, Lake Naivasha, Kenya. **Applied Geochemistry**, 18(11), 1789-1805.

Oreiro, S.G., Cupertino, J.A., Szatmari, P., Thomaz Filho, A., 2008. Influence of pre-salt alignments in post-Aptian magmatism in the Cabo Frio High and its surroundings, Santos and Campos basins, SE Brazil: an example of non-plume-related magmatism. **J. South Am. Earth Sci.**, 25:116-131

Osmundsen, P.T., Sommaruga, A., Skilbrei, J.R., Olesen, O., 2002. Deep structure of the Mid Norway rifted margin. **Norwegian Journal of Geology/Norsk Geologisk Forening**, 82(4).

Papaterra, G.E.Z., 2010. **Pré-sal: Conceituação Geológica sobre uma Nova Fronteira Exploratória no Brasil**. Master thesis. UFRJ, Rio de Janeiro. Brasil (in Portuguese).

Pedrosa-Soares, A.C., Alkmim, F.F., Tack, L., Noce, C.M., Babinski, M., Silva, L.C., Martins-Neto, M., 2008. Similarities and differences between the Brazilian and African counterparts of the Neoproterozoic Araçuaí–West Congo Orogen. In: Pankhurst, J.R., Trouw, R.A.J., Brito Neves, B.B., De Wit, M.J. (Eds.), West Gondwana: Pre-Cenozoic Correlations across the South Atlantic Region. **Geological Society, London, Special Publications,** 294, pp. 153–172.

Pereira, M.J., Feijó, F.J., 1994. Bacia de Santos. Estratigrafia das Bacias Sedimentares do Brasil. **Bol. Geociências Petrobras** 8, 219–234.

Peron-Pinvidic, G., Manatschal, G., Osmundsen, P.T., 2013. Structural comparison of archetypal Atlantic rifted margins: a review of observations and concepts. **Mar. Petrol. Geol.** 43, 21–47.

Peron-Pinvidic, G., Manatschal, G., et al., 2019. Rifted Margins: State of the Art and Future Challenges. **Front. Earth Sci.** 7 https://doi.org/10.3389/feart.2019.00218.

Peterman, Z.E., Hedge, C.E., Tourtelot, H.A., 1970. Isotopic composition of strontium in sea water throughout Phanerozoic time. **Geochimica et Cosmochimica Acta**, 34(1), 105-120.

Petersen, K.D., Schiffer, C., 2016. Wilson cycle passive margins: control of orogenic inheritance on continental breakup. **Gondwana Res**. 39, 131–144. https://doi.org/10.1016/j.gr.2016.06.012.

Pietzsch, R., Oliveira, D M., Tedeschi, L.R., Neto, J.V.Q., Figueiredo, M.F., Vazquez, J.C., de Souza, R.S., 2018. Palaeohydrology of the lower cretaceous pre-salt lacustrine system, from rift to post-rift phase, Santos Basin, Brazil. **Palaeogeogr. Palaeoclimatol. Palaeoecol.** 507, 60–80.

Pietzsch, R., Tedeschi, L.R., Oliveira, D.M., Anjos, C.W.D., Vazquez, J.C., Figueiredo, M.F., 2020. Environmental conditions of deposition of the Lower Cretaceous lacustrine carbonates of the Barra Velha Formation, Santos Basin (Brazil), based on stable carbon and oxygen isotopes: a continental record of pCO2 during the onset of the Oceanic Anoxic Event 1a (OAE 1a) interval? **Chem. Geol.** 535.

Planke, S., Eldholm, O., 1994. Seismic response and construction of seaward dipping wedges of flood basalts: Vøring volcanic margin. **Journal of Geophysical Research: Solid Earth**, 99(B5), 9263-9278.

Platt, N.H., Wright, V.P., 1991. Lacustrine carbonates: facies models, facies distributions and hydrocarbon aspects. In: Anadon, P, Cabrera, L.L. & Kelts, K. (eds) Lacustrine Facies Analysis**. International Association of Sedimentologists, Special Publications**, 13, 57–74.

Ponte, F.C., Asmus, H.E., 1976. The Brazilian margin basins-current state of knowledge. **Anais da Academia Brasileira de Ciências**, Rio de Janeiro, v. 48, supl., p. 215-240.

Ponte, F.C., Asmus, H.E., 1978. Geological framework of the Brazilian continental margin. **Geol. Rundsch**. 67, 201-235.

Pozo, M., Calvo, J.P., 2018. An overview of authigenic magnesian clays. **Minerals** 8 (520), 1–22.

Quirk, D.G., Hertle, M., Jeppesen, J.W., Raven, M., Mohriak, W.U., Kann, D.J., Nørgaard, M., Howe, M.J., Hsu, D., Coffey, B., Mendes, M.P., 2013. Rifting, subsidence and continental break-up above a mantle plume in the central South Atlantic. **Geological Society, London, Special Publications**, 369, 185-214. https://doi.org/10.1144/sp369.20

Ramsay, J.G., Huber, M.I., 1984. **The Techniques of Modern Structural Geology, Volume 1**: Strain Analysis. Academic Press.

Renne, P.R., Ernesto, M., Pacca, I.G., Coe, R.S., Glen, J.M., Prévot, M., Perrin, M., 1992. The age of Paraná flood volcanism, rifting of Gondwanaland, and the Jurassic-Cretaceous boundary. **Science**, 258(5084), 975-979.

Renne, P.R., Glen, J.M., Milner, S.C., Duncan, A.R., 1996. Age of Etendeka flood volcanism and associated intrusions in southwestern Africa. **Geology**, 24(7), 659-662.

Rhodes, M.K., Carroll, A.R., Pietras, J.T., Beard, B.L., Johnson, C.M., 2002. Strontium isotope record of paleohydrology and continental weathering, Eocene Green River Formation, Wyoming. **Geology**, 30(2), 167-170.

Riccomini, C., 1995. Padrão de fraturamentos do maciço alcalino de Cananéia, estado de São Paulo: relações com a tectônica mesozóica do sudeste do Brasil. **Revista Brasileira de Geociências**, 25(2), 79-84.

Riccomini, C., Sant'anna, L.G., Tassinari, C.C.G., 2012. Pré-sal: geologia e exploração. **Revista USP**, [s. l.], n. 95, p. 33-42.

Ricketts, J., Amato, J., Gavel, M., 2021. The origin and tectonic significance of the Basin and Range–Rio Grande rift boundary in southern New Mexico, USA. **GSA Today**, 31(10), 4-10.

Roure, F., Swennen, R., Schneider, F., Faure, J.L., Ferket, H., Guilhaumou, N., Osadetz, K., Robion, P., Vandeginste, V., 2005. Incidence and importance of tectonics and natural fluid migration on reservoir evolution in foreland foldand- thrust belts. **Oil & Gas Science and Technology** 60, 67-106.

Rowan, M.G., 1993. A systematic technique for the sequential restoration of salt structures. **Tectonophysics**, 228:331-348.

Rowan, M.G., Kligfield, R., 1989. Cross section restoration and balancing as aid to seismic interpretation in extensional terranes. **AAPG Bulletin**, 73:955–966.

Sabato-Ceraldi, T., Green, D., 2016. Evolution of the South Atlantic Lacustrine deposits in response to Early Cretaceous rifting, subsidence and lake hydrology. In: Sabato Ceraldi, T., Hodgkinson, R.A., Backe, G. (Eds.), Petroleum Geoscience of the West African Margin. **Geological Society, London, Special Publications**, p. 438.

Saller, A., Rushton, S., Buambua, L., Inman, K., McNeil, R., Dickson, J. T., 2016. Presalt stratigraphy and depositional systems in the Kwanza Basin, offshore Angola. **AAPG (Am. Assoc. Pet. Geol.) Bull**. 100 (7), 1135–1164.

Sans, M., Vergès, J., Gomis, J.M., Parès, J.M., Schiatarella, M., Travé, A., Doulcet, A., 1999. Layer parallel shortening in salt-detached folds: constraints on crosssection restoration. In: **Thrust Tectonics**, vol. 99. Royal Holloway University of London, pp. 321-324.

Santi, M.R., 2002. **Procedimentos Computacionais para o Balanceamento de Seções Geológicas.** Tese de Doutorado. Departamento de Engenharia Civil, Pontifica Universidade Católica do Rio de Janeiro, Rio de Janeiro.

Santi, M.R., Campos, J.L.E., Martha, L.F., 2002. A finite element approach for geological section reconstruction. In: **Gocad Meeting**, 22, Proceedings.

Santiago, R.M, Caxito, F.A., Neves, M.A., Dantas, E.L., Medeiros Júnior, E.B., Queiroga, G.N., 2020. Two generations of mafic dyke swarms in the Southeastern Brazilian coast: reactivation of structural lineaments during the gravitational collapse of the Araçuaí-Ribeira Orogen (500 Ma) and West Gondwana breakup (140 Ma), **Precambrian Research**, Volume 340, 105344, ISSN 0301-9268, https://doi.org/10.1016/j.precamres.2019.105344.

Sartorato, A.C.L., Tonietto, S.N., Pereira, E., 2020. Silicification and dissolution features in the brazilian Pre-salt Barra Velha formation: impacts in the reservoir quality and insights for 3D geological modeling. In **Rio Oil & Gas Expo and Conference** (pp. 1-3).

Schultz-Ela, D.D., 1992. Restoration of cross-sections to constrain deformation processes of extensional terranes. **Marine and Petroleum Geology**, 9:372-388.

Şengör, A.M.C., 2016. The structural evolution of the Albula Pass region, Graubünden, eastern Switzerland: the origin of the various vergences in the structure of the Alps. **Canadian Journal of Earth Sciences**, 53, 1279–1311.

Şengör, A.M.C., Görür, N., Şaroğlu, F., 1985. Strike-slip faulting and related basin formation in zones of tectonic escape: Turkey as a case study. In: BIDDLE, K.T. & CHRISTIE-BLICK, N. (eds) Strike-slip Deformation, Basin Formation, and Sedimentation. **Society of Economic Paleontologists and Mineralogists, Special Publications**, 37, 227–264.

Shaban, S.N., Scholz, C.A., Muirhead, J.D., Wood, D.A., 2021. The stratigraphic evolution of the Lake Tanganyika Rift, East Africa: Facies distributions and paleo-environmental implications. **Palaeogeography, Palaeoclimatology, Palaeoecology**, 575, 110474.

Silva, M.D.A., 2021. **Caracterização e análise estrutural do Campo de Tupi, Bacia de Santos**. Trabalho de Conclusão de Curso. Universidade Federal do Rio de Janeiro.

Sommer, V.P., Kuchle, J., De Ros, L.F., 2022. Seismic stratigraphic framework and seismic facies of the Aptian Pre-salt Barra Velha Formation in the Tupi Field, Santos Basin, Brazil. **Journal of South American Earth Sciences**, 118, 103947.

Souza, I.A., Ebert, H.D., Castro, J.C., Silva, G.H.T., 2007. A influência das falhas de transferência na porção norte da Bacia de Santos na formação de armadilhas capazes de conter hidrocarbonetos. **4◦ PDPETRO**, Campinas, SP, 1.1.0063-1 – 2.

Souza, R.S., Arienti, L.M., Viana, S.M., Falcão, L.C., Cuglieri, M.A., Silva Filho, R.P., Leite, C.O., Oliveira, V.C., Oliveira, D.M., Anjos, C., Amora, R., Carmo, I.D., Coelho, C.E., 2018. Petrology of the hydrothermal and evaporitic continental Cretaceous (Aptian) pre-salt carbonates and associated rocks, South Atlantic Santos Basin, offshore Brazil. In: **AAPG Annual Convention & Exhibition 2018**, Salt Lake City, Utah.

Stanton, N.S.G., Schmitt, R.S., 2007. Cronologia relativa das estruturas rúpteis e diques Meso-cenozóicos na porção onshore do Alto do Cabo Frio – região costeira e ilhas adjacentes, RJ. Resumos expandidos, **X Simpósio Nacional de Estudos Tectônicos – SNET**, Natal, RN.

Stanton, N., Ponte-Neto, C., Bijani, R., Masini, E., Fontes, S., Flexor, J.M., 2014. A geophysical view of the Southeastern Brazilian margin at Santos Basin: insights into rifting evolution. **J. S. Am. Earth Sci**. 55, 141–154.

Stern, R.J., Johnson, P.R., 2019. Constraining the opening of the Red Sea: Evidence from the Neoproterozoic margins and Cenozoic magmatism for a volcanic rifted margin. **Geological setting, palaeoenvironment and archaeology of the Red Sea**, 53-79.

Stewart K.S., Turner S., Kelley C.J., Hawkesworth C.J., Kirstein L., Mantovani M.S.M., 1996. 3-D $^{40}$Ar-$^{39}$Ar geochronology in the Paraná flood basalt province. **Earth Planet. Sci. Lett.,** 143:95-110.

Stica, J.M., Zalán, P.V., Ferrari, A.L., 2014. The evolution of rifting on the volcanic margin of the Pelotas Basin and the contextualization of the Paraná-Etendeka LIP in the separation of Gondwana in the South Atlantic. **Marine and Petroleum Geology** 50, p. 1-21.

Strozyk, F., Back, S., Kukla, P.A., 2017. Comparison of the rift and post-rift architecture of conjugated salt and salt-free basins offshore Brazil and Angola/Namibia, South Atlantic. **Tectonophysics**, 716, 204-224.

Szatmari, P., Milani, E.J., 2016. Tectonic control of the oil-rich large igneous carbonate-salt province of the South Atlantic rift. **Mar. Petrol. Geol.** 77, 567–596.

Talbot, M.R., 1990. A review of the palaeohydrological interpretation of carbon and oxygen isotopic ratios in primary lacustrine carbonates. **Chem. Geol. Isot. Geosci**. 80 (4), 261–279 (Amsterdam).

Talbot, M.R., Kelts, K., 1990. Paleolimnological signatures from carbon and oxygen isotopic ratios in carbonates from organic carbon-rich lacustrine sediments. In: KATZ, B. J. Lacustrine Basin Exploration: Case Studies and Modern Analogs. [S.l.]: **American Association of Petroleum Geologists**, p. 99-112. (Memoir series, 50).

Tedeschi, L. R., 2017. Doctor of Philosophy Thesis in: **Lower Cretaceous Climate Records and the Correlation between Marine and Lacustrine Settings (Europe and South America)**. University of Oxford.

Terra, G.J.S., Spadini, A.R., Franca, A.B., Sombra, C.L., Zambonato, E.E., Juschaks, L.C.S., Arienti, L.M., Erthal, M.M., Blauth, M., Franco, M.P., Matsuda, N.S., Da Silva, N.G.C., Moretti Jr., P.A., D'Avila, R.S.F., De Souza, R.S., Tonietto, S.N., Dos Anjos, S.M.C., Campinho, V.S., Winter, W.R., 2010. Classificação de rochas carbonáticas aplicável às bacias sedimentares brasileiras. **Bol. Geociências Petrobras** 18, 9–29.

Tetzner, W., Almeida, J.C.H., 2003. Registros da abertura do oceano Atlântico Sul no Cabo de Búzios: os diques toleíticos. Anais do **IX Simpósio Nacional de Estudos Tectônicos**, Búzios, RJ, 250-253.

Thompson, D.L., Stilwell, J.D., Hall, M., 2015. Lacustrine carbonate reservoirs from Early Cretaceous rift lakes of Western Gondwana: Pre-salt coquinas of Brazil and West Africa. **Gondwana Research**, 28(1), 26-51.

Tiab, D., Donaldson, E.C., 2016. Chapter 8 - Naturally Fractured Reservoirs, Editor(s): Djebbar Tiab, Erle C. Donaldson, **Petrophysics** (Fourth Edition), Gulf Professional Publishing, Pages 415-481, ISBN 9780128031889, https://doi.org/10.1016/B978-0-12-803188-9.00008-5.

Titeux, M.O., 2009. **Restauration et incertitudes structurales: changement d'échelles des propriétés mécaniques et gestion de la tectonique salifère.** Tese de Doutorado, Institut National Polytechnique de Lorraine, 205p.

Torsvik, T.H., Rousse, S., Smethurst, M.A., 2009. A new scheme for the opening of the South Atlantic Ocean and the dissection of an Aptian salt basin. **Geophys. J. Int.** 183, 29-34. https://doi.org/10.1111/j.1365-246X.2010.04728.x

Tosca, N.J., Macdonald, F.A., Strauss, J.V., Johnston, D.T., Knoll, A.H., 2011. Sedimentary talc in Neoproterozoic carbonate successions. **Earth and Planetary Science Letters**, 306(1-2), 11-22.

Tosca, N.J., Masterson, A.L., 2014. Chemical controls on incipient Mg-silicate crystallisation at 258C: implications for early and late diagenesis. **Clay Miner.** 49, 165–194.

Tosca, N.J., Wright, V.P., 2018. Diagenetic pathways linked to labile Mg-clays in lacustrine carbonate reservoirs: a model for the origin of secondary porosity in the cretaceous pre-salt Barra Velha Formation, offshore Brazil. **Geol. Soc. Lond. Spec. Publ.** 435, 33–46.

Trouw, R.A.J., Heilbron, M., Ribeiro, A., Valeriano, C., Paciullo, F., Almeida J.C.H., Tupinambá, M., 2000. The Central Segment of the Ribeira belt. In: Cordani U., Milani E., Thomaz-Filho A., Campos D. (eds.). **Geotectonics of South America**. Rio de Janeiro, CPRM, v. 1, p. 287-310.

Tucker, M.E., Dias-Brito, D., 2017. **Petrologia sedimentar carbonática**: iniciação com base no registro geológico do Brasil. Rio Claro, Obra: UNESP-IGCE-Unispetro, 208.

Turner, S., Regelous, M., Kelley, S., Hawkesworth, C., Mantovani, M., 1994. Magmatism and continental break-up in the South Atlantic: high precision $^{40}Ar$-$^{39}Ar$ geochronology. **Earth Planet. Sci. Lett.** 121, 333–348. https://doi.org/10.1016/0012-821X(94)90076-0

Tutolo, B.M., Tosca, N.J., 2018. Experimental examination of the Mg-silicate-carbonate system at ambient temperature: implications for alkaline chemical sedimentation and lacustrine carbonate formation. **Geochim. Cosmochim. Acta** 225, 80–101.

VanderLeest, R.A., Fosdick, J.C., Malkowski, M.A., Romans, B.W., Ghiglione, M.C., Schwartz, T.M., Sickmann, Z.T., 2022. Tectonic subsidence modeling of diachronous transition from backarc to retroarc basin development and uplift during Cordilleran orogenesis, Patagonian-Fuegian Andes. **Tectonics**, 41, e2021TC006891. https://doi.org/10.1029/2021TC006891

Valente, S.C., Dutra, T., Heilbron, M., Corval, A., Szatmari, P., 2009. Litogeoquímica de diques de diabásio da Faixa Colatina, ES. **Geochimica Brasiliensis**, 23(2), 177-192.

Van Hinte, J.E., 1978. Geohistory analysis - Application of micropaleontology in exploration geology. **American Association of Petroleum Geologists Bulletin**, 62, 201–222

Vendeville, B.C., Jackson, M.P.A., 1993. Some dogmas in salt tectonics challenged by modeling. In: **AAPG International Hedberg Research Conference**, Abstract Volume, p. 163–165.

Vieira, A.C., 2009. **Petrogênese e contexto geodinâmico das suítes basalticas toleíticas (de alto $TiO_2$ e baixo $TiO_2$) do Cretáceo inferior da porção centro-oriental do Enxame de Diques da Serra do Mar.** Tese de Doutorado, Faculdade de Geologia, Universidade do Estado do Rio de Janeiro, 244 p.

Vieira, R.A.B., Mendes, M.P., Vieira, P.E.C, Tagliari C.V., Bacelar, L.A.P., Feijó, F. J., 1994. Bacias do Espírito Santo e Mucuri. **Bol. Geoc. Petrobras**, 8, 195-202.

Vincentelli, M.G.C., Neves, M., Morales, N., 2016. Controle estrutural do Neógeno e Quaternário nas bacias de Campos e do Espírito Santo. São Paulo, UNESP, **Geociências**, v. 35, n. 1, p.47-62.

Wang, Y., Cerling, T. E., 1994. A model of fossil tooth and bone diagenesis: implications for paleodiet reconstruction from stable isotopes. **Palaeogeography, Palaeoclimatology, Palaeoecology,** 107(3-4), 281-289.

Watkins, J.M., Nielsen, L.C., Ryerson, F.J., DePaolo, D.J., 2013. The influence of kinetics on the oxygen isotope composition of calcium carbonate. **Earth Planet. Sci. Lett.** 375, 349–360.

Watkins, J.M., Hunt, J.D., Ryerson, F.J., DePaolo, D.J., 2014. The influence of temperature, pH, and growth rate on the δ18O composition of inorganically precipitated calcite. **Earth Planet. Sci. Lett.** 404, 332–343.

Weijermars, R., Jackson, M.P.A., Vendeville, B.C., 1993. Rheological and tectonic modelling of salt province. **Tectonophysics** 217, 143-174.

Weissel, J.K., Karner, G.D., 1989. Flexural uplift of rift flanks due to mechanical unloading of the lithosphere during extension. **Journal of Geophysical Research: Solid Earth,** 94(B10), 13919-13950.

Wennberg, O.P., McQueen, G., de Luca, P.V., Lapponi, F., Hunt, D., Chandler, A.S., Waldum, A., Camargo, G.N., Castro, E., Loures, L., 2021. Open fractures in pre-salt

silicified carbonate reservoirs in block BM-C-33, the Outer Campos Basin, offshore Brazil. **Petrol. Geosci.** 27 (4), petgeo2020–p2125.

Wernicke, B., 1985. Uniform-sense normal simple shear of the continental lithosphere. **Canadian Journal of Earth Sciences**, [s. l.], v. 22, ed. 1, p. 108-125.

White, W.M., 2013**. Geochemistry** / William M. White. Wiley-Blackwell.

White, R., Mckenzie, D., 1989. Magmatism at rift zones: The generation of volcanic continental margins and flood basalts. **JGR Solid Earth**, [s. l.], v. 94, ed. B6, p. 7685-7729.

Whiticar, M.J., Suess, E., 1998. The Cold Carbonate Connection Between Mono Lake, California and the Bransfield Strait, Antarctica. **Aquatic Geochemistry**, 4(3), 429-454.

Wickham, J., Moeckel, G., 1997. Restoration of structural cross-sections. **J. Struct. Geol.,** 19:975-986.

Wildman, M., 2015. **Reassessing the structural and geomorphic evolution of a 'classic' Atlantic type passive margin: an integrated study of the Namaqualand sector of the South African continental margin**. PhD thesis.

Winter, W.R., Jahnert, R.J., França, A.B., 2007. Bacia de Campos. **Boletim de Geociências da Petrobrás**, 15 (2): 511-529.

Woodcock, N.H., Fischer, M., 1986. Strike-slip duplexes. **Journal of Structural Geology** 8, 725–735.

Woodward N.B., Gray D.R., Spears D.B., 1986. Including strain in balanced cross sections. Journal of Structural Geology, 8(4):313-324.Wright, V. P., 2012. Lacustrine carbonates in rift settings: the interaction of volcanic and microbial processes on carbonate deposition. In: Garland, J., Neilson, J.E., Laubach, S., Whidden, K.J. (Eds.), Advances in Carbonate Exploration and Reservoir Analysis, vol. 370. **Geological Society of London, Special Publications**, pp. 39–47.

Wright, V.P., 2012. Lacustrine carbonates in rift settings: the interaction of volcanic and microbial processes on carbonate deposition. In: Garland, J., Neilson, J. E., Laubach, S., Whidden, K. J. (Eds.), Advances in Carbonate Exploration and Reservoir Analysis, vol. 370. **Geological Society of London, Special Publications**, pp. 39–47.

Wright, V.P., Barnett, A.J., 2015. An abiotic model for the development of textures in some South Atlantic Early Cretaceous lacustrine carbonates. In: Grotzinger, J.P., James, N. (Eds.), Microbial Carbonates in Space and Time: Implications for Global Exploration and Production, vol. 418. **The Geological Society of London, Special Publication**, pp. 209–219.

Wright, V.P., Barnett, A.J., 2017. Critically Evaluating the Current Depositional Models for the Pre-salt Barra Velha Formation. In: **Offshore Brazil**. AAPG Search and Discovery. Article #51439.

Wright, V.P., Barnett, A.J., 2020. The textural evolution and ghost matrices of the Cretaceous Barra Velha Formation carbonates from the Santos Basin, offshore Brazil. **Facies** 66, 7.

Yamamoto, K., Ishibashi, M., Takayanagi, H., Asahara, Y., Sato, T., Nishi, H., Iryu, Y., 2013. Early Aptian paleoenvironmental evolution of the bab basin at the southern Neo-tethys margin: response to global carbon-cycle perturbations across ocean anoxic event 1a. **Geochem. Geophys. Geosyst**. 14 (4), 1104–1130.

Ysaccis, R., El-Toukhy, M., Moreira, L., 2019. Maximizing the value of seismic data for a better regional understanding and exploration assessment in the Santos Basin. In: **Brazil**: Brazilian Geophysical Society, 16th International Congress, Proceedings, pp. 1–6.

Zalán P. V., Oliveira J.A.B., 2005. Origem e evolução estrutural do sistema de riftes cenozóicos do Sudeste do Brasil. **Boletim de Geociências da Petrobras**, 13(2):269-300.

Zalán, P.V., Severino, M.C.G., Rigoti, C.A., Magnavita, L.P., Oliveira, J.A.B., Vianna, A.R., 2011. An entirely new 3D-view of the crustal and mantle structure of a South Atlantic passive margin – Santos, Campos and Espírito Santo basins, Brazil. In: **AAPG Annual Conference and Exhibition**, vol. 13. AAPG, Houston, Texas, USA.

Zhao, Y., Zou, H., Li, N., Wei, W., Yuan, C., Fan, Q., Zhang, X., 2020. Petrogenesis of late Cenozoic basalts from Dalinor, Inner Mongolia: Implications for lateral mantle heterogeneity in eastern China. **Lithos**, 366-367, 105561.

# Appendix A – Supplementary material

Table A-1: Results from ICP-OES and parameters for final calculation of Ca, Fe, Mg, Mn, Rb and Sr concentrations in ppm.

| Sample | m1 | m2 | m3 | m4 | m5 | m4+m5 | Ca | Fe | Mg | Mn | Rb | Sr | Ca | Fe | Mg | Mn | Rb | Sr |
|---|---|---|---|---|---|---|---|---|---|---|---|---|---|---|---|---|---|---|
| depth (m) | (in g, which equals to mL) | | | | | | in ppm, prior to calculation | | | | | | in ppm, as final concentration | | | | | |
| 5081,5 | 1,174 | 0,011 | 0,983 | 0,507 | 9,436 | 9,943 | 118,9 | 0,31 | 42,19 | 0,39 | 0,27 | 1,42 | 110483 | 288 | 39203 | 362 | 251 | 1319 |
| 5085,9 | 1,174 | 0,012 | 0,979 | 0,506 | 9,5 | 10,006 | 182,2 | 0,47 | 32,77 | 0,95 | 0,42 | 1,48 | 154493 | 399 | 27787 | 806 | 356 | 1255 |
| 5089 | 1,198 | 0,009 | 0,98 | 0,505 | 9,427 | 9,931 | 166 | 0,31 | 10,39 | 0,4 | 0,39 | 1,06 | 175384 | 328 | 10977 | 423 | 412 | 1120 |
| 5095,1 | 1,176 | 0,009 | 0,978 | 0,52 | 9,526 | 10,046 | 164,8 | 0,07 | 10,85 | 0,22 | 0,38 | 1,39 | 178021 | 76 | 11720 | 238 | 410 | 1502 |
| 5098 | 1,197 | 0,01 | 0,981 | 0,503 | 9,437 | 9,940 | 82,51 | 0,23 | 39,76 | 0,23 | 0,19 | 0,75 | 86332 | 241 | 41602 | 241 | 199 | 785 |
| 5102,8 | 1,195 | 0,012 | 0,98 | 0,504 | 9,486 | 9,990 | 187,5 | 0,32 | 38,76 | 0,12 | 0,43 | 1,89 | 161475 | 276 | 33380 | 103 | 370 | 1628 |
| 5107,3 | 1,174 | 0,009 | 1,006 | 0,498 | 9,462 | 9,960 | 126,9 | 0,11 | 14,92 | 0,15 | 0,29 | 1,16 | 140435 | 122 | 16511 | 166 | 321 | 1284 |
| 5109,4 | 1,168 | 0,009 | 0,993 | 0,5 | 9,476 | 9,976 | 142,7 | 0,11 | 13,21 | 0,16 | 0,32 | 1,55 | 161767 | 125 | 14975 | 181 | 363 | 1757 |
| 5114,3 | 1,174 | 0,009 | 0,981 | 0,505 | 9,481 | 9,987 | 143,8 | 0,08 | 7,3 | 0,08 | 0,32 | 1,14 | 166985 | 93 | 8477 | 93 | 372 | 1324 |
| 5114,4 | 1,176 | 0,011 | 0,988 | 0,507 | 9,54 | 10,047 | 170,9 | 0,13 | 12,88 | 0,12 | 0,39 | 1,24 | 157524 | 120 | 11872 | 111 | 359 | 1143 |
| 5122,6 | 1,157 | 0,012 | 0,981 | 0,504 | 9,542 | 10,046 | 199,4 | 0,17 | 26,86 | 0,09 | 0,44 | 1,75 | 169759 | 145 | 22867 | 77 | 375 | 1490 |
| 5124 | 1,175 | 0,009 | 0,981 | 0,501 | 9,466 | 9,966 | 111,5 | 0,18 | 51,54 | 0,06 | 0,25 | 0,72 | 119490 | 193 | 55233 | 64 | 268 | 772 |
| 5135,7 | 1,176 | 0,011 | 0,981 | 0,505 | 9,532 | 10,037 | 129,8 | 0,21 | 34,9 | 0,09 | 0,29 | 1,23 | 121751 | 197 | 32736 | 84 | 272 | 1154 |
| 5137 | 1,156 | 0,009 | 0,981 | 0,502 | 9,498 | 10,000 | 123,9 | 0,16 | 30,23 | 0,12 | 0,29 | 1,11 | 140794 | 182 | 34352 | 136 | 330 | 1261 |
| 5138,9 | 1,167 | 0,011 | 0,981 | 0,508 | 9,558 | 10,066 | 177,9 | 0,29 | 19,41 | 0,24 | 0,42 | 1,12 | 167354 | 273 | 18259 | 226 | 395 | 1054 |
| 5147 | 1,167 | 0,009 | 0,981 | 0,502 | 9,535 | 10,038 | 79,96 | 1,15 | 39,7 | 0,18 | 0,19 | 0,81 | 88199 | 1268 | 43790 | 199 | 210 | 893 |
| 5148,5 | 1,177 | 0,012 | 0,981 | 0,507 | 9,481 | 9,989 | 173,5 | 0,34 | 33,34 | 0,45 | 0,41 | 1,35 | 144417 | 283 | 27751 | 375 | 341 | 1124 |
| 5151,8 | 1,19 | 0,012 | 0,981 | 0,493 | 9,492 | 9,985 | 211,1 | 0,59 | 11,58 | 0,17 | 0,5 | 1,28 | 178637 | 499 | 9799 | 144 | 423 | 1083 |
| 5156,8 | 1,176 | 0,011 | 0,981 | 0,587 | 9,46 | 10,047 | 188,8 | 0,22 | 16,91 | 0,27 | 0,45 | 1,52 | 167867 | 196 | 15035 | 240 | 400 | 1351 |
| 5158,8 | 1,177 | 0,012 | 0,981 | 0,506 | 9,507 | 10,012 | 154,3 | 3,82 | 10,23 | 0,14 | 0,37 | 0,82 | 134339 | 3326 | 8907 | 122 | 322 | 714 |
| 5160,3 | 1,194 | 0,009 | 0,981 | 0,505 | 9,543 | 10,048 | 138,9 | 0,64 | 23,06 | 0,14 | 0,33 | 1,2 | 158603 | 731 | 26331 | 160 | 377 | 1370 |
| 5166 | 1,167 | 0,009 | 0,981 | 0,504 | 9,574 | 10,078 | 69,25 | 0,19 | 20,71 | 0,02 | 0,16 | 0,43 | 74245 | 204 | 22204 | 21 | 172 | 461 |
| 5168,3 | 1,178 | 0,009 | 0,981 | 0,502 | 9,533 | 10,035 | 106,6 | 0,11 | 7,37 | 0,04 | 0,25 | 0,95 | 117554 | 121 | 8127 | 44 | 276 | 1048 |
| 5173,3 | 1,177 | 0,011 | 0,981 | 0,504 | 9,497 | 10,001 | 169,5 | 0,14 | 12,49 | 0,06 | 0,4 | 1,53 | 159914 | 132 | 11784 | 57 | 377 | 1443 |
| 5173,4 | 1,175 | 0,011 | 0,981 | 0,505 | 9,48 | 9,985 | 144,5 | 0,21 | 32,4 | 0,07 | 0,34 | 1,76 | 136109 | 198 | 30519 | 66 | 320 | 1658 |
| 5182,8 | 1,19 | 0,011 | 0,981 | 0,507 | 9,501 | 10,008 | 144,6 | 0,56 | 48,98 | 0,15 | 0,32 | 2 | 126942 | 492 | 42999 | 132 | 281 | 1756 |

# ANNEX A – Abstracts

## A.1 Analysis of the tectonic evolution in the Brazilian Atlantic margin via structural restoration and isotopic data

In: Geotop 2024 Student Meeting, 22-24th March, 2024, Stoneham, QC, Canada

Costa, Deniro; Novo, Tiago; Reis, Humberto; Stevenson, Ross

The discovery of giant accumulations of oil and natural gas, along the Brazilian Atlantic margin in continental lacustrine carbonate deposits, has raised great interest from industry and academia in the last decades. Most of the oil production in Brazil comes currently from the pre-salt reservoirs in the southeastern offshore basins. However, a limited number of studies detail the paleoenvironmental evolution and stratigraphic filling of the sag interval or have integrated a quantitative approach coupled with spatial and stratigraphic distribution and related to the depositional or structural context. Considering this scenario, structural restoration of 2D seismic sections can be applied to evaluate the dynamics of tectonic evolution to quantify deformation and describe fault distribution. In addition, isotopic analyses are essential to provide critical constraints on the environment of formation of the reservoir rocks. Section restoration is performed in the Santos, Campos and Espírito Santo basins on a regional scale, for the (i) post-salt, (ii) salt, (iii) sag and (iv) rift packages. Kinematic modeling includes decompaction and isostatic relief calculation, along with backstripping. Other methods comprise geomechanical, fracture and fault response. Isotopic analyses will be conducted in carbonate samples from a well located at the Tupi Field, Santos Basin, from sidewall coring facies (laminites, stromatolites, spherulitites and limestones). C and O stable isotopes provide information on the hydrological balance, (a)biotic component, water temperature and salinity/evaporation due to climate control. Sr radiogenic isotopes are sensitive indicators of lacustrine evolution. Results are expected to constrain the development of widely distributed burial faults formed during carbonate deposition and the influence of reactivated structures, which serve as pathways for fluid flow migration. Isotopic data will be compared to adjacent basins (Campos), equivalent African basins (Kwanza) and modern analogues basins.

A.2 Geochemical analysis of lacustrine carbonates and structural implications at the pre-salt, Santos Basin

In: 51º Congresso Brasileiro de Geologia, 13-17 de Outubro de 2024, Belo Horizonte/MG

**ID do trabalho:** 1848

**Área Técnica do trabalho:** TEMA 18 - Geocronologia e Geoquímica Isotópica

**Título do Trabalho:** Geochemical analysis of lacustrine carbonates and structural implications at the pre-salt, Santos Basin

**Forma de apresentação:** Oral

**Autores:** Costa, D F G[1]; Novo, T A[1]; Fonte Boa, T M R[1]; Reis, H L S[2]; Stevenson, R[3];

**Instituição dos Autores:** (1) UFMG - Belo Horizonte - MG - Brasil; (2) UFOP - Ouro Preto - MG - Brasil; (3) UQAM - Canada;

**Resumo do trabalho:**

Currently, most of Brazil's oil production comes from pre-salt reservoirs in the onshore basins of the Southeast, occurring in continental deposits of lacustrine carbonates. Although it has aroused great interest in the industrial and academic sectors in recent decades, a limited number of studies detail the paleoenvironmental evolution or integrate a quantitative approach associated with spatial/stratigraphic distribution and related to depositional or structural context. Our main objective, therefore, is to evaluate the correspondence of structures generated and/or reactivated during the tectonic evolution and the deposition of the pre-salt layers in the Santos Basin, focusing on the Barra Velha Formation and its isotopic signal, since it is the main hydrocarbon reservoir. In this way, the tectono-stratigraphic context is evaluated from the interpretation of 2D seismic sections. This makes it possible to analyze the dynamics of tectonic evolution, quantify and describe the distribution of faults in the pre-salt layers throughout the study area in the basin. Isotopic analyses are essential to provide critical constraints on the formation environment of the reservoir rocks in the

Iracema region of the Tupi field. Stable isotope analyses of C and O and radiogenic Sr were carried out on carbonate samples from sidewall borehole facies in a 101 m column. Major elements (Ca, Mg, Fe, Mn, Sr and Rb) also had their concentrations measured. The sample values of $\delta^{13}C$ vary between + 0.79 and + 3.16‰, with average values of +2.22‰. The values of $\delta^{18}O$ vary between -1.22 and + 3.86‰, with average values of +1.18‰. The values of $^{87}Sr/^{86}Sr$ vary between 0.7130 at the top of the section and 0.7144 at the bottom, with average values of 0.7135. The high $\delta^{13}C$ and $\delta^{18}O$ values mainly record the climatic effects responsible for controlling the deposition of sediments from the Barra Velha Formation. Environments with high temperatures and high salinity tend to favor the precipitation of dolomite and/or calcite rich in Mg. While the inflow waters are enriched in $\delta^{13}C$ due to evaporation in a restricted closed environment, the $\delta^{18}O$ isotopic signals may have been conserved to some extent, since the carbonates did not undergo intense diagenetic processes that could mobilize or reprecipitate Sr and Mg in large quantities. Other observations that corroborate the lower degree of alteration, preserving characteristics closer to the original carbonate, are high Ca/Mg and $\delta^{18}O$, in addition to the positive correlation between Ca and Sr. The same source or process introduced Rb and Sr, so during diagenesis, elements such as Sr can be replaced by Ca in the carbonates, while Rb can be incorporated into secondary mineral phases or associated clay materials. High $^{87}Sr/^{86}Sr$ values indicate a significant contribution of Sr from continental erosion or terrestrial sources, although there may be another source. Results indicate that the mapped structures may have participated in weak diagenetic processes in the well sampled, since the values obtained for isotopes are in line with those found in the Santos Basin. When compared to other basins, it is seen that they did not function as conduits that would allow the transportation of hydrothermal fluids, which would considerably alter the results obtained. Therefore, it is understood that the samples used preserved the characteristics close to the original carbonate and the structures served as conduits during diagenetic processes.

**Palavras-Chave do trabalho:** diagenesis; faults; Isotope Geochemistry; Tupi field.